

Review

# Metal Oxide Nanoparticles: Review of Synthesis, Characterization and Biological Effects

Andreea Mariana Negrescu <sup>1</sup>, Manuela S. Killian <sup>2</sup> , Swathi N. V. Raghu <sup>2</sup> , Patrik Schmuki <sup>3,4,5</sup>,  
Anca Mazare <sup>3,6,\*</sup>  and Anisoara Cimpean <sup>1</sup> 

<sup>1</sup> Department of Biochemistry and Molecular Biology, Faculty of Biology, University of Bucharest, 91-95 Splaiul Independentei, 050095 Bucharest, Romania

<sup>2</sup> Department of Chemistry and Biology, Chemistry and Structure of Novel Materials, University of Siegen, Paul-Bonatz-Str. 9-11, 57076 Siegen, Germany

<sup>3</sup> Department of Materials Science WW4-LKO, Friedrich-Alexander University, 91058 Erlangen, Germany

<sup>4</sup> Regional Centre of Advanced Technologies and Materials, Palacky University, Listopadu 50A, 772 07 Olomouc, Czech Republic

<sup>5</sup> Chemistry Department, King Abdulaziz University, Jeddah 80203, Saudi Arabia

<sup>6</sup> Advanced Institute for Materials Research (AIMR), National University Corporation Tohoku University (TU), Sendai 980-8577, Japan

\* Correspondence: anca.mazare@fau.de

**Abstract:** In the last few years, the progress made in the field of nanotechnology has allowed researchers to develop and synthesize nanosized materials with unique physicochemical characteristics, suitable for various biomedical applications. Amongst these nanomaterials, metal oxide nanoparticles (MONPs) have gained increasing interest due to their excellent properties, which to a great extent differ from their bulk counterpart. However, despite such positive advantages, a substantial body of literature reports on their cytotoxic effects, which are directly correlated to the nanoparticles' physicochemical properties, therefore, better control over the synthetic parameters will not only lead to favorable surface characteristics but may also increase biocompatibility and consequently lower cytotoxicity. Taking into consideration the enormous biomedical potential of MONPs, the present review will discuss the most recent developments in this field referring mainly to synthesis methods, physical and chemical characterization and biological effects, including the pro-regenerative and antitumor potentials as well as antibacterial activity. Moreover, the last section of the review will tackle the pressing issue of the toxic effects of MONPs on various tissues/organs and cell lines.

**Keywords:** metal oxide nanoparticles; nanotechnology; pro-regenerative potential; cancer therapy; antimicrobial activity; nanotoxicity



**Citation:** Negrescu, A.M.; Killian, M.S.; Raghu, S.N.V.; Schmuki, P.; Mazare, A.; Cimpean, A. Metal Oxide Nanoparticles: Review of Synthesis, Characterization and Biological Effects. *J. Funct. Biomater.* **2022**, *13*, 274. <https://doi.org/10.3390/jfb13040274>

Academic Editor: Elisa Boanini

Received: 21 October 2022

Accepted: 25 November 2022

Published: 5 December 2022

**Publisher's Note:** MDPI stays neutral with regard to jurisdictional claims in published maps and institutional affiliations.



**Copyright:** © 2022 by the authors. Licensee MDPI, Basel, Switzerland. This article is an open access article distributed under the terms and conditions of the Creative Commons Attribution (CC BY) license (<https://creativecommons.org/licenses/by/4.0/>).

## 1. Introduction

In the last few decades, the field of nanotechnology has become one of the most active areas of customizable materials science [1], with wide practicability in various clinical applications, due mainly to the specific size-dependent properties exhibited by the resulting nanomaterials as a direct consequence of a controlled synthesis procedure [2]. Amongst the already in use nanomaterials, nanoparticles (NPs) have received a great deal of attention due to their small size and large surface area [3], properties which provide researchers with novel ways of diagnosing and treating diseases that prior to this were thought to be unapproachable due to the size limitations. With multiple advantages such as high stability, simple preparation methods, excellent engineering control over aspects ranging from size, shape, porosity, etc. and cellular penetration capability, MONPs have grown into valuable materials for the drug and health-related industry [4]. Through the design and development of engineered MONPs, the limitations imposed by their bulk counterparts could be finally overcome, allowing researchers to make astounding breakthroughs in fields

such as specific drug delivery, bio-imaging, biomolecule sensors, etc. [5,6]. Moreover, due to their reduced size, metal oxide nanoparticles can interact on a more in-depth level with various cellular structures compared to their bulk counterparts, and, more importantly, they do not cause systemic toxicity due to their highly improved biocompatibility [5,6]. Currently, various types of MONPs are used in clinical practice as antibacterial and wound healing dressings, biosensors and anticancer and image contrast agents [7]. Of these, zinc oxide NPs (ZnO NPs), cerium oxide NPs (CeO<sub>2</sub> NPs), iron oxide NPs (Fe<sub>2</sub>O<sub>3</sub> NPs), silver oxide NPs (AgO NPs), magnesium oxide NPs (MgO NPs), titanium oxide NPs (TiO<sub>2</sub> NPs), nickel oxide NPs (NiO NPs), zirconium oxide NPs (ZrO NPs) and cadmium oxide NPs (CdO NPs) are the most promising candidates for biomedicine, with a considerable amount of research data available in recent literature regarding their biological in vitro and in vivo activity.

ZnO NPs are a nontoxic, biocompatible biomaterial, with unique abilities that may vary depending on their size, shape, orientation, morphology and aspect ratio [8]. They are widely used in commercial products such as sunscreens, ointments, food packaging and everyday-care products. Moreover, ZnO NPs exhibit a strong antibacterial effect, mainly attributed to their distinct characteristics, that is also dependent on dose, time and synthesis method [8]. In addition, due to their inherent anticancer activity, ZnO NPs have been approved by Food and Drug Administration (FDA) as a new and potent antitumor therapy [9]. It is generally accepted that in addition to the generation of high levels of reactive oxygen species (ROS), ZnO NPs can exhibit a selective cytotoxic effect against cancer cells through the induction of an impaired equilibrium of zinc-dependent protein activity [10]. However, ZnO NPs were shown to induce toxic effects in different cells and organisms, thereby requiring further studies meriting their therapeutic benefits over the potential toxicological risk [11].

CeO<sub>2</sub> NPs represent another type of MONPs widely used in biomedical applications due to their unusual antioxidant properties and anticancer activity. The basis for CeO<sub>2</sub> NPs activities lies in the thermodynamic efficiency of redox-cycling between 3+ and 4+ states on their surface [12] and their unusual ability to absorb and release oxygen [13]. It is worth noting that these NPs can also exhibit pro-oxidant effects at lower pH values [14] and high concentrations [15], and data found in the literature suggest that, depending on their synthesis procedure, dosage and exposure time, they can induce cytotoxic effects [16].

TiO<sub>2</sub> NPs are prevalently used in bone and tissue engineering due to their ability to induce cell migration, adhesion, osseointegration and wound healing [17,18]. However, they also serve as an excellent antibacterial agent [19,20], playing an important role in bacteria growth inhibition via ROS production in the presence of ultraviolet (UV) light [21,22]. Moreover, due to their ability to generate high levels of ROS, they also exhibit anticancer activity [23].

One of the most promising nanoscale biomaterials is represented by Fe<sub>2</sub>O<sub>3</sub> NPs, which can either be used as standalone agents (functionalized with other bioactive molecules/agents), embedded in composites, or bound to different types of cells [24]. Generally, Fe<sub>2</sub>O<sub>3</sub> NPs are mostly used as drug-delivery platforms for pro-regenerative purposes or anticancer therapies, where the selectively targeted release of an active drug is accomplished by either the use of specific binding proteins or by the influence of external magnetic fields [25,26]. In addition, various cells can be magnetically marked with these NPs, therefore allowing for a non-invasive in vivo monitoring of the efficiency of a therapy [27,28].

MgO NPs are primary non-poisonous nanomaterials, with biomedical applicability as drug-delivery systems for anticancer therapy and antibacterial dressings, especially as, being soluble, adverse effects due to remaining in the tissue are avoided [29].

NiO NPs are a class of nanomaterials with a wide variety of flexible properties and vast applicability in the biomedical field through their antibacterial, antifungal and anticancer activities [30].

Because of their favorable biodegradable, mechanical and optical characteristics, ZrO NPs have piqued the interest of researchers, but despite their high biomedical potential,

literature data regarding their role as antitumor, antibacterial and pro-regenerative materials are scarce [31].

Owing to their excellent antibacterial properties, which stem from their small size and morphology combined with the release of ions and ROS, CdO NPs play an important role in treating various bacterial and fungal diseases [32]. In addition, due to their unique physicochemical properties, CdO NPs exhibit better antitumor activity compared to any other heavy metal oxide nanoparticle, but only at lower concentrations [33].

Currently, MONPs are held at an enormous market value due to the significant improvements brought in various fields of nanobiomedicine and their immense potential for future applications.

The present review addresses in the first chapter, the various synthesis methods and characterization of the resulting MONPs, while the following chapters focus on the biological effects exhibited by the MONPs, particularly the pro-regenerative potential, anticancer activity and antibacterial properties. In addition to the positive aspects of MONPs, their very controversial biotoxicology is also discussed in detail alongside the future of these nanoparticles and if their positive therapeutic benefits can outweigh the potential risk caused by the toxic side effects.

## 2. Metal Oxide Nanoparticles: Synthesis, Characteristics, Surface Modification and Characterization

### 2.1. Synthesis Methods and Key Characteristics of Metal Oxide Nanoparticles

The synthesis of nanoparticles can be achieved with either a “top-down” or “bottom-up” approach. In the top-down approach, bulk materials are broken down into NPs by size reduction (via various lithographic techniques, milling, grinding, laser ablation, sputtering, etc.). In the bottom-up approach, NPs are obtained by chemical, physical and biological techniques (plant material, microbes, biological products, etc.).

Typically, chemical and physical synthesis routes (i.e., bottom-up approaches) are employed in the synthesis of MONPs, and result in an efficient quantity of obtained nanoparticles, but have the disadvantage of higher cost, presence of poisonous chemicals (e.g., absorbed on the NPs surface) leading to adverse effects when used in biomedical applications, the need to use of stabilizers, etc. [8,34–36].

Such synthesis routes include but are not limited to: (i) (chemical) precipitation, (ii) wet chemical synthesis, (iii) hydrothermal, (iv) solvothermal, (v) sol-gel, (vi) solid-state pyrolytic methods, (vii) thermal decomposition and (viii) microwave-assisted synthesis.

In order to overcome the disadvantages of MONPs synthesized through the usual classical routes that lead to adverse effects in biomedical applications, the green synthesis of MONPs, or biosynthesis, has gained significant attention due to the use of environmentally friendly and non-toxic reagents with diminished adverse/toxic effects, and result in increased biocompatibility. This approach includes, for example, the use of various biopolymers, plant leaf extracts, algae, surface active biosurfactants, etc. which offer higher specificity, biodegradability and biocompatibility [8,37,38]. Figure 1 shows an overview of the various synthesis routes used for manufacturing metal oxide nanoparticles.

Chemical precipitation is based, as the name suggests, on using a precipitating reagent (such as sodium hydroxide ammonium hydroxide or urea) in the metal precursor aqueous solution, and the resulting precipitate is annealed at high temperatures and converted to the corresponding MONPs. While such a synthesis method results in small-sized NPs, with a narrow distribution, and high purity, it can also lead to NPs with poor crystallinity and the risk of contamination can occur (from the intermediate formation). In the case of spontaneous precipitation, the process takes place without the addition of a precipitating reagent. Such precipitation methods are used for various MONPs, see for ZnO [39–42], CeO<sub>2</sub> [43–45], Fe<sub>2</sub>O<sub>3</sub> [46–48], TiO<sub>2</sub> [49], MgO [50,51] and NiO [52]. The wet chemical synthesis method is based on the chemical precipitation method with the addition of an additive to stabilize the formed NPs; for example, such a synthesis method is used for ZnO

NPs, with starch as the stabilizing agent [53], or for other MONPs (e.g., in the synthesis of  $\text{CeO}_2$  [54,55],  $\text{Fe}_2\text{O}_3$  [56],  $\text{TiO}_2$  [49],  $\text{MgO}$  [57] NiO [58,59],  $\text{ZrO}$  [60] and  $\text{CdO}$  [61,62]).

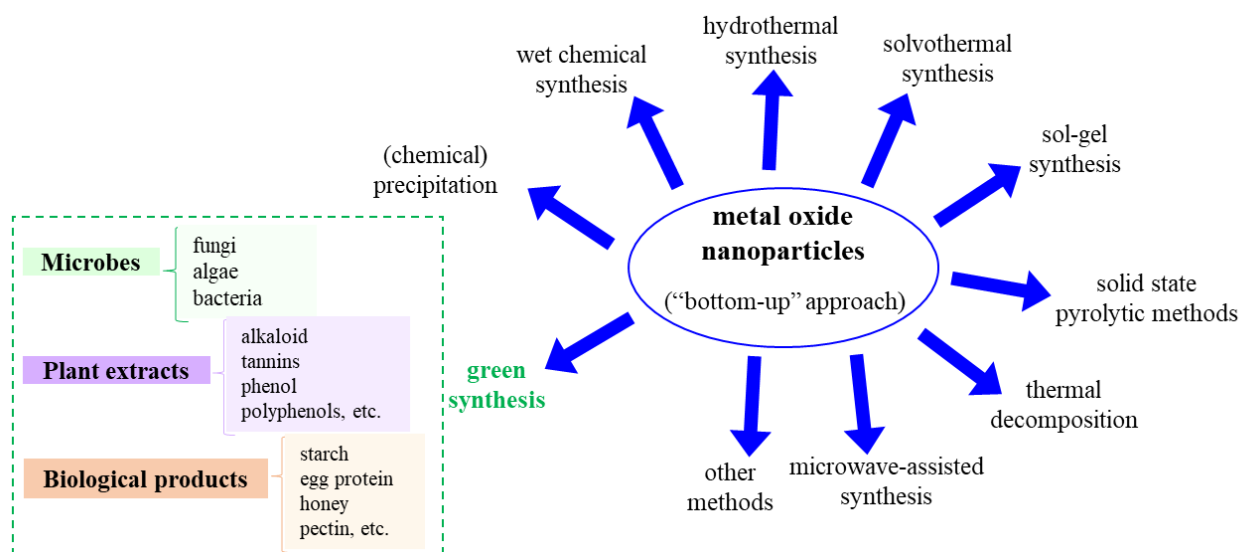


**Figure 1.** Possible metal oxide nanoparticle synthesis methods (“bottom-up” approach).

Hydrothermal synthesis of MONPs is widely used due to the extensive control exercised over the morphology/particle size and lowering of particle aggregation, combined with suitability for large-scale production and high purity. Nevertheless, long reaction times are involved and several post-processing steps are required, as will be further discussed. The synthesis typically involves sealing a metal precursor aqueous solution into a Teflon lined stainless-steel autoclave, together with a precipitating agent (e.g., NaOH) previously added dropwise to achieve the desired pH. The autoclave is then kept at a constant temperature (e.g., 80–200 °C) for a specific duration (e.g., 1–20 h), [63] followed by several washing steps and finally, annealing. Examples of hydrothermally grown MONPs include  $\text{ZnO}$  [64,65],  $\text{CeO}_2$  [66],  $\text{Fe}_2\text{O}_3$  [67],  $\text{TiO}_2$  [68],  $\text{MgO}$  [69,70], NiO [71,72] and  $\text{CdO}$  [73].

The solvothermal synthesis is similar to the hydrothermal method, except other solvents are used in place of water. Typically, the reaction vessels or autoclaves are operated in a temperature range of 100 to 1000 °C and a pressure range of 1 to 10,000 bar [74]. The solvents used typically include diethanolamine ( $\text{ZnO}$  NPs [75]), ethanol ( $\alpha\text{-Fe}_2\text{O}_3$  NPs [76]), methanol ( $\text{ZnO}$  NPs [77]) 1,4-butanediol ( $\gamma\text{-Fe}_2\text{O}_3$  NPs [78]), toluene ( $\text{TiO}_2$  NPs [79], NiO [80]) and ethylene glycol ( $\text{Fe}_3\text{O}_4$  NPs [81]). Nevertheless, in some syntheses, the use of a stabilizer is necessary, and when targeting biomedical applications, it should also be biocompatible (e.g., trisodium citrate [81]).

The sol-gel method is a conventional and industrial method widely used for the synthesis of various NPs [82], offering, especially, good control over their size, high purity and homogeneity and low temperatures (on the downside, the use of organic solvents, availability of necessary precursors and long reaction times pose challenges). The key lies in the production of a homogeneous sol from the precursors and its conversion into a gel, followed by the removal of the solvent from the gel and subsequent drying. The molecular precursor is usually the corresponding metal alkoxide, which is dissolved in water or alcohol and converted to a gel by heating and stirring by hydrolysis/alcoholysis [82]. Appropriate drying methods are necessary depending on the desired properties and application of the resulting NPs. A noteworthy point is the broad size-distribution of particles obtained via sol-gel processes. Examples of MONPs synthesized by sol-gel include the synthesis of  $\text{ZnO}$  NPs either by a modified sol-gel method resulting in a 25 nm NPs, which is smaller than with previously reported sol-gel processes [41], or by typical sol-gel processes [83]. Additionally, several other MONPs can typically be obtained via the sol-gel method, e.g.,  $\alpha\text{-Fe}_2\text{O}_3$  [84],  $\text{MgO}$  [63], NiO [85,86] and  $\text{CdO}$  [87].

Solid-state pyrolytic methods are based, as the name suggests, on the pyrolysis of the metal precursor, while the pyrolysis temperature controls the particle size and the additional chemicals and resulting by-products, and their dissolution can control the NP agglomeration [37]. For example, different sizes of ZnO NPs (8 to 35 nm) were obtained by adjusting the pyrolysis temperature of the reaction mixture [88].

MONPs obtained via thermal decomposition rely on heating the metal precursor above their decomposition temperature in a solvent with a high boiling point [89]. Such NPs have the advantage of being highly monocrystalline (i.e., a post-synthesis annealing is not necessary), but the yield of NPs is quite low. Typically, precursors are organometallic compounds dissolved in organic solvents, also containing surface-stabilizing agents, and the synthesis takes place at high temperatures in an inert atmosphere. Generally, an optimal precursor has to have a low decomposition temperature in order to result in a high surface area and low crystallite size. Moreover, high temperatures are avoided as they could lead to particle sintering, thus precluding the formation of NPs. The size of the NPs can be tuned through the reaction parameters, e.g., precursor, temperature, etc. This method is typically used in the synthesis of nanoparticles of ZnO [90], Fe<sub>2</sub>O<sub>3</sub> [91,92], CeO<sub>2</sub> [93], TiO<sub>2</sub> [94], MgO [95], NiO [96,97] and CdO [98].

Microwave-assisted synthesis of nanomaterials has also gained tremendous ground, as the rapid heating of the reaction system can be achieved by microwave radiation, resulting in an enhancement of the reaction rate (a several orders of magnitude increase due to generation of localized reaction sites) and, thus, in a reduction in the reaction time [89]. Though such a synthesis method cannot be scaled up (no control over the temperature and pressure of the process), due to the high NPs formation yield, reduced agglomeration and fast reaction rates it is advantageous for further research. Various MONPs were synthesized using microwave-assisted techniques, see microwave polyol synthesis (ZnO [99], CeO<sub>2</sub> [100]), microwave heating method ( $\alpha$ -Fe<sub>2</sub>O<sub>3</sub>,  $\beta$ -Fe<sub>2</sub>O<sub>3</sub>, Fe<sub>3</sub>O<sub>4</sub> [101], CdO [102]), solid-state microwave irradiation (NiO [103] NPs), microwave-assisted, solution-based synthesis of TiO<sub>2</sub> [104,105] or NiO [106], microwave-assisted hydrothermal methods (ZnO [107]), low-power microwave-assisted heating (ZnO [108]), surfactant-free microwave-assisted mixing (ZnO [109]), etc.

In addition, there are other reported synthesis methods, generally not valid for the synthesis of all MONPs, but for specific metal oxides. These include mechanochemical synthesis (mechanochemical reactions in different milling times—Fe<sub>2</sub>O<sub>3</sub> NPs [110]), coprecipitation via flow chemistry (Fe<sub>2</sub>O<sub>3</sub> NPs [111]), continuous flow synthesis (TiO<sub>2</sub> [112] or  $\gamma$ -Fe<sub>2</sub>O<sub>3</sub> [113] NPs), successive ionic layer adsorption and reaction (NiO [114]), direct chemical synthesis (NiO [115]), anodic arc plasma (NiO [116]) and so on.

The green synthesis of MONPs has received increased attention due to the use of environmentally friendly and non-toxic reagents, in contrast to other wet chemical synthesis methods, which employ noxious/toxic chemicals that can later be translated into the final products, therefore affecting the use of such NPs in pharmaceutical and other medical/biomedical applications. The advantages of green synthesis, besides the increased biocompatibility of the obtained NPs, are based on the control of the NPs morphology, lower costs and the fact that the enzymes and proteins found in the source materials are good reducing and capping agents [117]. In this respect, microbes (fungi, algae, bacteria), plant extracts of leaves, roots, fruits, or flowers (terpenoid, alkaloid, tannins, phenol, polyphenol, etc.) or various biological products (starch, egg protein, honey, agarose, pectin, etc.) are used [118–120]. Microbial synthesis of MONPs was shown to be an advantageous method due to its reduced toxicity compared to the typical high-pressure and chemical processes [121], but also because the microbes are not detrimentally affected by the synthesis conditions [122]. The green synthesis of MONPs using plant extracts is based on the fact that the plant extracts are employed in the bioreduction of metal ions and to synthesize and stabilize the NPs; similarly, the process is simple, fast and environmentally friendly. Overall, in green synthesis, the reaction rates are slower and only a limited variety of NP shape and size can be obtained. Due to the above-mentioned advantages, this synthesis

method is widely used for the growth of MONPs for biomedical applications, targeting various NPs such as Ag [121,123], or other metal oxides, as described in recent works or reviews (ZnO [8,37,117], Fe<sub>2</sub>O<sub>3</sub> [124,125], CeO<sub>2</sub> [117,119], TiO<sub>2</sub> [117,126,127], MgO [128], CuO [129], NiO [117,130], ZrO [131,132] or ZrO<sub>2</sub> [133] and CdO [62,134]).

On a final note, for more details with respect to the synthesis approach and methodology (used precursors, additives, stabilizers, or reactions conditions), the following reviews are recommended for the synthesis of various MONPs, i.e., for ZnO [8,37,120], CeO<sub>2</sub> [119,135–137], Fe<sub>2</sub>O<sub>3</sub> [124], TiO<sub>2</sub> [120,138], MgO [63,128,139,140], CuO [129,141], NiO [30,142,143] and CdO [144] NPs.

Additionally, in view of the biological effects (interactions with biofluids, cells, biomolecule, etc.) of such MONPs, these are influenced by a wide range of factors, such as NPs size, aggregation state, morphology and stability and, therefore, the synthesis methods are typically tailored towards achieving control over the NPs morphology, size and stability. For example, the physical and chemical properties of MONPs that have an impact on the interactions with cells are the (i) NPs morphology (shape, size), which controls aspects such as overcoming cell barrier, internalization and toxicity [145–148]; (ii) NPs surface area and surface energy, as this influences the number of active sites and can control reactivity [82,149]; (iii) crystal structure, which together with size, defects, media composition and aggregation, influences the dissolution of the metal ions, which can cause toxic effects [150,151]; (iv) surface chemistry, such as surface charge (zero-point of charge, acidity constant), dispersibility and aggregation, influence surface cascade reactions consequential for healing and subsequent biointegration [150–157]; (v) photocatalytic properties and chemical composition of the MONPs, as some nanoparticles can generate hydroxide or peroxide radicals and, furthermore, can (photo)release metal ions that may either promote adsorption reactions and/or facilitate favorable/unfavorable localized ‘-cidal’ effects [158–160].

## 2.2. Functionalization of Metal Oxide Nanoparticles for Biomedical Applications

The previous section discussed the various synthesis methods of MONPs, with an overview of ZnO, Fe<sub>2</sub>O<sub>3</sub>, CeO<sub>2</sub>, TiO<sub>2</sub>, MgO, NiO, ZrO and CdO NPs. While some of these NPs already present some biological effects in their bare nanoparticulate form, the performance and use of others type of NPs can be maximized by additional modifications. These modifications involve the surface functionalization of NPs such that they can elicit specific responses that may be biologically or chemically more favorable.

It should be noted that most of the synthesis processes result in hydrophobic NPs, as a result of synthesis conditions and due to the use of surfactants. This, in turn, limits the solubility of the NPs in aqueous or biological media [161]. There are many approaches for surface modifications and these include functionalization with drugs, polymers, biopolymers, inorganic materials, or bioconjugation (Figure 2). This is achieved by methods such as coating, conjugation strategies, in situ synthesis, self-assembly, surface encapsulation, or the synthesis of core-shell nanoparticles. After the surface modification, the functionalized nanoparticle is compatible with the biological environment, predominantly due to the hydrophilic nature of the coated shell [155,162].

With respect to drug functionalization, the key advantages of using MONPs are twofold. The first is connected to the possibility of localizing the drug to the target cell or area, which significantly increases the potency of the drug, while reducing the dosage and, thus, removing the issue of toxicity to the tissue. Secondly, having a surface coating (shell) on the MONPs can stabilize the nanoparticles, influence the size of the colloid particle and their bio-kinetics and distribution in the body, as well as diminishing their toxicity [155,161,163]. A wide range of specific drugs can be employed, such as anticancer, anticonvulsants, immunosuppressants, antibiotics, anti-inflammatory, antiviral, antifungal, or alternative, drugs. The drugs can either be covalently bound to the MONPs surface or via electrostatic interactions or via sequential functionalization [164] such that loading and release kinetics are governed by affinity to binding substrates and localized environments.

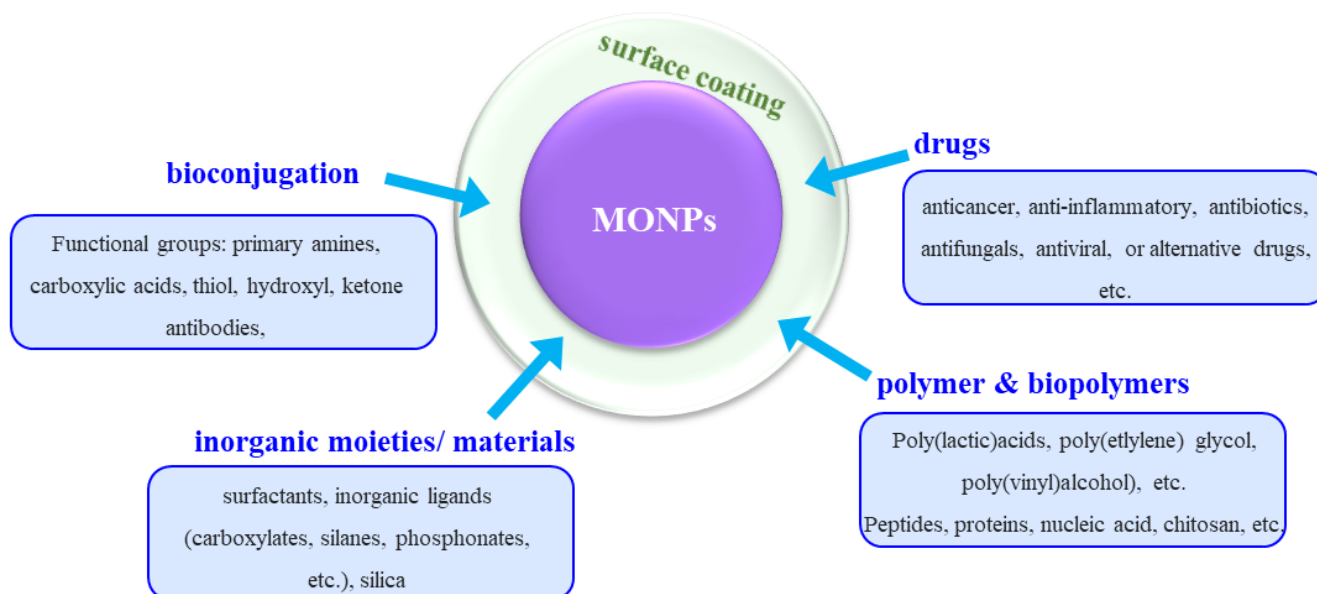


**Figure 2.** Schematic overview of the different surface modification/functionalization of MONPs usually applied for improving the biological effects.

MONPs can be modified by polymers and/or biopolymers, which also contributes to nanoparticle stability in physiological conditions, increase their activity towards biological interactions, and can be further used to introduce more diverse functionalities [161,165,166]. Such polymer coatings can be achieved by either replacing an initial coating on the MONPs (e.g., ligands) or by directly coating the polymer. Typical examples of polymers used include poly(ethylene glycol), poly(lactic-co-glycolic acid), poly(vinyl alcohol), poly(lactic acids), poly(vinylpyrrolidone), poly(alkyl cyanoacrylates), poly( $\epsilon$ -caprolactone), poly(methyl methacrylate), poly(ethyleneimine) and poly(dopamine) [155,161,167]. To further tackle the issue of toxicity of polymers at higher concentrations of longer treatment duration, an alternative is represented by using biopolymers such as peptides, proteins, dextran, chitosan, heparin, cellulose, lignin, etc. [155,161].

The use of inorganic moieties or materials such as surfactants, e.g., sodium dodecyl sulfate and sodium oleate, inorganic ligands such as carboxylates, silanes, phosphates and so on, or silica, is also widely employed for establishing a coating on the MONPs. For example, silica significantly increases NPs stability, biocompatibility and surface functionality with respect to biomedical applications, and is used for coating the surface of magnetic nanoparticles [161].

Another approach used for the functionalization of the MONPs is bioconjugation, which consists of the conjugation of NPs surfaces with biomolecules whose tailored properties evoke favorable interactions in the biological environment [168]. Often, linker molecules are necessary to obtain good adhesion and functionality of the immobilized biomolecules [169]. These conjugations enable the NPs to reach and effectively interact with site-specific cells [161,170].

Furthermore, the functionalization method also depends on the chemical nature and surface properties of the chosen nanoparticles, and thus there is no universal method valid for all MONPs. For detailed information with respect to specific functionalization approaches targeting the discussed MONPs of the present review, readers are referred to the following literature reports—ZnO [155,161], Fe<sub>2</sub>O<sub>3</sub> [155,161,163,171], CeO<sub>2</sub> [172], TiO<sub>2</sub> [23,155,173,174], MgO [139,140] NPs, or recent functionalization approaches (NiO [175] NPs).

### 2.3. Characterization of Metal Oxide Nanoparticles for Biomedical Applications

The typical characterization techniques for MONPs also in view of targeting biomedical applications are based on evaluating the: (a) morphology and composition—scanning

electron microscopy (SEM) and transmission electron microscopy (TEM), combined with energy dispersive X-ray (EDX) analysis; (b) crystallographic structure—X-ray diffraction analysis (XRD); (c) molecular groups and chemical bonding—Fourier-transform infrared spectroscopy (FTIR), or time-of-flight secondary ion mass spectrometry (ToF-SIMS); (d) NPs' chemical and compositional properties—X-ray photoelectron spectroscopy (XPS); (e) synthesis mechanism—thermogravimetric analysis and differential thermal analysis (TGA–DTA); and (f) evaluation of the bandgap adsorption peak—UV-Vis spectroscopy. Moreover, other typical characterization techniques include the evaluation of the zeta potential, which is crucial in evaluating the effective electric charge of the nanoparticles (without or with further functionalization of the NPs). The different characterization techniques are also chosen as a function of the MONPs evaluated, due to the specifics of the metal oxide material and/or their further modifications.

### 2.3.1. MONPs—Morphology Evaluation

From the above characterization methods, electron-microscopy techniques are crucial for the evaluation of the nanostructure and the NPs morphology with respect to particle size (mean and distribution), as well as providing detailed structural information at the atomic scale [176].

Representative TEM images of different MONPs obtained by various synthesis methods are shown in Figure 3. Namely, Figure 3a shows a representative high-resolution transmission electron microscopy (HRTEM) image of ZnO NPs obtained by a green synthesis using *E. prostrata* leaf extract as a capping agent—the NPs have an average size of 29 nm, ranging from 16 to 85 nm, showing also a triangular, radial, hexagonal, rod, or rectangular shape [177]. The SAED pattern is also included (selected area electron diffraction pattern) confirming the high crystallinity of the NPs. Figure 3b shows the HRTEM image demonstrating the formation of small-sized CeO spherical particles (diameter ~5 nm), obtained by a simple wet chemistry method [178,179]. Balaji et al. [180] have synthesized different sizes of biogenic ceria (CeO<sub>2</sub>) NPs, with diameters of 50, 20, 10 and 5 nm, by hydrothermal synthesis in the presence of *E. globulus* leaf extract—Figure 3c shows the HRTEM image of the CeO<sub>2</sub> NPs with 20 nm diameter. Moreover, the authors confirmed the formation of CeO<sub>2</sub> particles with a fringe space of 3.1 Å, also corroborated by the XRD data, demonstrating a (111) plane (3.24 Å) of CeO<sub>2</sub> NPs [180]. Rufus et al. [181] have reported on the green synthesis of α-Fe<sub>2</sub>O<sub>3</sub> NPs (environmentally benign, by the use of guava leaves, *Psidium guajava*) via a simple precipitation method. While SEM confirmed the quasi-spherical shape of the NPs, with diameters in the 20–48 nm range and an average diameter of 35 nm (weight of iron and oxygen from EDX was 62.55% and 37.45%), further TEM characterization corroborated the irregular shape of the NPs with an average size of ~38 nm (Figure 3c) and a rhombohedral structure (lattice fringe width of 0.27 nm corresponding to the (104) facets of the rhombohedral structure—Figure 3d).

TiO<sub>2</sub> NPs obtained by thermal decomposition from titanium oxysulfate and urea (precursor ratio 1:0.4) are shown in Figure 3e [94], and the diameter of the NPs can be controlled by the urea amount—in this case, the NPs had diameters in the 20–40 nm range. MgO NPs obtained by a sol-gel method with the addition of a surfactant (in order to prevent agglomeration) are shown in Figure 3f, having some light agglomeration but with a narrow distribution of the particle size (average size 15.7 nm) [70]. Hydrothermally grown NiO NPs with an average size of 29 nm are shown in Figure 3h (authors confirmed the NPs size by STM measurements) [182]. Green-synthesized ZrO NPs, using the leaves of *L. speciosa*, are shown in Figure 3i, with an average particle size of 56.8 nm with a tetragonal morphology (this could be due to the green synthesis, as the biomolecules are capping the NPs) [131]. CdO NPs obtained by a recently reported annealing of polyvinyl alcohol and para-aminobenzoic acid complexes (from an aqueous solution containing metal chloride as a precursor) [183], with an average diameter of 58 nm, are shown in Figure 3j.

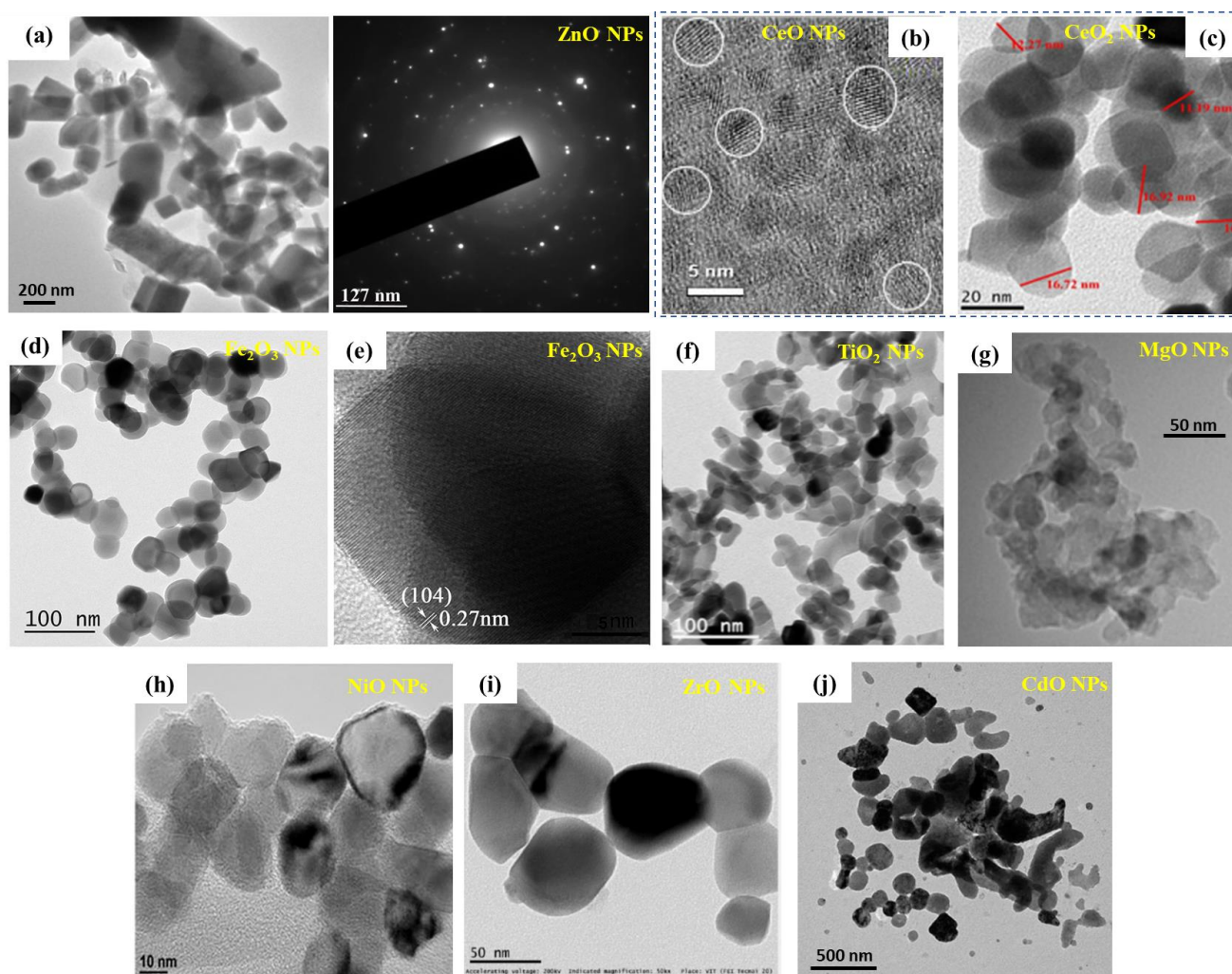


**Figure 3.** Morphology of MONPs: (a) HRTEM image showing green-synthesized ZnO NPs (*E. prostrata* leaf extract) together with the SAED pattern (reprinted from ref. [177]). (b) HRTEM image demonstrating spherical crystalline CeO NPs, diameter ~5 nm, representative crystallites with lattice fringes in white circles (reprinted with permission from ref. [178]). Copyright 2021 Elsevier). (c) HRTEM image of green-synthesized 20 nm CeO<sub>2</sub> NPs (hydrothermal method mediated by *E. globulus* leaf extract (reprinted from ref. [180])). (d,e) green-synthesized  $\alpha$ -Fe<sub>2</sub>O<sub>3</sub> nanoparticles (guava leaves, *Psidium guajava*): (d) TEM micrograph, (e) HRTEM image of a single nanocrystal showing lattice fringes with a spacing of 0.27 nm (reprinted with permission from ref. [181]). Copyright 2016 Royal Society of Chemistry). (f) TEM image of TiO<sub>2</sub> NPs obtained by thermal decomposition (reprinted from ref. [94]). (g) HRTEM image of MgO NPs obtained by a sol-gel method (reprinted from ref. [70]). Copyright© 2019 Alfaro et al.). (h) TEM image of hydrothermal NiO NPs (reprinted from ref. [182]). Copyright 2017 AIP Publishing). (i) HRTEM image of ZrO NPs obtained by a green synthesis (reprinted from ref. [131]). Copyright 2017 Elsevier). (j) TEM image of CdO NPs obtained by the annealing of formed complexes (reprinted from ref. [183]).

Figure 3 clearly shows the variety in NPs shape and size, consequently dependent on the synthesis procedure, together with the progress made into avoiding NP agglomeration via the use of additional capping or stabilizing agents (e.g., plant-based extracts to further ensure the NPs eco-friendliness and biocompatibility, and, thus, their use in biomedical application).

### 2.3.2. MONPs—Crystallographic Structure Evaluation

X-ray diffraction represents a widely used characterization technique in material science in order to determine the crystallographic structure of the materials, and it is also

a crucial evaluation tool for MONPs. Especially as some synthesis techniques require an annealing/thermal treatment step, known also as post-synthesis, to crystallize the NPs (e.g., chemical precipitation), while other methods result directly in the formation of crystalline NPs (e.g., hydrothermal synthesis).

XRD is especially needed in the case of synthesis methods where the effect of the thermal treatment on the crystallinity of the NPs has to be evaluated. For example, for the green synthesis of ZnO NPs in the presence of cyanobacterium from *A. Platensis* [184], a wurtzite structure was confirmed (Figure 4a (peaks at 2 theta degree 31.7°, 34.5°, 36.1°, 47.4°, 56.3°, 63.1° and 67.9°, which matched to the (100), (002), (101), (102), (110), (103) and (112) planes, respectively), with an average crystal size of  $\approx 45$  nm (computed from the XRD analysis by the Debye–Scherrer equation)). In the green synthesis of CeO<sub>2</sub> NPs in the presence of *Prosopis farcta* leaf extract [185], the authors evaluated the impact of the temperature on the synthesis and determined a fluorite cubic structure of the CeO<sub>2</sub> NPs; a similar structure was reported when synthesis was performed with *Eleagnus angustifolia* leaves [186].

Overall, XRD represents a necessary characterization technique to evaluate the crystallinity, lattice parameters, Miller indices and crystallite size for most of the studied MONPs (e.g., ZnO [177,184,187], Fe<sub>2</sub>O<sub>3</sub> [84], MgO [188], NiO [182], ZrO [131,132] and CdO [183]), irrespective of the synthesis method.

### 2.3.3. MONPs—Chemical and Compositional Evaluation

The chemical and compositional structure of the MONPs, without or with further functionalization, can be evaluated by several complementary techniques. FTIR can be used to identify the chemical bonds and characteristic functional groups, especially in view of functionalized MONPs or biomedical composites [189,190]. For example, for the green-synthesized ZnO NPs (cyanobacterium from *A. Platensis* [184] of Figure 4a), the functional groups and chemical structures can be determined by FTIR (Figure 4b). Peaks are observed and their assignments were: 3415 cm<sup>-1</sup>—N–H overlap with a stretching O–H band, 3000 cm<sup>-1</sup>—stretching CH<sub>2</sub> of asymmetric and symmetric carbohydrates and/or lipids, 1600 cm<sup>-1</sup>—stretching C=O vibration of proteins or remaining acetate, 1410 cm<sup>-1</sup>—C–N stretching bond of amino acid, 1341 cm<sup>-1</sup>—vibration bending of the C–H (absorption wave of CH<sub>2</sub> or CH<sub>3</sub> of proteins), 1025 cm<sup>-1</sup>—C–O–C ether of polysaccharides, 676 cm<sup>-1</sup>—C=C bonds and 503 cm<sup>-1</sup>—Zn–O absorption band [184]. In addition to confirming the formation of the ZnO nanoparticles, data show the role of organic substances present in the *A. platensis* extract in the reduction, capping and stabilization of the biosynthesized ZnO NPs [184].

EDX can be used to evaluate the elemental composition of the NPs, and EDX coupled with TEM provides local chemical composition and mapping of the NPs. Similarly, for the ZnO NPs synthesized via a green route (cyanobacterium from *A. Platensis* [184]) of Figure 4a,b, EDX was employed to evaluate the quantitative elemental structure and confirmed the presence of Zn, O, Na, C and Al with weight percentages of 56.6, 20.4, 15.3, 4.5 and 3.2%, respectively (Figure 4c); thus, confirming the ZnO NPs formation through the use of the metabolites in the *A. platensis* filtrate [184].

XPS provides information on the chemical and compositional properties of surfaces and is especially employed to confirm the composition of the NPs, as well as their further modification/functionalization. Typically, the adventitious carbon peak is used to calibrate the measured spectra, nevertheless, recent works have shown the limitations and how to reliably determine the chemical states [194–196] and to accurately fit the peaks of interest [196,197]. Using, as an example, the green-synthesized ZnO NPs [184], the authors confirmed the presence of Zn(II) [184,198]. Namely, Figure 4d shows the high-resolution Zn 2p peak and its deconvolution into the doublet with Zn 2p<sub>3/2</sub> at 1021.4 eV and Zn 2p<sub>1/2</sub> at 1044.2 eV, and the doublet with the 2p<sub>3/2</sub> at 1023.25 eV and 2p<sub>1/2</sub> at 1045.55 eV (with satellite peaks at 1036.25, 1037.3, 1039, 1040.05, and 1041.65 eV, verifying the oxide species) [184,198]. Additionally, for MONPs, deconvolution of the O1s peak can also be performed to verify the presence of the metal oxide, and in the case of biosynthesis or further functionalization peak fitting of the C1s peak is also crucial. For example, for the

biosynthesized ZnO NPs, the authors verified the hydrocarbon composition produced in their reaction medium with peak fitting of the C1s (five peaks at 284.48, 285.75, 287.9, 287.05 and 288.9 eV for C(H, C), C–N, C–O, C=O and C–O–C [184]), and the oxide structure by fitting the O1s peak (overlap of the O in ZnO with that in NaO; Na KL1 at 536.75 and O(C, H), O=C and C–O–C at 531, 532.2 and 535.3 eV, respectively) [184].

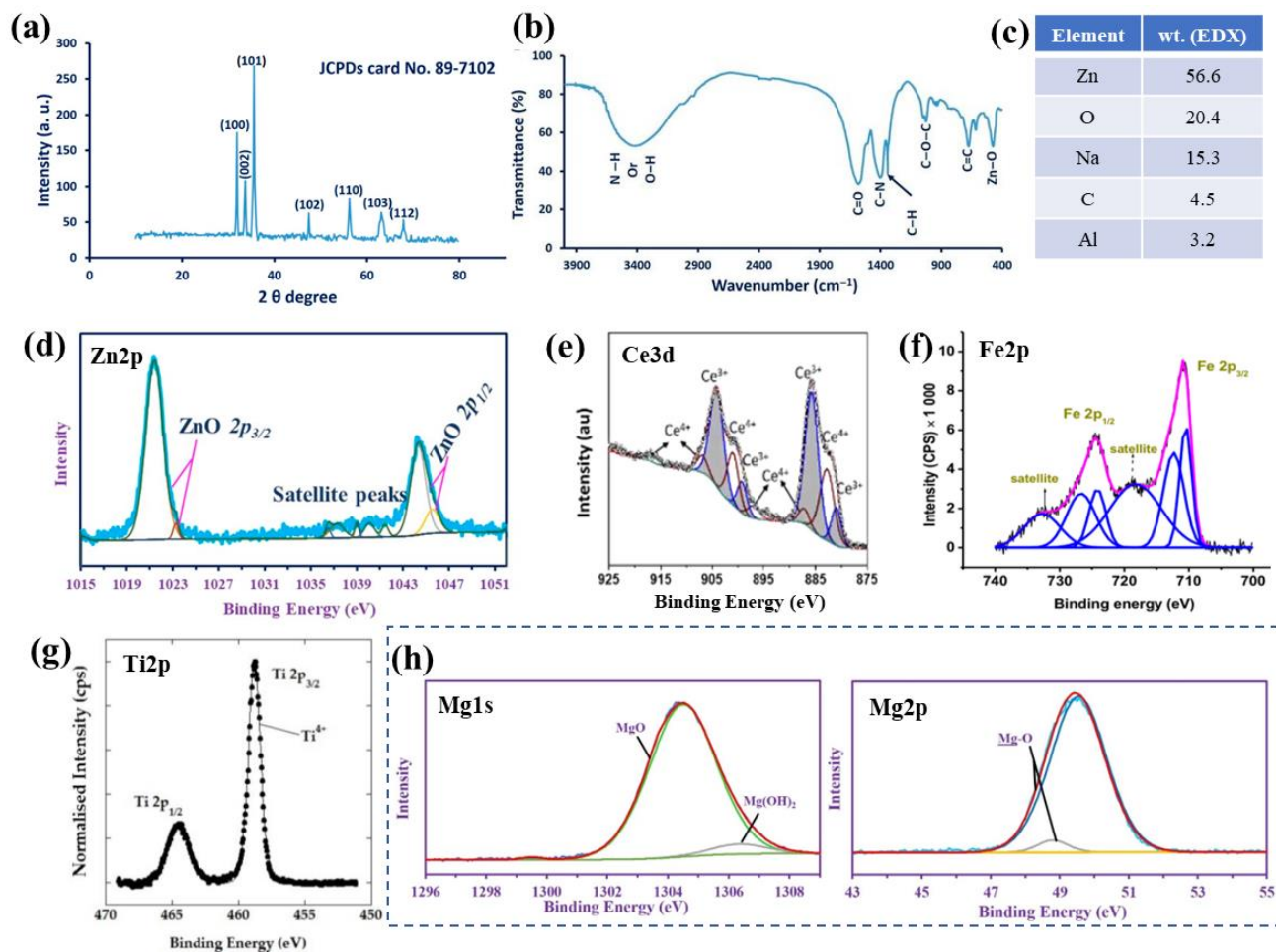


**Figure 4.** Green-synthesized ZnO NPs in the presence of *A. platensis* (cyanobacterium): (a) XRD patterns, (b) FTIR spectrum, (c) weight percentage from EDX (data from ref. [184]), and (d) high-resolution XPS peak of Zn2p (a,b,d: reprinted from ref. [184]). High-resolution XPS spectra for (e) Ce3d of CeO NPs (reprinted with permission from ref. [178]. Copyright 2021 Elsevier), (f) Fe3d in Fe<sub>2</sub>O<sub>3</sub> NPs (solvochemical synthesis in the presence of double capping agents) (reprinted from ref. [191]), (g) Ti2p in TiO<sub>2</sub> NPs synthesized by microwave-assisted method (reprinted from ref. [192]), and (h) Mg1s and Mg2p in MgO NPs (biosynthesis in the presence of metabolites from *Penicillium chrysogenum*) (reprinted from ref. [193]).

Figure 4e–h further show the typical high-resolution XPS peak of the corresponding metal element from the CeO, Fe<sub>2</sub>O<sub>3</sub>, TiO<sub>2</sub> and MgO NPs. From these MONPs, the spectra of Ce 3d and Fe 2p are quite complex. Namely, Figure 4e presents the Ce 3d peak of CeO NPs [178] with the 3d doublet (3d<sub>5/2</sub> and 3d<sub>3/2</sub>) indicating the Ce<sup>3+</sup> and Ce<sup>4+</sup> states with 60% of the cerium being present as Ce<sup>3+</sup> (Ce<sup>3+</sup> peaks of two spin-orbit features: ~880.6, 885.5, 898.8 and 903.7 eV and Ce<sup>4+</sup> peaks of three spin-orbit features: 882.5, 887.1, 897.2, 900.7, 906.8 and 916.3 eV). The XPS spectra clearly show the presence of both chemical states, and the presence of the peak at 916.3 eV enables the clear differentiation between the Ce<sup>3+</sup> and Ce<sup>4+</sup> states, as this peak arises only for the Ce<sup>4+</sup> state [199–201]. In addition, the authors [178] evaluated the O1s spectra and reported a typical asymmetry as a result

of the  $O^{2-}$  ions from different chemical environments (e.g., oxygen bound to  $Ce^{4+}$ ,  $Ce^{3+}$  and  $H^+$ ) thus further corroborating the dual oxidation states. In the case of Fe 2p, Figure 4f shows a typical Fe 2p peak and its deconvolution, for monodisperse magnetic  $\gamma$ - $Fe_2O_3$  nanoparticles obtained by the solvothermal method (with double capping agents) [191]. The differentiation between iron oxides is possible as the spectrum of Figure 4f is typical to the  $Fe^{3+}$  state of the  $\gamma$ - $Fe_2O_3$  NPs, consistent with literature data [202,203], that is with Fe 2p<sub>3/2</sub> at 710.85 eV and Fe 2p<sub>1/2</sub> at 724.42 eV, with their corresponding satellites at 732.78 and 718.44 eV [191].

Typically, the Ti 2p peak corresponding to  $TiO_2$  (NPs, or other nanomorphologies) is more straightforward with respect to the peak shape and chemical state, due to the presence of only one oxidation state of titanium. For example, Figure 4g shows a typical Ti 2p spectrum of  $TiO_2$  NPs, obtained, in this case, by a microwave-assisted method [192], and confirms the presence of Ti 2p<sub>3/2</sub> and Ti 2p<sub>1/2</sub> at 458.8 and 464.5 eV, respectively (attributed to  $Ti^{4+}$  of anatase  $TiO_2$  [204,205]). The authors also evaluated the O1s peak, which was deconvoluted into three peaks including 530.1 eV—assigned to oxygen bonded to titanium (O-Ti), 531.6 eV—oxygen bound to carbon (impurities from the synthesis, i.e., urea or acetylacetone) and 532.8 eV—adsorbed oxygen (O-H bonds of chemisorbed water) [192]. Similarly, in the case of MgO NPs, for example, obtained by (biosynthesis harnessing the metabolites secreted by *Penicillium chrysogenum* [193], the presence of MgO as the main species was confirmed. Briefly, the Mg1s spectrum was deconvoluted into MgO at 1304.44 eV (94.74%) and  $Mg(OH)_2$  at 1306.28 eV (5.26%), and the Mg 2p confirmed this point with Mg-O bonds at 49.49 eV (95.89%) and Mg-OH bonds at 48.74 eV (4.11), as shown in Figure 4h—consistent with literature data [205,206] and further confirmed with the deconvolution of the Mg 2s spectra [193].

For NiO NPs, the typical Ni 2p peaks, i.e., Ni 2p<sub>3/2</sub> and Ni 2p<sub>1/2</sub>, can be observed at binding energies of 853.7–855.42 eV with a split spin-orbit of 17.3 eV [205], and, additionally, with satellite peaks at 861.5, 867.16 and 879.3 eV [207]. In the case of CdO NPs, the Cd 3d peaks attributed to the cadmium oxide are expected at 405 eV (Cd 3d<sub>5/2</sub>) and 412 eV (3d<sub>3/2</sub>) [205,208].

Characterization techniques for establishing the chemical and compositional structure of MONPs are crucial for linking the structure of the NPs with their biological effects, and, in addition, prove necessary when the NPs are loaded with active molecules or have functionalized surfaces [209]. Even when used independently as ‘active’ agents in various composites targeting specific effects such as in the case of drug-loading/release, linking process and subsequent interactions, characterization techniques offer insights into interaction chemistry/behavior, etc.

### 3. Biological Effects

#### 3.1. Pro-Regenerative Potential

Over the last few years, in the field of biomedical research, nanotechnology has offered numerous promising approaches for increasing the transition of regenerative medicine from research to clinical practice [24]. Amongst the variety of materials used in nanotechnology, NPs, especially MONPs, are a widely spread class of materials with unique physical and chemical properties that possess numerous advantages and multiple applications in the biological and biomedical fields [210] (Figure 5). One such application is in wound healing. Trauma, distinct skin conditions, burns, or removal of the skin due to surgical procedures, resulting in superficial or deep wounds, which can be prone to pathogenic colonization and further complications if not protected and treated properly [7]. In this context, suitable wound dressing materials that possess antibacterial properties and the ability to promote wound healing are necessary [211].

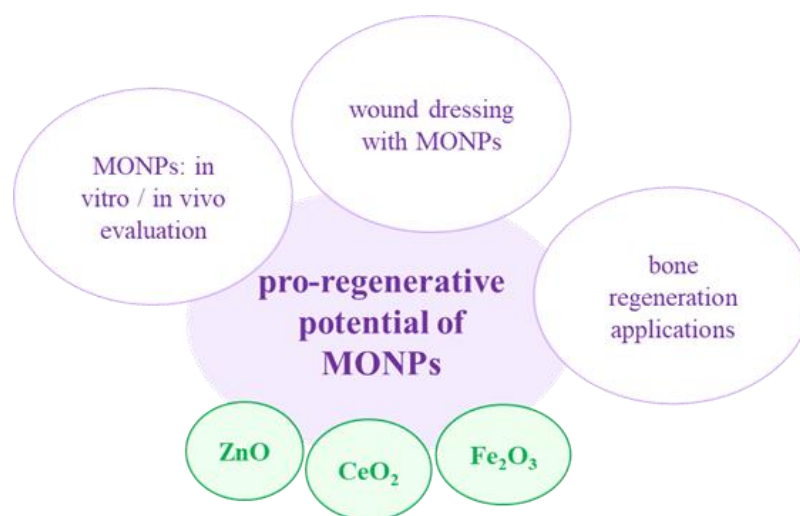


**Figure 5.** MONPs and their use in pro-regenerative potential.

Taking this aspect into account, several wound dressings loaded with MONPs have proved able to decrease the infection and contraction time of the wound, without any significant side effects [212]. One such example of MONPs is ZnO NPs, which have been used with success in numerous wound dressings due to their strong antibacterial activity and stimulating effect on epithelial cells [213]. Raguvaran et al. [214] loaded ZnO NPs onto sodium alginate-gum acacia hydrogels (SAGA-ZnO NPs) and observed that, at low concentrations, these MONPs exerted wound-healing effects on sheep fibroblasts, whereas high concentrations proved to exhibit a cytotoxic effect. Moreover, the loaded hydrogel reduced the inherent toxic effect of the ZnO NPs, while keeping the antibacterial and healing properties of the NPs.

It is a well-known fact that wound healing is a complex process in which the presence of oxidative stress due to an over-production of ROS can lead to injured cells and tissues [215]. Keeping this in mind, numerous *in vitro* and *in vivo* studies focused on the suitability of MONPs for skin-wound repair and regeneration through the inhibition of ROS generation. For example, Davan et al. [216] observed in a rat model that spherical shape CeO<sub>2</sub> NPs (with a size of 160 nm) were capable of enhancing the wound closure rate and collagen deposition, without scarring tissue. Similar results were observed in wound dressings loaded with CeO<sub>2</sub> NPs; for example, Naseri-Nosar et al. [217] loaded poly( $\epsilon$ -caprolactone) (PCL)/gelatin films with CeO<sub>2</sub> NPs and the results suggested that the film containing 1.5% CeO<sub>2</sub> NPs is favorable in terms of L929 cells proliferation. In another study, Wu et al. [218] designed tissue adhesives using assembled ultra-small CeO<sub>2</sub> NPs onto the surface of mesoporous silica NPs and the *in vitro* results showed the ability of the newly developed product to impair the exacerbation of ROS-mediated side effects and promote the wound healing process. Moreover, the *in vivo* results indicated a significantly low ROS level and a reduced local inflammatory activity, coupled with an improved wound healing and lack of scar tissue.

Another type of MONPs used for wound dressing studies are Fe<sub>2</sub>O<sub>3</sub> NPs. One such study by Pai et al. [219] demonstrated that a composite thin film of poly( $\epsilon$ -caprolactone)-Fe<sub>2</sub>O<sub>3</sub> NPs exhibited a strong antibacterial activity and promoted NIH 3T3 mouse fibroblasts proliferation. Similarly, Grumezescu et al. [220] prepared an absorbable wound dressing based on anionic polymers such as sodium alginate and carboxymethylcellulose and Fe<sub>2</sub>O<sub>3</sub> NPs, and the results showed low cytotoxicity to human progenitor cells coupled with a powerful antibacterial activity. Another study showed the promising potential for wound healing of a silk fibroin-Fe<sub>2</sub>O<sub>3</sub> NPs dressing that is biocompatible with human adipose stem cells (ASCs) [221]. Anghel et al. [222] developed a wound dressing coated with a nanofluid containing Fe<sub>2</sub>O<sub>3</sub> NPs and two natural microbicidal compounds and observed that the coating exhibited anti-adherence and anti-biofilm properties against

*Pseudomonas aeruginosa* (*P. aeruginosa*) and *Staphylococcus aureus* (*S. aureus*). Moreover, Fe<sub>2</sub>O<sub>3</sub> NPs possess unique magnetic characteristics which can be used in order to achieve an accelerated wound-healing process. For example, Wu et al. [223] functionalized Fe<sub>2</sub>O<sub>3</sub> NPs with basic fibroblast growth factor (bFGF) and reported an increased cell proliferation and macrophage polarization towards a pro-healing M2 phenotype. In a rat model, the administration of Fe<sub>2</sub>O<sub>3</sub> NPs-loaded mesenchymal stem cells (MSCs) and their magnetically enhanced migration to the injury site improved skin regeneration and enhanced the anti-inflammatory effects and angiogenic process compared with only the injected MSCs [224].

In addition to their potential as wound dressings, MONPs (ZnO, CeO<sub>2</sub> and Fe<sub>2</sub>O<sub>3</sub>) have been used in bone-regeneration applications due to their ability to augment the bone-healing process. For example, in a study by Tang et al. [210], *Scutellaria baicalensis* (SB)-ZnO NPs, i.e., with the addition of the Chinese herb *Scutellaria baicalensis* (generally used to treat bone and joint ailments), were investigated for their effects on osteoblast differentiation and osteoclast formation. The reported results indicated the ability of the SB-ZnO NPs to improve bone regeneration via osteoblast proliferation and differentiation enhancement and inhibition of osteoclast formation. Khader and Arinze [225] incorporated ZnO NPs in a PCL scaffold and the in vitro results suggested that the slow release of ZnO NPs from the structure of the composite benefited both the osteogenic and chondrogenic differentiation of MSCs. Garino et al. [226] evaluated the behavior of ZnO nanocrystals (NCs), with a diameter of 20 nm and partially chemically functionalized by anchoring amino-propyl groups, in terms of biocompatibility, cell proliferation and differentiation—it was suggested that the proposed NCs were capable of promoting bone tissue proliferation even at high concentrations. In another study, Zhou et al. [227] evaluated the effects of CeO<sub>2</sub> NPs on the proliferation, differentiation and mineralization of primary osteoblasts and the results indicated that the biological activity of bone cells is size, concentration- and exposure time-dependent, with positive results at higher concentrations and with smaller size nanoparticles. Moreover, Yuan et al. [228] demonstrated that CeO<sub>2</sub> NPs (average diameter 17 nm) are capable of inhibiting osteoclast formation and activity at high concentrations through the over-production of ROS. Similar results were reported by Wei et al. [178], where 5 nm CeO<sub>2</sub> NPs were observed to enhance MSCs proliferation, osteogenic differentiation and mineralization. Li et al. [229] deposited CeO<sub>2</sub> NPs on a titanium surface and investigated the underlying mechanism of new bone formation both in vitro and in vivo. The results showed that the prepared oxide NPs found in a mixed Ce<sup>3+</sup>/Ce<sup>4+</sup> valence state promoted the new bone formation and mineralization even in the absence of specific osteogenic agents. Similar results were observed in another study [15], where in the absence of osteogenic agents, glass foam-based scaffolds coated with CeO<sub>2</sub> NPs were able to enhance the collagen production and osteogenic differentiation of human mesenchymal stem cells (HMSCs), in comparison to CeO<sub>2</sub> NPs-free scaffolds. In addition, Singh et al. [230] developed PCL nanofiber scaffolds functionalized with Fe<sub>2</sub>O<sub>3</sub> NPs and observed improved cell adhesion and osteogenic activity of osteoblasts; while Cojocar et al. [231] reported improved biocompatibility and bone cell proliferation for the newly developed biodegradable composite based on chitosan, calcium phosphate, hyaluronic acid and Fe<sub>2</sub>O<sub>3</sub> NPs. Similarly, Lee et al. [232] loaded a nanoscaffold based on halloysite nanotubes with Fe<sub>2</sub>O<sub>3</sub> NPs and observed that due to the osteoinductive abilities of the Fe<sub>2</sub>O<sub>3</sub> NPs, the developed nanoscaffold was able to elicit an improved osteogenic differentiation of human adipose tissue-derived mesenchymal stem cells (hADMSCs) through the enhancement of osteoblast formation. Moreover, Zeng et al. [233] fabricated magnetic biomimetic hydroxyapatite (HA) scaffolds immersed in Fe<sub>2</sub>O<sub>3</sub> NPs solutions and observed that, after cell proliferation, the murine pre-osteoblast MC3T3-E1 cell line and the rat osteosarcoma ROS 17/2.8 cell line experienced a promotion of the proliferative and differentiation processes. Similarly, in a study by Tanasa et al. [234], the presence of an applied magnetic field in scaffolds based on silk fibroin, poly(2-hydroxyethyl methacrylate) and Fe<sub>2</sub>O<sub>3</sub> NPs (7 nm) led to an improvement in the proliferative state and differentiation capacity of the MC3T3-E1 pre-osteoblast cells.

However, despite the on-going progress made in this field, there are still many challenges that need to be overcome in order to obtain a successful transition from research to clinical practices; thus, further studies regarding the physicochemical characterization and *in vitro* and *in vivo* cytotoxic potentials of the MONPs are still required.

### 3.2. Antitumor Effect

#### 3.2.1. General Considerations

Cancer, a heterogeneous disease, which affects billions of people and is considered to be one of the main causes of mortality worldwide, represents a serious health problem. With the recent World Cancer Report by the World Health Organization stating that in 2020 the incidence of cancer increased to 19.3 million from 18.1 million in 2018, the growth trend is bound to continue, reaching up to almost 28.4 million cases per year in 2040 [235]. According to the National Cancer Institute (National Institute of Health), patients diagnosed with cancer are currently presented with several treatment options, which may include surgery, radiation therapy, hormone therapy, targeted therapy, biomarker testing, stem cell transplantation, etc. However, each of these therapies possesses the potential to impact the patients' life quality, especially radiation and chemotherapy, which can cause side effects due to their difficulties in differentiating between cancer and normal cells, resulting in systematic toxicity [236]. The surgical approach might appear as a better option, but it has its limitations too, namely in the form of post-surgical scars and the inability to remove all of the tumoral mass, therefore requiring additional side therapy such as radiation, chemotherapy, or, in extreme cases, both. In this context, targeted therapies minimize the side effects whilst improving patient care. New approaches for cancer treatment continue to be studied and developed, and one such strategy includes the use of MONPs against tumor development and progression, due to their intrinsic antitumor effects [10]. The exhibited anticancer activity of MONPs is related to their unique physicochemical properties, which are either related to their intrinsic features, such as their antioxidant action or depend on activities based on the application of external stimuli [10]. In addition, MONPs possess the ability to transport anticancer drugs to a specific tumor location. This specific targeting is achieved by using either an active or passive process. Passive targeting is mainly based on the enhanced permeability and retention effect, meaning that the leaky vasculature found in tumoral tissue allows MONPs to diffuse rapidly and kill cells [237]. However, some adverse effects are associated with drug delivery via passive targeting; for example, the leaky vasculature found in the tumoral mass can also be present in inflamed tissue; therefore, rendering the targeted drug delivery less than ideal due to the lack of precision. Conversely, drug delivery via active processes can reduce the side effects caused by passive targeting, due to the fact that the NPs are functionalized and directed specifically against the cancer cells. Thus, through biomolecule or ligand binding to the surface of the NPs, the targeted delivery of anticancer agents to tumor cells instead of normal ones, can be improved [10].

#### 3.2.2. Applications of ZnO NPs in Cancer Therapy

In anticancer therapy, MONPs are used experimentally to kill tumor cells both *in vitro* and *in vivo*. Amongst several biomedical applications, the use of ZnO NPs in cancer therapy has been well explored. The antitumor activity of ZnO NPs stems from both the ability to generate ROS and their electrostatic properties [37]. The selective toxicity of ZnO NPs against cancer cells has been demonstrated in an *in vitro* study through the use of co-cultured C2C12 myoblastoma cells and 3T3-L1 adipocytes. The results showed that the levels of ROS and p53, bax/bcl-2 ratio and caspase (CASP)-3 enzyme activity were increased in co-cultured C2C12 cells in comparison with the 3T3-L1 adipocytes, suggesting that the ZnO NPs selectively induced apoptosis in the C2C12 cancer cell [238]. In addition, Wahab et al. [239] demonstrated the specificity of ZnO NPs by investigating their toxic effects against malignant T98G human gliomas and KB epidermoids in comparison to non-tumoral HEK kidney cells. The ZnO NPs were found to exhibit a strong cytotoxic effect against the T98G cancer cells, a moderate effect against the KB cells and an insignificant

effect on the healthy kidney cells. Similarly, Premanathan et al. [240] reported that ZnO NPs are capable of inhibiting the proliferation of human myeloblastic leukemia cells in comparison to normal peripheral blood mononuclear cells. In addition, Pandurangan et al. [241] investigated the cytotoxicity of ZnO NPs in human cervical carcinoma cells and it was demonstrated that the cancer cells' viability was significantly reduced, therefore suggesting the possible cytotoxic effect of ZnO NPs through the overproduction of ROS. Furthermore, ZnO NPs (80, 150, 260 and 400 nm in average diameter) were reported to exhibit a cytotoxic effect on ovarian cancer cells, through the induction of acute oxidative and proteotoxic stress, which led to cell death via apoptosis [242]. In another study, Shahnaz et al. [243] observed that ZnO NPs (12–26 nm) were able to induce cytotoxic effects on the HCT-116 colon cancer cell line in comparison to the Vero cell line. In addition to studies with ZnO NPs as standalone agents, numerous studies focused on modified ZnO NPs due to their improved stability and increased selectivity for specific cells. Results showed that surface modifications using Triton-X, polyethylene glycol (PEG), or hyaluronan did not affect the antitumor activity of the ZnO NPs but did improve their safety towards normal cells due to their biocompatible coating [244–246]. In other studies, ZnO NPs have been coated with doxorubicin (DOX), cisplatin and paclitaxel (PTX) and the results indicated that their cytotoxic effect increased significantly in combination with this type of MONPs [53,239]. Wu and Zhang [247] investigated the anticancer effect of both chitosan-coated and uncoated ZnO NPs in HeLa cells exposed to different concentrations and the results obtained showed that both coated and uncoated NPs exhibited reduced cytotoxicity when exposed to smaller concentrations, whereas the chitosan-coated positively charged ZnO NPs caused enhanced cytotoxicity at higher concentrations, possibly through the increased cellular internalization and subsequent ROS production, which caused cellular death by apoptosis. Given the fact that ZnO NPs possess inherent antitumor properties, researchers have used them as drug-delivery platforms for several active biomolecules and drugs. ZnO NPs-based drug-delivery systems (DDS) possess several advantages, such as (i) low risk of systemic toxicity due to the inhibition of a premature release of the loaded drug; (ii) they offer the loaded drugs an increased aqueous solubility and improved hydrophobicity; (iii) they increase the drugs' efficiency by transporting them to the targeted cells/tissues/organs via an active process; and (iv) show a low risk of cytotoxic effects towards normal or healthy cells/tissues/organs.

Presently, only four types of DDS based on ZnO NPs are mainly adopted: (i) mesoporous silica nanoparticles (MSN)-based DDS; (ii) porous ZnO NPs where the active drugs are loaded inside the pores; (iii) ZnO NPs/polymer core-shell nanocomposites where the drugs are loaded into the hydrophobic shell; and (iv) ZnO NPs/drug complex [248]. Zhang et al. [249] developed a multifunctional MSN-based charge reversal and ZnO quantum dots (QDs) targeted drug-delivery system for combined cancer therapy. In order for the MSNs to be able to escape easily and more rapidly from endosomes, they were functionalized with cell-penetrating deca-lysine peptide, while the positively charged ZnO QDs were used to cap the DOX-loaded MSN pores through electrostatic interactions. The results indicated a synergistic anticancer effect in Hep G2 cells through the targeted release of DOX from the uncapped MSN pores into the cytosol. Similarly, Cai et al. [250] designed ZnO QDs functionalized with hyaluronic acid (HA) for pH-responsive delivery of DOX in A549 cells. The mechanism behind this drug-delivery platform is based on the recognition of highly expressed CD44+ cells and the release of drugs through the rupture of the metal-DOX complex due to the dissolution of ZnO NPs in the acidic intracellular compartment. It was demonstrated that the HA-functionalized ZnO QDs-DOX exhibited higher cytotoxicity compared to the non-targeted ZnO QDs-DOX due to the increased intracellular uptake. In another study, Wang et al. [251] reported the successful delivery of certain immunostimulating agents such as ovalbumin and polyinosinic-polycytidylic acid, with the help of hollow ZnO nanospheres for cancer immunotherapy, showing that the combination of the drug-loaded NPs significantly reduced the tumor growth and metastasis to the inguinal lymph node in the E.G7-OVA cell line. Akbarian et al. [252] developed a DDS for paclitaxel

(PTX) based on chitosan-coated ZnO NPs and observed that the PTX-loaded ZnO-chitosan NPs exhibited a cytotoxic effect on MCF-7 cells, and a minimal effect on normal fibroblasts, suggesting that these newly developed ZnO-chitosan NPs could be used as a promising drug-delivery platform for PTX. A biocompatible co-polymer encapsulated ZnO NPs with an interior hydrophobic core designed for efficient encapsulation of curcumin proved to exhibit a higher cytotoxic effect against human gastric cancer cells in comparison to nanocurcumin [253], while a ZnO/ferulic acid stable nanohybrid showed a synergistic antitumor potential in human carcinoma Huh-7 and HepG2 cell lines through the induction of ROS, oxidative stress and DNA damage, followed by cycle arrest in the S phase and intrinsic apoptosis pathways. Moreover, the in vivo results indicated a significant reduction in the number of hepatic nodules and tumor-associated toxicity in hepatocellular carcinoma (HCC) bearing mice [254].

Abbasian et al. [255] synthesized cationic cellulose based ZnO nanocomposites and investigated the targeted and pH-responsive delivery of methotrexate (MTX) into MCF-7 breast cancer cells. The anticancer agent MTX was loaded into the newly developed nanocarriers via electrostatic interactions generated between the drug’s carboxyl groups and the cationic moiety of the NPs and by the formation of ZnO complexes at the chelating sites of MTX. The results showed a higher cytotoxicity against the MCF-7 cells in comparison to the free MTX, probability due to its increased intracellular uptake. Table 1 summarises additional in vitro and in vivo studies focused on investigating the antitumor potential of ZnO NPs either as stand-alone agents or as drug-delivery platforms.

**Table 1.** Supplementary in vitro and in vivo studies focusing on evaluating the anticancer activity of ZnO NPs as standalone agents or as drug carriers.

MONPs	Cell Line	Observations	Ref.
	human prostate cancer cells (PC3 cell line); non-small cell lung cancer cells (A549 cell line)	↓ serum levels of tumor markers; ↓ levels of hepatocyte integrity and oxidative stress markers	[256]
	human skin melanoma (B16F10 cell line); human skin melanoma (A375 cell line)	↓ ERK (extracellular signal-regulated kinases) enzyme and other cancer-associated kinases	[257]
	human colon carcinoma (LoVo cell line)	severe oxidative stress → DNA damage	[258]
	human cervical carcinoma cells (HeLa cell line)	↑ mRNA expression of p53; ↑ levels of ROS	[241]
	hepatocellular carcinoma (Hep-G2 cell line)	dose-dependent cytopathic effects	[177]
ZnO NPs	Caco-2	↑ ROS and 8-oxodG levels; micronuclei and DNA damage	[259]
	cervical cancer cells (SiHa cell line)	dose-dependent cytotoxic effects via mitochondria apoptotic and necrotic death	[260]
	human breast cancer cells (MCF-7 cell line)	dose-dependent cytotoxicity against tumor cells when treated for 24 h	[261]
	human breast cancer cells (MDA-MB-231 cell line)	dose-dependent antitumor activity within the concentration interval of 12.5–200 µg/mL after a 24 h treatment	[246]
	Human skin melanoma (A375 cell line)	↓ cell viability; ↑ROS generation; ↑ apoptosis confirmed by chromosomal condensation assay and caspase-3 activation; ↓ density and a round morphology	[262]

**Table 1.** Cont.

MONPs	Cell Line	Observations	Ref.
ZnO NPs	human lung cancer cells (A549 cell line)	dose-dependent cytotoxic effect via ROS overproduction; ↑ membrane damage; ↑ oxidative stress; ↓ mitochondrial membrane potential	[263]
	wild type EGFR A549 and EGFR-mutated CL 1–5 cells	↑ cytotoxic effect in CL 1–5 cells compared to A549 cells	[264]
ZnO/SiO <sub>2</sub> core-shells NPs	human prostate adenocarcinoma (LNCaP and Du145 cell lines)	↑ radiation-induced reduction in the cell survival rate	[265]
PEG-ZnO NPs	breast cancer cells (MCF-7; MDA-MB-231; MDA-MB-468; T-47D cell lines)	↑ cytotoxic effect against all breast cancer cells at a concentration of 25 µg/mL when treated for 24 h	[244]
daunorubicin-ZnO NPs	human lung cancer cells (A549 cell line)	no premature drug leakage; relevant therapeutic concentrations; liposome incorporated NPs demonstrated a pH-responsive release of the active drug	[266]
	sensitive leukaemia cells (K562 cell line) resistant leukaemia cells (K561/A02)	↑ sensitivity of the drug-resistant tumor cell line; ↑ accumulation of daunorubicin; ↑ cell membrane permeation; ↑ uptake of daunorubicin into both cell types	[267]
DOX-ZnO NPs	human breast cancer cells (MCF-7 cell line)	↑ cytotoxicity for the drug-loaded NPs	[53]
isoorientin-DOX ZnO NPs	hepatocellular carcinoma (HepG-2)	dose- and time-dependent antitumor activity; ↑ synergistic anticancer activity; ↑ cell death through mitochondrial dysfunction; Akt and ERK1/2 inhibited phosphorylation and JNK and P38 enhanced phosphorylation; no significant damage to normal healthy liver cells	[268]
photofrin-ZnO NPs	human lung cancer cells (A549 cell line)	↑ ROS production and cell death	[269]
Folic acid (FA)-functionalised-PTX-ZnO NPs	human breast cancer cells (MCF-7 and MDA-MB-231)	combined passive and active targeting of paclitaxel; ↑ efficacy of paclitaxel against subcutaneous tumors in vivo	[270]
DOX-ZnO/PEG nanocomposites	human cervical cancer cells (HeLa)	↑ antitumor activity; ↑ cancer cell injury via ROS under UV irradiation; ↑ intracellular concentration of DOX with an enhanced anticancer effect	[271]

↑ indicates enhancement; ↓ indicates inhibition.

### 3.2.3. Applications of CeO<sub>2</sub> NPs in Cancer Therapy

Cerium oxide NPs are a novel and very interesting compound, which are currently pursued in various in vitro and in vivo studies for their potential use in cancer treatment (Table 2). Being originally investigated for their antioxidant activity and ability to protect normal cells/tissues from radiation-induced damage associated with cancer therapy in the intestine [272], head and neck [273], breasts [274] and lungs [275], the use of CeO<sub>2</sub> NPs has expanded beyond the prevention of adverse side effects of other cancer treatments. For example, data found in the literature indicates the inherent toxicity of CeO<sub>2</sub> NPs towards various cancer cells such as pancreatic carcinoma cells [276], hepatocellular carcinoma cells [277], epithelial cancer cells [278], melanoma cells [279], ovarian cancer cells [280], etc. Taking this into account, the use of CeO<sub>2</sub> NPs in cancer therapy is ever-growing, with the NPs being used both as the primary treatment and as an adjuvant treatment for the already in-use therapies [281]. In 2006, Lin et al. [282] evaluated the antitumor activity of different concentrations of CeO<sub>2</sub> NPs in A549 human lung cancer cells and observed a dose- and time-dependent cytotoxicity towards the tumor cells through the induction of ROS and

implicitly oxidative stress. Similarly, the inherent toxic effect of CeO<sub>2</sub> NPs was reported on human colon cancer cells (HCT-15) in a dose- and time-dependent manner [283].

**Table 2.** Overview of in vitro and in vivo studies focusing on evaluating the anticancer activity of CeO<sub>2</sub> NPs as standalone agents or as drug carriers.

MONPs	Cell Line	Observations	Ref.
CeO NPs	human lung cancer cells (A549 cell line)	↑ free-radical production; ↑ oxidative stress; ↑ cytotoxic effect against cancerous cells	[282]
	human prostate cancer cells (PC-3 cell line)	↑ antitumor affect against cancer cells; no injury caused to normal healthy cells	[284]
	ovarian cancer cells (A2780 cell line); A2780 xenograft murine model	concentrations in the range of 25–50 μM exhibited an anti-angiogenic effect in ovarian cancer cells; ↓ tumor size in vivo	[280]
	human colon cancer cells (HCT 15 cell line)	↓ cell viability via ROS overproduction	[283]
	human neuroblastoma cells (IMR31 cell line)	↑ ROS production that resulted in oxidative stress; ↑ cytotoxicity and genotoxicity	[285]
	Fibrosarcoma (WEHI146 cell line)	↑ antitumor activity by increasing ROS generation and inducing apoptosis	[286]
camptothecin-CeO <sub>2</sub> NPs	human pancreatic cancer cells (BxPC-3 cell line)	↓ cell viability	[287]
chlorin e6-CeO <sub>2</sub> NPs	Human breast cancer cells (MCF-7/ADR cell line); MCF-7/ADR xenograft murine model	exhibited photodynamic therapy against drug-resistant breast cancer cells and in vivo tumors	[44]
DOX-CeO <sub>2</sub> NPs	human ovarian cancer cells (A2780; SKOV-3 and CAOV-3 cell lines)	↓ cell proliferation rates; ↑ apoptosis of cancerous cells compared to free DOX	[288]
curcumin-CeO <sub>2</sub> NPs	neuroblastoma cells (IMR-32; SMS-KAN; SK-N-AS, LA-N-6)	induced significant cell death in all of the mentioned cancer cells	[289]
DOX-CeO <sub>2</sub> NPs	human liver cancer cells (HEPG-2 cell line)	induced a synergistic antitumor activity on cancer cells	[290]

↑ indicates enhancement; ↓ indicates inhibition.

Kumari et al. [285] investigated the cytotoxic effect of CeO<sub>2</sub> either as NPs or as microparticles for 24 h in human neuroblastoma cells and the results indicated that the tumor cells treated with NPs showed a higher production of ROS and subsequently a higher cytotoxic effect in comparison to the microparticle structure. Another cell line sensitive to CeO<sub>2</sub> NPs toxicity is WEHI1164, which was demonstrated by Nourmohammadi et al. [286] to exhibit a dose-dependent sensitivity. Furthermore, Renu et al. [284] prepared cerium oxide NPs via two different methods in order to obtain ceric oxide NPs with a +3 oxidation state (hydrolysis) and cerous oxide NPs with a +4 oxidation state (hydrothermal) and the results demonstrated that the hydrothermal NPs possessed a higher cytotoxicity towards prostate cancer cells compared to the hydrolysis NPs, mainly due to their increased cellular uptake. However, when compared to normal mouse fibroblast cell line L929, no toxic effects could be observed. Furthermore, Giri et al. [280] investigated the in vivo effect of CeO<sub>2</sub> NPs on A2780 xenograft tumor mice models and after intraperitoneal administration of NPs for every third day up to 30 days. They observed that the tumor weight and the abdominal circumference in the treated mice were significantly reduced compared to the untreated mice. These results suggested that such NPs possess the ability to inhibit metastasis and the angiogenic process in ovarian cancer cells and implicitly reduce ovarian tumor growth. In another in vivo study, Hijaz et al. [43] evaluated the anticancer effect of CeO<sub>2</sub> NPs modified with folic acid in A2780 xenograft tumor mice models and it was reported that the folic acid-tagged NPs were more efficient in attenuating the tumor growth in the treated mice compared to the untreated animals.

Recently, CeO<sub>2</sub> NPs have also been widely used as effective drug-delivery platforms for various active drugs. This drug-delivery property of CeO<sub>2</sub> NPs is based on their inherent cytotoxicity towards tumor cells, exhibiting a synergistic anticancer effect. In 2014, Muhammad et al. [287] designed a redox-responsive CeO<sub>2</sub> NPs capped MSN-camptothecin delivery platform for the active transport of an anticancer drug into the human pancreatic cancer cells and reported that such a drug-delivery platform was capable of inducing a dose- and time-dependent cytotoxic effect on the tumor pancreatic cells, mainly due to its active intracellular uptake and dissolution of the NPs in the highly acidic microenvironment, which led to the release of the encapsulated drug. Moreover, Li et al. [44] developed a CeO<sub>2</sub> NPs-based drug-delivery platform by conjugating a photosensitizer, chlorin e6 and folic acid on polyethylenimine-PEGylation CeO<sub>2</sub> NPs for a targeted photodynamic treatment against drug-resistant human breast cancer cells and xenograft murine models. Under near-infrared irradiation (NIR), the newly developed drug-delivery system was capable of generating ROS, leading to a reduction in the P-glycoprotein expression, and an increase in the lysosomal membrane permeabilization, which in turn results in cytotoxic effects towards breast cancer cells even at lower doses. Furthermore, the *in vivo* results revealed that in the presence of the irradiation procedure, the mice treated with the CeO<sub>2</sub> NPs system showed a visible reduction in tumor growth up to almost 98%. In another study, a CeO<sub>2</sub> NPs-DOX drug-delivery system exhibited a higher degree of apoptosis and inhibition of the cell proliferative rates compared to free DOX in human ovarian cancer cells [288]. Doxorubicin was used as a loading agent in another study by Zhang et al. [290] where a multifunctional and pH/GSH (glutathione) dual-responsive drug-delivery system using porous CeO<sub>2</sub> NPs was developed in order to target human liver cancer cells. The authors reported a synergistic anticancer effect against the tumoral liver cells, probably due to the low intracellular pH and high GSH levels inside the lysosomes present in the cancer cells. Sulthana et al. [289] designed polyacrylic acid (PAA)-coated CeO<sub>2</sub> NPs loaded with a combination of drugs (Hsp90 inhibitor, ganatespib and DOX) for the treatment of non-small-cell lung cancer. They observed that this delivery platform led to a reduction in cell viability to almost 80% in comparison to the single drug-delivery system. In addition, Kalashnikova et al. [291] explored the anticancer effects of dextran-coated CeO<sub>2</sub> NPs loaded with curcumin in human childhood neuroblastoma and reported that the newly developed DDS was capable of inducing a significant toxic effect on the neuroblastoma cells without affecting the healthy cells.

#### 3.2.4. Applications of Fe<sub>2</sub>O<sub>3</sub> NPs in Cancer Therapy

Due to their non-toxic, biodegradable and cheap nature, Fe<sub>2</sub>O<sub>3</sub> NPs have been extensively studied as potential candidates for different cancer therapies [292,293]. Fe<sub>2</sub>O<sub>3</sub> NPs are magnetic biomaterials that can be directed and concentrated by external magnetic fields, e.g., NIR or oscillating magnetic fields (MF), and removed easily once the treatment is brought to completion [294]. Data found in the literature indicate that Fe<sub>2</sub>O<sub>3</sub> NPs are capable of killing tumor cells without affecting normal healthy tissue due to the increased *in vivo* sensitivity of tumors to heat damage. This allows the use of a specific cancer therapy called hyperthermia, where magnetic NPs can target tumors in a heat-specific manner through the alternation of fields, hysteresis and frictional heating [295]. Anticancer hyperthermia therapy implies the use of heat temperatures above 40 °C. For example, Hilger et al. [296] injected supermagnetic NPs into immunodeficient mice models with implanted breast adenocarcinoma cells and observed an increase in temperature within the tumor region of up to 73 °C, but only after applying a 400 kHz magnetic field. Therefore, by employing the use of Fe<sub>2</sub>O<sub>3</sub> for cancer therapy, the risk of damaging healthy tissue is significantly reduced, while the selectivity for cancer cells is greatly improved [10]. Moreover, magnetic Fe<sub>2</sub>O<sub>3</sub> NPs allow for differential functionalization or surface loading, which can be especially useful for magnetically assisted drug-delivery treatments. Therefore, this type of NPs can be coupled with antitumor agents, either by covalent binding or through co-encapsulation in various polymeric matrices. To date, several active molecules, such as

DOX and PTX have been loaded and tested as potential anticancer agents [297,298]. For example, Plichta et al. [299] reported a reduction in human glioblastoma cells' viability when treated with magnetic  $\gamma$ -Fe<sub>2</sub>O<sub>3</sub> NPs conjugated with DOX at low concentrations, while in A549 lung cancer cells, PEG-functionalized  $\gamma$ -Fe<sub>2</sub>O<sub>3</sub> NPs conjugated with DOX were capable of inducing an increase in the viability rate, possible due to the insufficient release of DOX from the system. However, when an alternating magnetic field (AMF) was employed, the NPs exhibited excellent thermal effects that favored the release of DOX from the delivery platform and implicitly the death of the lung cancer cells [300]. Likewise, Lungu et al. [301] reported the anticancer effect of DOX-conjugated carboxymethylcellulose sodium (CMCNa) coated- $\gamma$ -Fe<sub>2</sub>O<sub>3</sub> NPs, through the inhibition of tumor cell proliferation, cell membrane disruption and induction of human breast cancer cells' death. In addition, Plichta et al. [302] observed a 10–20% decrease in the survival rate of human cervix carcinoma cells (HeLa cell line) and human osteosarcoma cells (MG-63 cell line) under the action of DOX-conjugated polymer-coated  $\gamma$ -Fe<sub>2</sub>O<sub>3</sub> NPs compared to free DOX treatment. Quan et al. [303] developed human serum albumin (HSA)-coated Fe<sub>2</sub>O<sub>3</sub> NPs (HINP) conjugated with DOX and observed that in a 4T1 murine breast cancer xenograft model, DOX-HINP induced a reduction in tumor growth comparable to Doxil (a liposome-based DOX formula used as a treatment for various types of cancer) and superior to free Dox. This increased antitumor effect of magnetic NPs coupled with DOX is probably due to the activation of the hydroxyl radicals, which in turn damages mitochondria, lipids, proteins, DNA and other structures found in the cancer cells, leading in the end to their apoptosis and necrosis [10].

### 3.2.5. Antitumor Effects of MgO NPs

Another class of biomaterials with a strong antitumor effect consists of MgO-based NPs. Mubarakali et al. [304] investigated their effect on human breast cancer MCF-7 cells and the results indicated an inhibition of the cell proliferation rates accompanied by specific cytomorphological characteristics of apoptosis. Moreover, Karthik et al. [305] evaluated the cytotoxic activity of MgO NPs against the A549 cancer cell line and it was observed that, by increasing the NPs' concentration, the percentage of dead cells gradually grew up to almost 50%. Similarly, in another study, MgO NPs showed a strong toxic effect against A549 lung carcinoma cells through the increase in ROS, which in turn damaged the mitochondrial membrane potential and activated the apoptotic pathways [188]. In addition, due to the chemical stability of the MgO NPs (as obtained or with further modifications) under harsh conditions, their high tolerability in the human body and biodegradability [306–311], these biomaterials can be used with success in drug-delivery applications.

### 3.2.6. Antitumor Effects of CuO NPs

Data found in the literature also reported on the anticancer effect of CuO NPs [7]. For example, these NPs showed a cytotoxic effect on human lung cancer cells and breast cancer cells, through the induction of apoptosis via enhanced production of ROS [312]. In another study, CuO NPs were used to treat mouse subcutaneous melanoma and metastatic lung tumors, based on B16-F10 mouse melanoma cells, through intratumoral and systemic injections, respectively [313]. The observations suggested that this type of NPs was capable of downsizing the growth of melanoma, inhibiting the metastasis of B16-F10 cells and increasing the survival chances of the mice models. Furthermore, the in vitro results on HeLa cells indicated that CuO NPs affected the mitochondria, which resulted in the release of cytochrome C and the activation of caspase-3 and -9, therefore inducing cell death. Moreover, CuO NPs were reported to possess a cytotoxic effect on human liver carcinoma cells in a dose-dependent manner, via ROS overproduction and, subsequently, induced oxidative stress [314].

### 3.2.7. Antitumor Potential of TiO<sub>2</sub> NP

TiO<sub>2</sub> NPs are a prevalent material used in various biomedical applications, including cancer treatment [10]. Photocatalyzed TiO<sub>2</sub> NPs have been reported as a potential strategy for cancer cell eradication. In one in vivo study, TiO<sub>2</sub> NPs exposed to light irradiation suppressed tumor growth in glioma-bearing mice and increased the survival rate of the mice models [315]. Furthermore, nitrogen-doped anatase NPs demonstrated a higher visible light absorbance in comparison to the neat TiO<sub>2</sub> NPs, inducing an almost 93% cell death of melanoma cells under UV light [316]. Similar results were observed in another study with colloidal ruthenium complex-loaded TiO<sub>2</sub> NPs against melanoma cancer cells [317] and the results indicated that, under UV light, the number of dead cells increased in comparison with visible light illumination. However, the in situ penetration of UV light is low and dangerous to the human organism, therefore, a strategy to overcome this limitation is represented by the surface-functionalization of the TiO<sub>2</sub> NPs. Recently, the efficacy of NIR on crystallized shells comprised of TiO<sub>2</sub> NPs coated in order to form core/shell nanocomposites has been reported against HeLa cells and in a tumor model using female Balb/c nude mice [318]. Moreover, the study of Lucky et al. [319] reported the use of core-shell up-conversion nanoparticles with a thin and continuous layer of TiO<sub>2</sub> against oral squamous cell carcinoma and their ability to reduce the in vivo generation of tumors. Venkatasubbu et al. [320] developed PTX-loaded HA/TiO<sub>2</sub> NPs and evaluated their antitumor activity in diethylnitrosamine (DEN)-induced hepatocarcinoma in animal models and observed an enhanced anticancer activity for the modified PTX-loaded HA/TiO<sub>2</sub> NPs compared to pure PTX. Similarly, in another study, the treatment of ovarian cancer cells with hyaluronic acid-TiO<sub>2</sub> NPs loaded with cisplatin resulted in an improvement of intracellular drug accumulation when compared to free cisplatin [321]. Moreover, through the adjustment of the nanocarriers' size and shape, a possible increase in drug accumulation in the microenvironment could be achieved, and various in vivo studies have demonstrated that elongated nanocarriers can be retained more efficiently at the tumor sites after intravenous injection and can deliver larger quantities of therapeutic drugs [322–324]. In this context, non-spherically shaped TiO<sub>2</sub> nanoparticles with an elongated geometry could represent a possible drug-delivery strategy with higher efficiency. For example, Kafshgari et al. [325] fabricated well-separated, uniformly shaped and easily detachable anodic TiO<sub>2</sub> nanotubes (NTs) and nanocylinders (NCs) through a time-varying electrochemical anodization protocol to investigate their potential application in cancer therapy. Accordingly, the newly fabricated nanotubes and nanocylinders were conjugated with DOX and their cellular uptake and cytotoxicity in HeLa cells were evaluated. The reported data indicated that the single and uniformly shaped pH-responsive anodic TiO<sub>2</sub> NTs and TiO<sub>2</sub> NCs possessed low cytotoxicity. When conjugated with the antitumor agent, they were easily incorporated into the cells and subsequently released their drug cargo into acidic intracellular compartments. In another study, Fe<sub>2</sub>O<sub>3</sub> NPs-loaded TiO<sub>2</sub> NTs were designed with the purpose of magnetic targeted guidance and site-specific drug delivery and the results suggested that the nanocarriers could be controlled and guided toward the cancer cells through a static gradient magnetic field [326]. In addition, the site-specific delivery of incorporated drugs was demonstrated through the nanocarriers' conjugation with camptothecin, when a 90% killing efficiency of HeLa cells was achieved and with oligonucleotides for cell transfections demonstrating a 100% cellular uptake [326].

### 3.2.8. Antitumor Effects of Other Metal Oxide Nanoparticles

The antitumor activity of NiO NPs has been lightly recorded in the specialized literature. Abbasi et al. [327] evaluated the anticancer effects of NiO NPs against the Hep G2 cancer cell line and observed that the pathogenic cells treated with increasing concentrations of nanoparticles exhibited a decrease in their survival rate that was dose-dependent. Thus, the highest concentration of NiO NPs induced a reduction in the survival rate by up to 84%, results that indicated a strong anticancer potential for this type of NPs. Similarly, Lingaraju et al. [130] synthesized via a green route NiO NPs and investigated their antitu-

mor potential against A549 and Hep G2 cell lines. The results showed a dose-dependent cytotoxic effect against the cells treated with different concentrations of NiO NPs, probably due to the internal accumulation of nanoparticles and high stress, which in the end led to cellular death via apoptosis. Moreover, Zhang et al. [328] used green-synthesized NiO NPs to evaluate their anticancer activity on various tumor cell lines and the reported data indicated that the newly obtained NPs could decrease the viability of esophageal cancer cells up to 50% compared to other cancer cell lines such as colon cancer cells.

As with NiO NPs, the number of relevant works regarding the antitumor activity of ZrO NPs is very limited, despite their biomedical potential. One study investigated the cytotoxic effect of newly synthesized ZrO NPs against the MCF-7 cell line and the reported data suggested that, compared to the control group, the survival rate of the MCF-7 cancer cells was reduced in a dose-dependent manner [131]. Tabassum et al. [329] evaluated the cytotoxicity of ZrO NPs against the MDA-MB-231 cell line and observed a diminishing trend in the cells' survival rate that was directly linked to the increase in the nanoparticles' concentrations. In another study, a dose-dependent reduction in the survival rates of MDA-MB-231 and Hep G2 cancer cells was observed after exposure for 72 h to iron-manganese-doped sulfated ZrO NPs [330]. Another cell line with a high sensitivity to ZrO NPs is the A549 cell line, where in a study by Balaji et al. [331] after 24 h of treatment, a reduced level of viable cells could be observed.

As stated above, CdO NPs possess the ability to control cancer cells via the destruction of their cellular membrane, but this antitumor potential is rarely studied and reported in the specialized literature, with only a few articles investigating the cytotoxic effect against cancer cells. One such study, by Skheel et al. [32] evaluated the cytotoxic effects of green-synthesized CdO NPs against human colon cancer cells (HT29) and the obtained data demonstrated their significant antitumor effect against the studied cancer cells. Moreover, Gowri et al. [33] showed that, even at a minimal concentration, ZrO NPs are able to induce an inhibitory effect against human cervical cancer cells, thus implying their promising potential as anticancer agents.

### 3.3. Antibacterial Activity

The ever-increasing resistance of different pathogens towards antibiotics coupled with the need for biomedical devices, such as implants, wound dressings, catheters and stents, with a wide range of antibacterial activity, forced researchers to identify and develop new strategies in the battle against various bacterial agents. In the last 20 years, nanotechnology has offered a solution in the form of a variety of nanoparticles that have been proven by *in vitro* and *in vivo* studies to possess antibacterial effects (Table 3). Of these, metal oxide nanoparticles such as Ag<sub>2</sub>O, TiO<sub>2</sub>, CuO, ZnO and MgO have been identified to exhibit antibacterial activity against several bacterial species [332].

Literature data indicate that MONPs can interfere with different cellular processes of pathogens, either through the generation of ROS, which causes oxidative stress, or either through their dissolution and release of toxic free metal ions [333] (Figure 6). In addition, the antibacterial effectiveness of MONPs is dictated by their characteristics, such as size and surface properties, determined by their synthesis parameters [334,335].

For example, it was demonstrated that smaller nanoparticles exhibited a stronger bactericidal effect compared to both bigger NPs and their bulk counterpart [333,336,356,357], while NPs with positively charged surfaces possessed a stronger binding force for the negatively charged surfaces of various bacterial agents, therefore leading to an enhanced antibacterial activity [334].

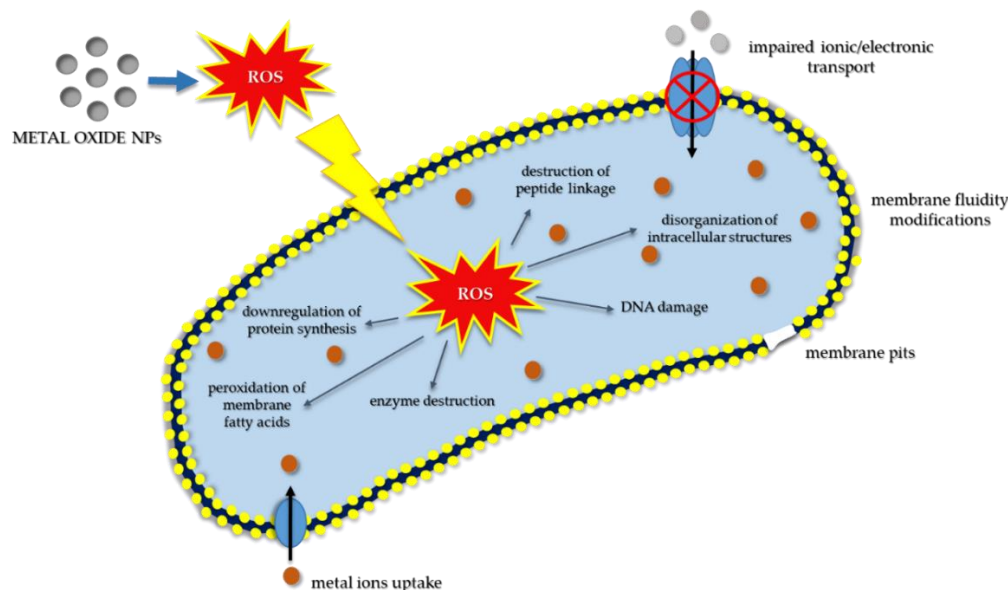


**Figure 6.** Schematic representation of various mechanisms of antibacterial activity of the MONPs, illustrating the possible interactions of MONPs with the bacteria cell wall, membrane structures, DNA, enzymes and other proteins and the influence of ROS on membrane stability, protein function and synthesis.

**Table 3.** Metal oxide NPs with antibacterial activity: mechanism of action and characteristics.

MONPs	Mechanism of Action	Factors that Influence MONPs Effectiveness	Antibacterial Activity and Characteristics	Ref.
Ag <sub>2</sub> O	dissolution and ion release from the NPs surface → pits and gaps in the bacteria membrane → disruption of the metabolic processes due to ion interaction with disulfide or sulfhydryl enzymes → DNA damage	NPs shape and size	action on drug-resistant bacteria; high stability	[336–340]
CeO	dissolution and ion release → ROS generation → DNA damage → cellular death	NPs concentration and surface properties	efficient against both Gram-positive/Gram-negative bacteria	[341,342]
CuO	dissolution and ion release → vital enzyme damaging	NPs size and shape	efficient against Gram-positive/Gram-negative bacteria; high stability	[343–345]
MgO	loss of cell membrane integrity → extracellular leakage of intracellular contents → cellular death	NPs concentration, pH and size	efficient against both Gram-positive/Gram-negative bacteria; high stability; low cost	[346–348]
TiO <sub>2</sub>	ROS overproduction → oxidative stress → lipid peroxidation → membrane fluidity	NPs size, shape and crystal structure	high stability	[349–352]
ZnO	dissolution and ion release + ROS generation → membrane dysfunction → NPs internalization into the cell	NPs concentration and size	efficient against both Gram-positive/Gram-negative bacteria; high stability; effectiveness against spores	[353–355]

### 3.3.1. Antibacterial Activity of ZnO NPs

The antibacterial activity of ZnO NPs stems from their high solubility and Zn<sup>+</sup> ion release, which, once in contact with the bacterial cells, will end up being absorbed. At this intracellular level, the free Zn<sup>+</sup> ions will interact with the thiol group of respiratory enzymes and inhibit their action, leading to an overproduction of ROS and free radicals,

which in turn will cause oxidative stress. This will result in membrane, mitochondria and DNA damage and ultimately bacterial cell death [358]. Data from the specialized literature indicate the bactericidal effect of ZnO NPs against both Gram-positive and Gram-negative bacteria, but also against spores, which in general possess resistance against high pressures and temperatures [354]. Moreover, it was reported that the antibacterial activity of ZnO NPs is tightly related to their size and concentration. For example, (i) Padmavaty et al. [359] showed that the bactericidal activity of ZnO NPs increased with the decrease in particle size, while (ii) Zhang et al. [249] demonstrated that the bacterial response to ZnO NPs is both dose- and time-dependent, with positive results being observed in low-dose ranges and smaller exposure periods; similarly, (iii) Hosseinkhani et al. [360] reported a decrease in the number of bacteria with the decrease in the NPs size, while (iv) Emami-Karvani et al. [361] investigated the effect of ZnO NPs against both Gram-positive (*Escherichia coli*) and Gram-negative (*S. aureus*) bacteria and the results indicated that the antibacterial activity of ZnO NPs is both size- and concentration-dependent. Furthermore, several studies investigated the synergistic action of ZnO NPs with antibiotics as an alternative treatment for various bacterial diseases. In this context, Ghasemi and Jalal [362] evaluated the effect of ZnO NPs on the effectiveness of two antibiotics, namely ciprofloxacin and ceftazidime, against an opportunistic pathogen, *Acinetobacter baumannii*, which causes a wide range of diseases (e.g., meningitis and pneumonia) and reported that, in the presence of sub-inhibitory concentrations of ZnO NPs, the antibacterial activity of both antibiotics was enhanced. In addition, ZnO NPs have been demonstrated to possess antibacterial activity against *Vibrio cholerae* [363], *Camphylobacter jejuni* [364], *Mycobacterium tuberculosis* [365], etc., namely to pathogenic agents responsible for a wide range of illnesses such as severe watery diarrhoea, dysentery and tuberculosis.

### 3.3.2. Antibacterial Activity of TiO<sub>2</sub> NPs

The antibacterial properties of TiO<sub>2</sub> NPs are associated with their specific characteristics such as crystal structure, size and shape [350], with the proposed mechanism of action being correlated to their ability to generate ROS and cause DNA damage [351,366]. Thus, in a study conducted by Roy et al. [351], it was reported that TiO<sub>2</sub> NPs were able to improve the antibacterial activity of a wide range of antibiotics, such as cephalosporins, tetracycline, glycopeptides and macrolides, against *methicillin-resistant S. aureus* (MRSA). In addition, it was demonstrated that the photocatalytic properties of TiO<sub>2</sub> NPs facilitate the eradication of bacteria. For example, Carré et al. [352] suggested that the antibacterial photocatalytic activity of these NPs is accompanied by lipid peroxidation that causes membrane fluidity enhancement and lowers the cell's integrity. However, despite the enhancement offered by ultra-violet (UV) light exposure, the use of TiO<sub>2</sub> NPs under UV light is limited due to the genetic damage observed in human cells and tissues [349].

### 3.3.3. Antibacterial Potential of CuO NPs

Due to their unique physicochemical and biological characteristics, antibacterial activities and low cost of preparation, CuO NPs have attracted the attention of researchers all over the world [Wu et al., 2002; Usman et al., 2013]. Mahapatra et al., 2008, investigated the antibacterial activity of CuO NPs against various bacteria including *Salmonella paratyphi*, *Shigella strains*, *Klebsiella pneumoniae* (*K. pneumoniae*) and *P. aeruginosa* and reported that these nanoparticles were able to reduce the number of bacteria through membrane crossing and enzyme damage, which in turn led to cell death. In another study, Azam et al., 2012, evaluated the effect of CuO NPs against two Gram-positive bacteria and two Gram-negative bacteria and the results showed that the antibacterial effect against both groups of bacteria was size- and concentration-dependent. Moreover, Ahamed et al. [345] showed that the CuO NPs exhibited significant antibacterial activity against a wide range of bacterial strains such as *Enterococcus faecalis*, *K. pneumoniae*, *E. coli*, *P. aeruginosa*, *Shigella flexneri*, *S. aureus*, *Proteus vulgaris*, *S. typhimurium*, etc.

### 3.3.4. Antibacterial Activity of MgO NPs

Data from the literature highlight a strong antibacterial activity of MgO NPs, which can be correlated to their ability to generate superoxide on their surface and increase the pH of the microenvironment by particle hydration with water [348]. In addition, Jin and He [346] demonstrated that this type of MONPs is capable of damaging the membrane, resulting in a leakage of the intracellular contents and, in the end, cell death. MgO NPs exhibit antibacterial effects against both Gram-positive and Gram-negative bacteria [347]. For example, Sawai et al. [367] reported that MgO NPs possess antibacterial effectiveness against *S. aureus* and *E. coli*, while another study proved the particles' efficiency against *E. coli* and *Salmoella stanely*, but in a concentration-dependent manner [346]. Vidic et al. [347] investigated the antibacterial potential of a combined nanostructure of ZnO-MgO and their results indicated a high antibacterial activity against the Gram-positive bacterium, *B. subtilis*, while the pure MgO NPs revealed a moderate activity against both *B. subtilis* and *E. coli* bacteria.

### 3.3.5. Antibacterial Potential of Ag<sub>2</sub>O NPs

Ag<sub>2</sub>O NPs have also been discovered to possess great antibacterial effectiveness against both regular and drug-resistant bacteria, turning them into potential novel alternatives to most in-use antibiotics [349]. In a study by Sondi and Salopek-Sondi et al. [368], it was suggested that the antibacterial mechanism of action for Ag<sub>2</sub>O NPs is due to their ability to induce cell death through oxidative stress caused by arresting the cell cycle in the G<sub>2</sub>/M phase as a direct consequence of DNA damage.

### 3.3.6. Antibacterial Activity of CeO<sub>2</sub> NPs

In terms of CeO<sub>2</sub> NPs, there is widespread research on their antibacterial action [369–371] with studies showing their effectiveness against nitrogen-fixing bacteria and Gram-negative bacteria. In contrast to other MONPs, it was discovered that CeO<sub>2</sub> NPs cannot penetrate the bacteria membrane [341]; therefore, the hypothesized mechanism of action is based on the generation of oxidative stress in lipids and proteins found in the plasma membrane and on the disruption of the electron-flow and bacterial respiration [155]. Ravishankar et al. [342] reported that CeO<sub>2</sub> NPs exhibited a concentration-dependent antibacterial activity against *P. aeruginosa* and a lack of activity against Gram-positive bacteria.

### 3.3.7. Antibacterial Activity of Other Metal Oxide Nanoparticles

Even though the exact mechanism of the NiO NPs antibacterial activity is not yet fully understood, data reported in the literature indicate their antibacterial effect against various Gram-positive and Gram-negative bacteria such as *B. subtilis*, *S. aureus*, *E. coli* and *P. aeruginosa* [30]. For example, in one study, the newly developed NiO NPs were shown to have strong antibacterial activity against *S. aureus* and *B. subtilis*, while the least-susceptible strains were found to be *P. aeruginosa* and *K. pneumoniae* [327]. Moreover, Lingaraju et al. [130] demonstrated the nanoparticles' strong antibacterial activity against *E. coli* and only a moderate effect on the *S. aureus* and *K. aerogenes* strains.

As with other MONPs, ZrO<sub>2</sub> NPs exhibit an antibacterial effect on both Gram-positive and Gram-negative bacteria. Gowri et al. [372] evaluated the antibacterial potential of the ZrO<sub>2</sub> NPs against *E. coli* and *S. aureus* and observed that the inhibition zones in the case of cotton fabrics treated with ZrO<sub>2</sub> NPs were greatly improved. Furthermore, Kumaresan et al. [373] revealed the nanoparticles' ability to inhibit the growth of bacteria strains such as *E. coli*, *Salmonella typhi* and *B. subtilis*. In another study, *Penicillium* was used to synthesize ZrO<sub>2</sub> NPs and it was observed that, even at minimum concentrations, the nanoparticles had strong antibacterial activity against *P. aeruginosa* and *E. coli* [374].

The antibacterial activity of CdO NPs was tested against three Gram-positive (*S. aureus*, *S. pneumoniae* and *B. subtilis*) and three Gram-negative bacteria (*Proteus vulgaris*, *P. aeruginosa* and *S. typhi*) at three different concentrations. The results indicated that the maximum zone of inhibition was obtained against *P. vulgaris* suggesting that this bacterial strain is more

susceptible to CdO NPs, and this can be explained through structural differences in the cell membranes. Moreover, *S. aureus* showed the least zone of inhibition, thus indicating the reduced antibacterial activity of these NPs on this bacterial strain [33]. In addition, Shkeel et al. [375] prepared CdO NPs with the use of aqueous plant extracts from the Curcuma rhizome and investigated their antibacterial effect against a variety of human pathogens such as *P. aeruginosa*, *K. pneumoniae*, *S. aureus*, *E. coli*, *Candida albicans* and *Trichophyton rubrum* and reported a superior activity in the area of antimicrobial strain inhibition.

Considering the strong antibacterial activity of MONPs, their use in combination therapy could represent a feasible strategy to overcome the current rise in bacterial resistance and biomedical device-mediated infection. However, further studies are still required in order to minimize the toxicity of nanoparticles before they can be employed as potential alternatives for antibiotics and disinfectants for biomedical applications.

#### 4. Toxicological Effects of Metal Oxide Nanoparticles

Due to their unique and novel characteristics, MONPs have become the main focus of a wide range of in vitro and in vivo studies, consequently turning them into potential but powerful scientific tools, with diverse applicability in the biological field [241]. However, despite their multiple therapeutic effects, the potential toxicity of MONPs has been a rising concern, as numerous in vitro and in vivo studies report controversial results [376]. Different toxicity mechanisms, such as oxidative stress/lipid peroxidation/cell wall damage as a result of an overproduction of ROS [377,378], metal ion release [379–381] and an impaired interaction between the nanoparticles and the targeted cells [382–384], have been suggested (Figure 7). However, no singular, indisputable and precise identification of the toxicity mechanism involving MONPs has been made.

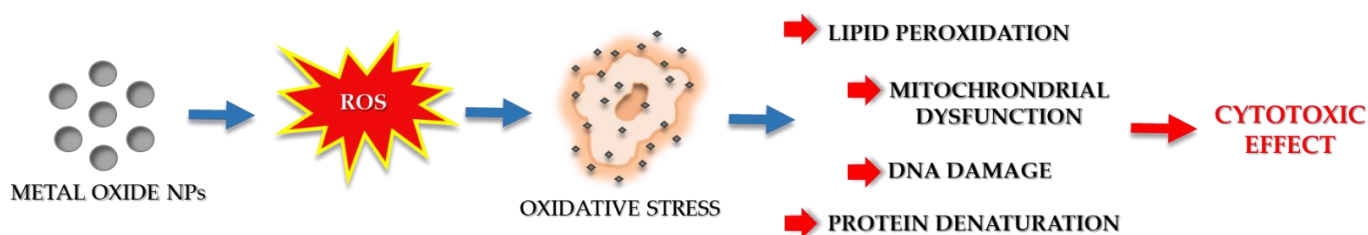


**Figure 7.** Schematic representation of the possible toxicity mechanisms of metal oxide nanoparticles.

Furthermore, it is a well-known fact that the toxicological risk of any given substance is determined both by its inherent toxicity and exposure time. Therefore, if the exposure time is kept to a minimal threshold, the toxicity risk might be reduced even though the MONPs possess a powerful cytotoxic effect [385]. Owing to the ever-growing importance of MONPs in the fields of biology and medicine, an incremental need for risk assessment of the toxic effect of MONPs should be further studied and characterized. The following section will outline the most recent in vitro and in vivo toxicity studies of various MONPs synthesized via different techniques.

##### 4.1. In Vitro Studies

Despite being recognized as one of the most widely used non-toxic mineral nanostructures, TiO<sub>2</sub> NPs exhibit various specific properties that could possess a potentially unknown cytotoxic effect toward the human organism. Several in vitro studies reported the toxic effects of TiO<sub>2</sub> NPs in various cell types such as COS-1, NIH-3T3, TK6, WIL2-NS, NIH-3T3, etc. [386–389]. Magdolenova et al. [389] reported that the cytotoxic effects displayed by the TiO<sub>2</sub> NPs are mainly attributed to the type of dispersion procedure used during toxicological investigations, while Kang et al. [387] and Akhal'tseva et al. [390] observed DNA damage and micronuclei generation in human lymphocytes and the human lymphoblast TK6 cell line after TiO<sub>2</sub> NPs treatment. However, since different testing protocols influence a variety of nanoparticle interactions, it may have a divergent impact on the toxicity results

and the data reported in the literature are inconsistent and often conflicting with numerous *in vitro* studies disconfirming the cytotoxic potential of TiO<sub>2</sub> NPs [391]. In common with TiO<sub>2</sub> NPs, ZnO NPs also present a widespread range of applicability in biomedicine, with numerous studies reporting on their multiple therapeutic benefits [11]. However, in the last few years, the use of ZnO NPs has become debatable, mainly after it was discovered that they induce an over-accumulation of ROS and subsequently cause cytotoxic effects on certain specific organs and cell lines [11]. Data reported in literature assign the biotoxicity of these nanoparticles on their high solubility, a property responsible for the increase in the free intracellular Zn<sup>2+</sup> ion concentration released into the microenvironment [11]. As a direct consequence, in an *in vitro* system, the cellular Zn homeostasis disruption has been associated with oxidative stress, mitochondrial dysfunction and, ultimately, higher toxicity [392] (Figure 6). Nonetheless, important aspects that should be taken into consideration when assessing ZnO NPs toxicity are the concentration, the time of exposure to the particles and whether or not their toxicity could be reversible [258]. For example, Sahu et al. [393] reported that exposure to 50 nm ZnO NPs at concentrations of between 5 and 100 µg/mL decreased cell viability through the generation of oxidative stress, in a concentration-dependent manner, ultimately resulting in DNA damage and cell apoptosis. Moreover, Huang et al. [394] showed that 20 nm ZnO NPs exerted a concentration- and time-dependent cytotoxic effect on BEAS-2B human lung epithelial cells; while Wu et al. [395] and Ng et al. [396] demonstrated that the nanoparticles' cytotoxic effect on the primary human bronchial epithelial cell line BEAS-2B was induced by 24–70 nm ZnO NPs and 22.5 nm ZnO NPs, respectively.

In addition to specific cell lines derived from the airways, a vast number of *in vitro* studies focused on the toxic effects of ZnO NPs on various immune cells, such as macrophages and monocytes. In the RAW 264.7 macrophage-like cell line, 20 nm ZnO NPs led to the induction of intracellular Ca<sup>2+</sup> flux, a process followed closely by reduced mitochondrial membrane potential and, finally, to the loss of membrane integrity [397]. However, similarly sized ZnO NPs did not activate the inflammasome in the THP-1 human monocytic cell line, therefore, no cytotoxic effects could be observed. Moreover, it was reported that monocytes are more sensitive to 4–20 nm sized ZnO NPs and that with NPs size reduction, the cytotoxicity and ROS generation were significantly increased [398]. As stated above, the manifold effects of CeO<sub>2</sub> NPs have motivated researchers all over the world to pursue these MONPs as therapeutic agents for a number of diseases, including cancer, with various *in vitro* and *in vivo* studies demonstrating their cytotoxic effects on a wide range of tumor cells [281]. However, data published in the specialized literature indicate that CeO<sub>2</sub> NPs can also display minimal *in vitro* toxicity to non-cancerous cells, most likely due to the impact of various unknown cellular and micro-environmental stimuli on the manifestation of anti- and pro-oxidant behavior [281]. For example, several *in vitro* reports showed that the uptake of CeO<sub>2</sub> NPs could induce oxidative stress, DNA damage, aberrant cell signaling, substrate dephosphorylation and modifications at the transcriptional and post-translational levels [277,399,400]. However, due to the distinct properties of the synthesized ceria NPs and the poor correlation between their cytotoxic effects with particle size/surface characteristics and cell type, the majority of the reported data regarding their toxicity are often contradictory [376]. As with other MONPs, the intracellular and *in vivo* toxicity of Fe<sub>2</sub>O<sub>3</sub> nanoparticles arise from the over-production of ROS, which can damage cells by peroxidizing lipids, disrupting DNA, modulating gene transcription, changing proteins and ultimately lowering the physiological function of cells, followed by their death (Figure 6). The cytotoxic effect of Fe<sub>2</sub>O<sub>3</sub> NPs has been investigated *in vitro* on a wide range of cell lines such as human lung epithelial cells, human epidermal keratinocytes, BRL3A rat liver cells, Cos-7 monkey fibroblasts, etc. [401], but reported end results were contradictory mainly due to the wide variety of cell lines employed. For example, amine-modified Fe<sub>2</sub>O<sub>3</sub> NPs at a concentration of 224 µg/mL were shown to induce an up to 25% reduction in the astrocytes derived from a mouse brain, while human dermal fibroblasts and fibrosarcoma cells did not present the same drastic changes in their survival rate [402]. Moreover, the toxicity of Fe<sub>2</sub>O<sub>3</sub>

NPs has been demonstrated to be strongly dose-dependent, with concentrations higher than 300 µg/mL usually inducing cytotoxic effects after a prolonged exposure time [403,404]; Dwivedi et al. [358] reported that cell death is a dose-dependent phenomenon and it was associated with increasing concentrations of NPs, which led to the generation of ROS-mediated oxidative stress. In vitro studies are a step toward clinical practices, especially due to the reproducibility of material behavior and cellular response. However, one of their considerable challenges lies in the inability to replicate cellular conditions in 'live' systems, which may curtail the data of in vitro test to effectively ascertain in vivo response, which will be looked into in the following section.

#### 4.2. In Vivo Studies

Regardless of the in vitro toxicity evaluation of MONPs, in vivo studies are scarcely reported. This section presents the most relevant in vivo animal investigations concerning the toxic effects of these metal oxide nanoparticles. The in vivo toxicity of ceria NPs was evaluated in a series of studies that demonstrated that animal exposure to certain concentrations of CeO<sub>2</sub> NPs led to lung inflammation, lung injury, alveolar macrophage functional alteration, induction of phospholipidosis and release of pro-inflammatory and fibrotic mediators [405]. Moreover, reported data suggest that ceria NPs can induce myocardial fibroblast proliferation and collagen accumulation in rat models [406]. In addition, CeO<sub>2</sub> NPs could lead to systemic toxicity, since cerium is not a mineral found normally in the human body, therefore lacking an intrinsic clearance mechanism for its subsequent elimination [376]. As with CeO<sub>2</sub> NPs, in vivo toxicity studies of TiO<sub>2</sub> NPs showed stronger inflammatory activity in comparison to their micro-sized counterparts, leading to lung inflammation and, consequently, cancer in rats after nanoparticle inhalation and intratracheal instillation [388,407,408]. Moreover, Trouiller et al. [409] and Sycheva et al. [410] reported that TiO<sub>2</sub> NPs administered either through drinking water or gavage could induce micronuclei and DNA damage in the peripheral blood cells and bone marrow of adult male mice, while Lindberg et al. [411] observed that, after five days inhalation of TiO<sub>2</sub> NPs, no DNA damage occurred in the peripheral blood lymphocytes of mice. As stated above, the system distribution of ZnO NPs can lead to toxic manifestations in various organs of the body, based on their concentration, the administered dose and its route, and the exposure time. Taking this into consideration, a wide range of in vivo studies demonstrated that ZnO NPs could affect organs such as the liver, kidneys, spleen, stomach, pancreas, lungs and heart, but also the neurological and lymphatic systems. For example, ZnO NPs inhalation caused a size-dependent severe inflammatory response and fibrosis in the alveolar and tracheobronchial tissues, due to the dissolution of nanoparticles by the acidic lung fluid, which in turn increased their concentration and, implicitly, their pulmonary cytotoxicity [412]. Moreover, Han et al. [413] reported that the administration of ZnO NPs via intraperitoneal injection resulted in neurotoxic effects, such as an attenuated learning ability and memory. Similarly, Elshama et al. [414] identified significant histopathological and ultrastructural alterations in the brains and spinal cords of rats as a direct consequence of increased ROS after prolonged exposure to high doses of intraperitoneally administered ZnO nanoparticles. Furthermore, in a study by Li et al. [415], it was demonstrated that both intraperitoneal and oral administration of ZnO NPs had, as a direct consequence, the systemic distribution and toxic accumulation of nanoparticles in different organs such as the liver, lungs, kidneys and spleen. In addition, it was shown that in male rat models, the nanoparticles were able to alter the body's metabolism by elevating the levels of liver enzymes. Similar results were reported by Soheili et al. [416], who, apart from the elevated levels of liver enzymes, observed higher levels of glucose, thus suggesting that ZnO NPs are also harmful to some extent to pancreatic cells. In another study, Esmaeilloua et al. [417] demonstrated that the cytotoxic effects of ZnO NPs on organs such as the lungs, liver and kidneys could be also dependent on their physicochemical characteristics, such as size and specific surface area. Similarly, Kim et al. [418] reported that the oral administration of a wide range of doses of 100 nm sized ZnO NPs with various surface charges and for

a prolonged period of time were capable of inducing an assortment of histopathological alterations such as squamous and glandular cell hyperplasia in the stomach, acinar pancreatic cells apoptosis, retinal atrophy and suppurative inflammation in the prostate. Despite the scarcely available data on the effects of the ZnO NPs on the reproductive system and fetal development, Hong et al. [419] showed that the repeated oral administration of ZnO NPs for short periods of time in pregnant rat models led to maternal and developmental toxicity. When it comes to the *in vivo* interaction between Fe<sub>2</sub>O<sub>3</sub> NPs and biological systems, the process becomes quite complicated and dynamic [420–422]. When these NPs are administered and enter an organism through various routes, their absorption can occur through interactions with different biological components, e.g., proteins and cells, only to be afterward distributed into different organs where they either remain or end up being metabolized [423]. Taking this into consideration, it was expected that organs that are enriched with reticuloendothelial systems, such as the lungs, liver and spleen, would take up the majority of iron oxide nanoparticles administered via different routes. *In vivo* studies demonstrated that Fe<sub>2</sub>O<sub>3</sub> NPs that entered the body both via inhalation and the intravenous route, accumulated in the lungs, brain, spleen, testes and liver, while only intravenous Fe<sub>2</sub>O<sub>3</sub> NPs were found to accumulate in the brain, spleen and kidneys [424,425]. In addition, different types of animal models also displayed different toxicity profiles for Fe<sub>2</sub>O<sub>3</sub> NPs, e.g., differences in liver function in terms of the levels of aspartate aminotransferase and alanine aminotransferase, were observed in different types of animal models upon intravenous administration of the same concentration of iron oxide NPs [426].

In summary, the toxicity of MONPs remains an overly controversial subject, and further standardized studies are still required in order to understand the exact mechanism through which nanoparticles exert their cytotoxic effects and the ways through which this present liability could be overcome.

## 5. Conclusions and Future Perspectives

Due to their small size and unique characteristics, NPs possess different properties compared to their bulk counterparts, thus exhibiting an ever-growing biomedical potential, mainly due to their inherent ability to induce an over-production of ROS and implicitly cell death. These unique properties turn MONPs into suitable anticancer, antibacterial and pro-regenerative tools, either as standalone agents or as drug-delivery platforms for various bioactive molecules. However, despite the multiple advantages that MONPs bring into clinical practice, the major drawback that poses a great challenge for researchers all over the world is their inherent toxicity and the lack of a consensus regarding the guidelines and regulatory frameworks for *in vitro* and *in vivo* testing of their toxicological effects.

With this in mind, systematic documentation of the complementary *in vitro* and *in vivo* protocols used to evaluate specific NPs responses would be beneficial and more than likely eliminate the limitations imposed by their toxicity, especially if it would present both as a standardized method of synthesis and as testing protocols. From the point of view of synthesis and functionalization, firstly, due to the variety of synthesis methods, there is difficulty in evaluating the influence of the NPs size and morphology, and, secondly, as a result of differences in the chemical and surface properties of the same metal oxide NPs synthesized by different methods, there is a disparity in the performance and actual functionalization of such NPs.

Each MONP synthesis method comes with its own advantages, and from the different bottom-up approaches discussed in the present review, typically precipitation, sol-gel, hydrothermal and various biosynthesis methods are extensively used in both laboratory and industrial synthesis. Furthermore, biosynthesis or green synthesis possesses a huge potential for the advancement of green research in the field of MONPs with biomedical applications due to its effectiveness, low costs, sustainability and environmental and human health safety benefits.

Once this challenge of systematic documentation is addressed and overcome, the future of MONPs in the biomedical field will hold an even greater promise, not only for

multifunctional therapeutic strategies but also for early disease diagnosis as theranostic platforms for in-depth and non-invasive cellular and tissue imaging. Moreover, recent advances in the design and development of MONPs allow them to deliver, with minimal effects, active drugs for lethal diseases that demand site-specific treatment. This characteristic was and will continue to be heavily exploited in cancer treatment, with researchers seeking multi-functional therapies and remote control of NPs functions. Furthermore, this will open the door for the introduction of personalized medicine, which will pave the way for safer, more effective and tailored treatment options for patients with cancer. Therefore, it is expected that the coming years should witness an increase in the number of clinical trials and an improvement in the life of cancer patients.

**Author Contributions:** Conceptualization, A.M. and A.C.; writing—original draft preparation, A.M.N., M.S.K., S.N.V.R., P.S., A.M., A.C.; writing—review and editing, A.M.N., A.M., A.C.; visualization, A.M., A.C.; supervision, A.M., A.C.; project administration, A.M. All authors have read and agreed to the published version of the manuscript.

**Funding:** This research received no external funding.

**Conflicts of Interest:** The authors declare no conflict of interest.

## References

1. Chaudhury, K.; Kandasamy, J.; Kumar, H.S.V.; RoyChoudhury, S. Regenerative nanomedicine: Current perspectives and future directions. *Int. J. Nanomed.* **2014**, *9*, 4153–4167. [[CrossRef](#)]
2. Chung, E.J.; Rinaldi, C.; Leon, L. (Eds.) *Nanoparticles for Biomedical Applications*; Elsevier: Amsterdam, The Netherlands, 2020; ISBN 9780128166628.
3. Rizvi, S.A.A.; Saleh, A.M. Applications of nanoparticle systems in drug delivery technology. *Saudi Pharm. J.* **2018**, *26*, 64–70. [[CrossRef](#)] [[PubMed](#)]
4. Sánchez-Moreno, P.; Ortega-Vinuesa, J.L.; Peula-García, J.M.; Marchal, J.A.; Boulaiz, H. Smart Drug-Delivery Systems for Cancer Nanotherapy. *Curr. Drug Targets* **2018**, *19*, 339–359. [[CrossRef](#)]
5. Rostami, M.; Nasab, A.S.; Fasihi-Ramandi, M.; Badiei, A.; Rahimi-Nasrabadi, M.; Ahmadi, F. The ZnFe<sub>2</sub>O<sub>4</sub>@mZnO-N/RGO nano-composite as a carrier and an intelligent releaser drug with dual pH- and ultrasound-triggered control. *New J. Chem.* **2021**, *45*, 4280–4291. [[CrossRef](#)]
6. Biswas, S.; Bellare, J. Bioactivity, Biocompatibility, and Toxicity of Metal Oxides. In *Metal Oxides for Biomedical and Biosensor Applications*; Elsevier: Amsterdam, The Netherlands, 2022; pp. 3–33.
7. Augustine, R.; Hasan, A. Emerging applications of biocompatible phytosynthesized metal/metal oxide nanoparticles in healthcare. *J. Drug Deliv. Sci. Technol.* **2020**, *56*, 101516. [[CrossRef](#)]
8. Mirzaei, H.; Darroudi, M. Zinc oxide nanoparticles: Biological synthesis and biomedical applications. *Ceram. Int.* **2017**, *43*, 907–914. [[CrossRef](#)]
9. Shen, C.; James, S.A.; de Jonge, M.D.; Turney, T.W.; Wright, P.F.A.; Feltis, B.N. Relating Cytotoxicity, Zinc Ions, and Reactive Oxygen in ZnO Nanoparticle-Exposed Human Immune Cells. *Toxicol. Sci.* **2013**, *136*, 120–130. [[CrossRef](#)] [[PubMed](#)]
10. Vinardell, M.P.; Mitjans, M. Antitumor Activities of Metal Oxide Nanoparticles. *Nanomaterials* **2015**, *5*, 1004–1021. [[CrossRef](#)]
11. Elshama, S.S.; Abdallah, M.E.; Abdel-Karim, R.I. Zinc Oxide Nanoparticles: Therapeutic Benefits and Toxicological Hazards. *Open Nanomed. J.* **2018**, *5*, 16–22. [[CrossRef](#)]
12. Korsvik, C.; Patil, S.; Seal, S.; Self, W.T. Superoxide dismutase mimetic properties exhibited by vacancy engineered ceria nanoparticles. *Chem. Commun.* **2007**, *10*, 1056–1058. [[CrossRef](#)]
13. Deshpande, S.; Patil, S.; Kuchibhatla, S.V.; Seal, S. Size dependency variation in lattice parameter and valency states in nanocrystalline cerium oxide. *Appl. Phys. Lett.* **2005**, *87*, 133113. [[CrossRef](#)]
14. Asati, A.; Santra, S.; Kaittanis, C.; Nath, S.; Perez, J.M. Oxidase-Like Activity of Polymer-Coated Cerium Oxide Nanoparticles. *Angew. Chem. Int. Ed.* **2009**, *48*, 2308–2312. [[CrossRef](#)] [[PubMed](#)]
15. Karakoti, A.S.; Tsigkou, O.; Yue, S.; Lee, P.D.; Stevens, M.M.; Jones, J.R.; Seal, S. Rare earth oxides as nanoadditives in 3-D nanocomposite scaffolds for bone regeneration. *J. Mater. Chem.* **2010**, *20*, 8912–8919. [[CrossRef](#)]
16. Yokel, R.A.; Hussain, S.; Garantziotis, S.; Demokritou, P.; Castranova, V.; Cassee, F.R. The yin: An adverse health perspective of nanoceria: Uptake, distribution, accumulation, and mechanisms of its toxicity. *Environ. Sci. Nano* **2014**, *1*, 406–428. [[CrossRef](#)]
17. Haugen, H.J.; Monjo, M.; Rubert, M.; Verket, A.; Lyngstadaas, S.P.; Ellingsen, J.E.; Rønold, H.J.; Wohlfahrt, J.C. Porous ceramic titanium dioxide scaffolds promote bone formation in rabbit peri-implant cortical defect model. *Acta Biomater.* **2013**, *9*, 5390–5399. [[CrossRef](#)] [[PubMed](#)]
18. Martin, P.; Leibovich, S.J. Inflammatory cells during wound repair: The good, the bad and the ugly. *Trends Cell Biol.* **2005**, *15*, 599–607. [[CrossRef](#)] [[PubMed](#)]

19. Fu, G.; Vary, P.S.; Lin, C.-T. Anatase TiO<sub>2</sub> Nanocomposites for Antimicrobial Coatings. *J. Phys. Chem. B* **2005**, *109*, 8889–8898. [[CrossRef](#)]
20. Kaviyarasu, K.; Geetha, N.; Kanimozhi, K.; Magdalane, C.M.; Sivaranjani, S.; Ayeshamariam, A.; Kennedy, J.; Maaza, M. In vitro cytotoxicity effect and antibacterial performance of human lung epithelial cells A549 activity of Zinc oxide doped TiO<sub>2</sub> nanocrystals: Investigation of bio-medical application by chemical method. *Mater. Sci. Eng. C* **2017**, *74*, 325–333. [[CrossRef](#)]
21. Hu, C.; Lan, Y.; Qu, J.; Hu, X.; Wang, A. Ag/AgBr/TiO<sub>2</sub> Visible Light Photocatalyst for Destruction of Azodyes and Bacteria. *J. Phys. Chem. B* **2006**, *110*, 4066–4072. [[CrossRef](#)]
22. Battin, T.J.; von der Kammer, F.; Weillhartner, A.; Ottofuelling, S.; Hofmann, T. Nanostructured TiO<sub>2</sub>: Transport Behavior and Effects on Aquatic Microbial Communities under Environmental Conditions. *Environ. Sci. Technol.* **2009**, *43*, 8098–8104. [[CrossRef](#)]
23. Jafari, S.; Mahyad, B.; Hashemzadeh, H.; Janfaza, S.; Gholikhani, T.; Tayebi, L. Biomedical Applications of TiO<sub>2</sub> Nanostructures: Recent Advances. *Int. J. Nanomed.* **2020**, *15*, 3447–3470. [[CrossRef](#)] [[PubMed](#)]
24. Friedrich, R.P.; Cicha, I.; Alexiou, C. Iron Oxide Nanoparticles in Regenerative Medicine and Tissue Engineering. *Nanomaterials* **2021**, *11*, 2337. [[CrossRef](#)] [[PubMed](#)]
25. Kumar, A.; Jena, P.K.; Behera, S.; Lockey, R.F.; Mohapatra, S.; Mohapatra, S. Multifunctional magnetic nanoparticles for targeted delivery. *Nanomed. Nanotechnol. Biol. Med.* **2010**, *6*, 64–69. [[CrossRef](#)] [[PubMed](#)]
26. Cicha, I.; Alexiou, C. Cardiovascular applications of magnetic particles. *J. Magn. Magn. Mater.* **2021**, *518*, 167428. [[CrossRef](#)]
27. Mathiasen, A.B.; Hansen, L.; Friis, T.; Thomsen, C.; Bhakoo, K.; Kastrop, J. Optimal Labeling Dose, Labeling Time, and Magnetic Resonance Imaging Detection Limits of Ultrasmall Superparamagnetic Iron-Oxide Nanoparticle Labeled Mesenchymal Stromal Cells. *Stem Cells Int.* **2013**, *2013*, 353105. [[CrossRef](#)]
28. Parashurama, N.; Ahn, B.-C.; Ziv, K.; Ito, K.; Paulmurugan, R.; Willmann, J.K.; Chung, J.; Ikeno, F.; Swanson, J.C.; Merk, D.R.; et al. Multimodality Molecular Imaging of Cardiac Cell Transplantation: Part II. In Vivo Imaging of Bone Marrow Stromal Cells in Swine with PET/CT and MR Imaging. *Radiology* **2016**, *280*, 826–836. [[CrossRef](#)]
29. Nejati, M.; Rostami, M.; Mirzaei, H.; Rahimi-Nasrabadi, M.; Vosoughifar, M.; Nasab, A.S.; Ganjali, M.R. Green methods for the preparation of MgO nanomaterials and their drug delivery, anti-cancer and anti-bacterial potentials: A review. *Inorg. Chem. Commun.* **2022**, *136*, 109107. [[CrossRef](#)]
30. Narender, S.S.; Varma, V.V.S.; Srikar, C.S.; Ruchitha, J.; Varma, P.A.; Praveen, B.V.S. Nickel Oxide Nanoparticles: A Brief Review of Their Synthesis, Characterization, and Applications. *Chem. Eng. Technol.* **2022**, *45*, 397–409. [[CrossRef](#)]
31. Alsharari, S.S.; Alenezi, M.A.; Al Tami, M.S.; Soliman, M. Recent advances in the Biosynthesis of Zirconium Oxide Nanoparticles and their Biological Applications. *Baghdad Sci. J.* **2022**, 41–57. [[CrossRef](#)]
32. Skheel, A.Z.; Jaduaa, M.H.; Abd, A.N. Green synthesis of cadmium oxide nanoparticles for biomedical applications (antibacterial, and anticancer activities). *Mater. Today Proc.* **2021**, *45*, 5793–5799. [[CrossRef](#)]
33. Gowri, S.; Gopinath, K.; Arumugam, A. Experimental and computational assessment of mycosynthesized CdO nanoparticles towards biomedical applications. *J. Photochem. Photobiol. B Biol.* **2018**, *180*, 166–174. [[CrossRef](#)]
34. Khorsand Zak, A.; Razali, R.; Abd Majid, W.H.; Darroudi, M. Synthesis and characterization of a narrow size distribution of zinc oxide nanoparticles. *Int. J. Nanomed.* **2011**, *6*, 1399. [[CrossRef](#)] [[PubMed](#)]
35. Hudlikar, M.; Joglekar, S.; Dhaygude, M.; Kodam, K. Latex-mediated synthesis of ZnS nanoparticles: Green synthesis approach. *J. Nanopart. Res.* **2012**, *14*, 865. [[CrossRef](#)]
36. Singhal, G.; Bhavesh, R.; Kasariya, K.; Sharma, A.R.; Singh, R.P. Biosynthesis of silver nanoparticles using *Ocimum sanctum* (Tulsi) leaf extract and screening its antimicrobial activity. *J. Nanopart. Res.* **2011**, *13*, 2981–2988. [[CrossRef](#)]
37. Mishra, P.K.; Mishra, H.; Ekielski, A.; Talegaonkar, S.; Vaidya, B. Zinc oxide nanoparticles: A promising nanomaterial for biomedical applications. *Drug Discov. Today* **2017**, *22*, 1825–1834. [[CrossRef](#)]
38. Mohanta, Y.K.; Nayak, D.; Mishra, A.K.; Chakrabartty, I.; Ray, M.K.; Mohanta, T.K.; Tayung, K.; Rajaganesh, R.; Vasanthakumaran, M.; Muthupandian, S.; et al. Green Synthesis of Endolichenic Fungi Functionalized Silver Nanoparticles: The Role in Antimicrobial, Anti-Cancer, and Mosquitocidal Activities. *Int. J. Mol. Sci.* **2022**, *23*, 10626. [[CrossRef](#)]
39. Srivastava, V.; Gusain, D.; Sharma, Y.C. Synthesis, characterization and application of zinc oxide nanoparticles (n-ZnO). *Ceram. Int.* **2013**, *39*, 9803–9808. [[CrossRef](#)]
40. Sharma, R.K.; Ghose, R. Synthesis of zinc oxide nanoparticles by homogeneous precipitation method and its application in antifungal activity against *Candida albicans*. *Ceram. Int.* **2015**, *41*, 967–975. [[CrossRef](#)]
41. Hayat, K.; Gondal, M.A.; Khaled, M.M.; Ahmed, S.; Shemsi, A.M. Nano ZnO synthesis by modified sol gel method and its application in heterogeneous photocatalytic removal of phenol from water. *Appl. Catal. A Gen.* **2011**, *393*, 122–129. [[CrossRef](#)]
42. Wang, Y.; Zhang, C.; Bi, S.; Luo, G. Preparation of ZnO nanoparticles using the direct precipitation method in a membrane dispersion micro-structured reactor. *Powder Technol.* **2010**, *202*, 130–136. [[CrossRef](#)]
43. Hijaz, M.; Das, S.; Mert, I.; Gupta, A.; Al-Wahab, Z.; Tebbe, C.; Dar, S.; Chhina, J.; Giri, S.; Munkarah, A.; et al. Folic acid tagged nanoceria as a novel therapeutic agent in ovarian cancer. *BMC Cancer* **2016**, *16*, 220. [[CrossRef](#)] [[PubMed](#)]
44. Li, H.; Liu, C.; Zeng, Y.-P.; Hao, Y.-H.; Huang, J.-W.; Yang, Z.-Y.; Li, R. Nanoceria-Mediated Drug Delivery for Targeted Photodynamic Therapy on Drug-Resistant Breast Cancer. *ACS Appl. Mater. Interfaces* **2016**, *8*, 31510–31523. [[CrossRef](#)] [[PubMed](#)]
45. Chang, H.-Y.; Chen, H.-I. Morphological evolution for CeO<sub>2</sub> nanoparticles synthesized by precipitation technique. *J. Cryst. Growth* **2005**, *283*, 457–468. [[CrossRef](#)]

46. Kundu, M.; Karunakaran, G.; Van Minh, N.; Kuznetsov, D. Improved Electrochemical Performance of Nanostructured Fe<sub>2</sub>O<sub>3</sub> Anode Synthesized by Chemical Precipitation Method for Lithium-ion Batteries. *J. Clust. Sci.* **2017**, *28*, 1285–1293. [[CrossRef](#)]
47. Nazari, M.; Ghasemi, N.; Maddah, H.; Motlagh, M.M. Synthesis and characterization of maghemite nanopowders by chemical precipitation method. *J. Nanostruct. Chem.* **2014**, *4*, 99–104. [[CrossRef](#)]
48. Carvalho, M.D.; Henriques, F.; Ferreira, L.P.; Godinho, M.; Cruz, M.M. Iron oxide nanoparticles: The Influence of synthesis method and size on composition and magnetic properties. *J. Solid State Chem.* **2013**, *201*, 144–152. [[CrossRef](#)]
49. Buraso, W.; Lachom, V.; Siriya, P.; Laokul, P. Synthesis of TiO<sub>2</sub> nanoparticles via a simple precipitation method and photocatalytic performance. *Mater. Res. Express* **2018**, *5*, 115003. [[CrossRef](#)]
50. Pilarska, A.; Pauksza, D.; Ciesielczyk, F.; Jesionowski, T. Physico-chemical and dispersive characterisation of magnesium oxides precipitated from the Mg(NO<sub>3</sub>)<sub>2</sub> and MgSO<sub>4</sub> solutions. *Pol. J. Chem. Technol.* **2010**, *12*, 52–56. [[CrossRef](#)]
51. Song, X.; Sun, S.; Zhang, D.; Wang, J.; Yu, J. Synthesis and characterization of magnesium hydroxide by batch reaction crystallization. *Front. Chem. Sci. Eng.* **2011**, *5*, 416–421. [[CrossRef](#)]
52. Bahadur, J.; Sen, D.; Mazumder, S.; Ramanathan, S. Effect of heat treatment on pore structure in nano-crystalline NiO: A small angle neutron scattering study. *J. Solid State Chem.* **2008**, *181*, 1227–1235. [[CrossRef](#)]
53. Sharma, H.; Kumar, K.; Choudhary, C.; Mishra, P.K.; Vaidya, B. Development and characterization of metal oxide nanoparticles for the delivery of anticancer drug. *Artif. Cells Nanomed. Biotechnol.* **2016**, *44*, 672–679. [[CrossRef](#)] [[PubMed](#)]
54. Karakoti, A.S.; Monteiro-Riviere, N.A.; Aggarwal, R.; Davis, J.P.; Narayan, R.J.; Self, W.T.; McGinnis, J.; Seal, S. Nanoceria as antioxidant: Synthesis and biomedical applications. *JOM* **2008**, *60*, 33–37. [[CrossRef](#)] [[PubMed](#)]
55. Wong, L.L.; Pye, Q.N.; Chen, L.; Seal, S.; McGinnis, J.F. Defining the Catalytic Activity of Nanoceria in the P23H-1 Rat, a Photoreceptor Degeneration Model. *PLoS ONE* **2015**, *10*, e0121977. [[CrossRef](#)] [[PubMed](#)]
56. Lassoued, A.; Dkhil, B.; Gadri, A.; Ammar, S. Control of the shape and size of iron oxide ( $\alpha$ -Fe<sub>2</sub>O<sub>3</sub>) nanoparticles synthesized through the chemical precipitation method. *Results Phys.* **2017**, *7*, 3007–3015. [[CrossRef](#)]
57. Sutradhar, N.; Sinhamahapatra, A.; Roy, B.; Bajaj, H.C.; Mukhopadhyay, I.; Panda, A.B. Preparation of MgO nano-rods with strong catalytic activity via hydrated basic magnesium carbonates. *Mater. Res. Bull.* **2011**, *46*, 2163–2167. [[CrossRef](#)]
58. Bahari Molla Mahaleh, Y.; Sadrnezhaad, S.K.; Hosseini, D. NiO Nanoparticles Synthesis by Chemical Precipitation and Effect of Applied Surfactant on Distribution of Particle Size. *J. Nanomater.* **2008**, *2008*, 470595. [[CrossRef](#)]
59. Krishnakanth, R.; Jayakumar, G.; Irudayaraj, A.A.; Raj, A.D. Structural and Magnetic Properties of NiO and Fe-doped NiO Nanoparticles Synthesized by Chemical Co-precipitation Method. *Mater. Today Proc.* **2016**, *3*, 1370–1377. [[CrossRef](#)]
60. Lang, J.; Wang, J.; Zhang, Q.; Li, X.; Han, Q.; Wei, M.; Sui, Y.; Wang, D.; Yang, J. Chemical precipitation synthesis and significant enhancement in photocatalytic activity of Ce-doped ZnO nanoparticles. *Ceram. Int.* **2016**, *42*, 14175–14181. [[CrossRef](#)]
61. Ranjithkumar, R.; Irudayaraj, A.A.; Jayakumar, G.; Raj, A.D.; Karthick, S.; Vinayagamorthy, R. Synthesis and Properties of CdO and Fe doped CdO Nanoparticles. *Mater. Today Proc.* **2016**, *3*, 1378–1382. [[CrossRef](#)]
62. Nasrullah, M.; Gul, F.Z.; Hanif, S.; Mannan, A.; Naz, S.; Ali, J.S.; Zia, M. Green and Chemical Syntheses of CdO NPs: A Comparative Study for Yield Attributes, Biological Characteristics, and Toxicity Concerns. *ACS Omega* **2020**, *5*, 5739–5747. [[CrossRef](#)]
63. Tang, Z.-X.; Lv, B.-F. MgO nanoparticles as antibacterial agent: Preparation and activity. *Braz. J. Chem. Eng.* **2014**, *31*, 591–601. [[CrossRef](#)]
64. Baruwati, B.; Kumar, D.K.; Manorama, S.V. Hydrothermal synthesis of highly crystalline ZnO nanoparticles: A competitive sensor for LPG and EtOH. *Sens. Actuators B Chem.* **2006**, *119*, 676–682. [[CrossRef](#)]
65. Ramimoghadam, D.; Bin Hussein, M.Z.; Taufiq-Yap, Y.H. Hydrothermal synthesis of zinc oxide nanoparticles using rice as soft biotemplate. *Chem. Cent. J.* **2013**, *7*, 136. [[CrossRef](#)] [[PubMed](#)]
66. Maria Magdalane, C.; Kaviyarasu, K.; Siddhardha, B.; Ramalingam, G. Synthesis and characterization of CeO<sub>2</sub> nanoparticles by hydrothermal method. *Mater. Today Proc.* **2021**, *36*, 130–132. [[CrossRef](#)]
67. Wang, F.; Qin, X.F.; Meng, Y.F.; Guo, Z.L.; Yang, L.X.; Ming, Y.F. Hydrothermal synthesis and characterization of  $\alpha$ -Fe<sub>2</sub>O<sub>3</sub> nanoparticles. *Mater. Sci. Semicond. Process.* **2013**, *16*, 802–806. [[CrossRef](#)]
68. Gomathi Thanga Keerthana, B.; Solaiyammal, T.; Muniyappan, S.; Murugakoothan, P. Hydrothermal synthesis and characterization of TiO<sub>2</sub> nanostructures prepared using different solvents. *Mater. Lett.* **2018**, *220*, 20–23. [[CrossRef](#)]
69. Huang, L.; Li, D.-Q.; Lin, Y.-J.; Wei, M.; Evans, D.G.; Duan, X. Controllable preparation of Nano-MgO and investigation of its bactericidal properties. *J. Inorg. Biochem.* **2005**, *99*, 986–993. [[CrossRef](#)]
70. Alfaro, A.; León, A.; Guajardo-Correa, E.; Reúquen, P.; Torres, F.; Mery, M.; Segura, R.; Zapata, P.A.; Orihuela, P.A. MgO nanoparticles coated with polyethylene glycol as carrier for 2-Methoxyestradiol anticancer drug. *PLoS ONE* **2019**, *14*, e0214900. [[CrossRef](#)]
71. Kumar, A.; Sanger, A.; Kumar, A.; Chandra, R. Single-step growth of pyramidally textured NiO nanostructures with improved supercapacitive properties. *Int. J. Hydrogen Energy* **2017**, *42*, 6080–6087. [[CrossRef](#)]
72. Cao, S.; Peng, L.; Han, T.; Liu, B.; Zhu, D.; Zhao, C.; Xu, J.; Tang, Y.; Wang, J.; He, S. Hydrothermal synthesis of nanoparticles-assembled NiO microspheres and their sensing properties. *Phys. E Low-Dimens. Syst. Nanostruct.* **2020**, *118*, 113655. [[CrossRef](#)]
73. Somasundaram, G.; Rajan, J.; Sangaiya, P.; Dilip, R. Hydrothermal synthesis of CdO nanoparticles for photocatalytic and antimicrobial activities. *Results Mater.* **2019**, *4*, 100044. [[CrossRef](#)]

74. Walton, R.I. Subcritical solvothermal synthesis of condensed inorganic materials. *Chem. Soc. Rev.* **2002**, *31*, 230–238. [[CrossRef](#)] [[PubMed](#)]
75. Razali, R.; Zak, A.K.; Majid, W.A.; Darroudi, M. Solvothermal synthesis of microsphere ZnO nanostructures in DEA media. *Ceram. Int.* **2011**, *37*, 3657–3663. [[CrossRef](#)]
76. Abdul Rashid, N.M.; Haw, C.; Chiu, W.; Khanis, N.H.; Rohaizad, A.; Khiew, P.; Abdul Rahman, S. Structural- and optical-properties analysis of single crystalline hematite ( $\alpha$ -Fe<sub>2</sub>O<sub>3</sub>) nanocubes prepared by one-pot hydrothermal approach. *CrystEngComm* **2016**, *18*, 4720–4732. [[CrossRef](#)]
77. Zhang, X.L.; Qiao, R.; Kim, J.C.; Kang, Y.S. Inorganic Cluster Synthesis and Characterization of Transition-Metal-Doped ZnO Hollow Spheres. *Cryst. Growth Des.* **2008**, *8*, 2609–2613. [[CrossRef](#)]
78. Chaianansutcharit, S.; Mekasuwandumrong, O.; Prasertdam, P. Effect of Organic Solvents on Iron Oxide Nanoparticles by the Solvothermal Method. *Cryst. Growth Des.* **2006**, *6*, 40–45. [[CrossRef](#)]
79. Kim, C.-S.; Moon, B.K.; Park, J.-H.; Choi, B.-C.; Seo, H.-J. Solvothermal synthesis of nanocrystalline TiO<sub>2</sub> in toluene with surfactant. *J. Cryst. Growth* **2003**, *257*, 309–315. [[CrossRef](#)]
80. Ghosh, M.; Biswas, K.; Sundaresan, A.; Rao, C.N.R. MnO and NiO nanoparticles: Synthesis and magnetic properties. *J. Mater. Chem.* **2006**, *16*, 106–111. [[CrossRef](#)]
81. Liu, J.; Sun, Z.; Deng, Y.; Zou, Y.; Li, C.; Guo, X.; Xiong, L.; Gao, Y.; Li, F.; Zhao, D. Highly Water-Dispersible Biocompatible Magnetite Particles with Low Cytotoxicity Stabilized by Citrate Groups. *Angew. Chem. Int. Ed.* **2009**, *48*, 5875–5879. [[CrossRef](#)]
82. Bokov, D.; Jalil, A.T.; Chupradit, S.; Suksatan, W.; Ansari, M.J.; Shewael, I.H.; Valiev, G.H.; Kianfar, E. Nanomaterial by Sol-Gel Method: Synthesis and Application. *Adv. Mater. Sci. Eng.* **2021**, *2021*, 5102014. [[CrossRef](#)]
83. Hasnidawani, J.N.; Azlina, H.N.; Norita, H.; Bonnia, N.N.; Ratim, S.; Ali, E.S. Synthesis of ZnO Nanostructures Using Sol-Gel Method. *Procedia Chem.* **2016**, *19*, 211–216. [[CrossRef](#)]
84. Raja, K.; Jaculine, M.M.; Jose, M.; Verma, S.; Prince, A.A.M.; Ilangovan, K.; Sethusankar, K.; Das, S.J. Sol-gel synthesis and characterization of  $\alpha$ -Fe<sub>2</sub>O<sub>3</sub> nanoparticles. *Superlattices Microstruct.* **2015**, *86*, 306–312. [[CrossRef](#)]
85. Wu, Y.; He, Y.; Wu, T.; Chen, T.; Weng, W.; Wan, H. Influence of some parameters on the synthesis of nanosized NiO material by modified sol-gel method. *Mater. Lett.* **2007**, *61*, 3174–3178. [[CrossRef](#)]
86. Thota, S.; Kumar, J. Sol-gel synthesis and anomalous magnetic behaviour of NiO nanoparticles. *J. Phys. Chem. Solids* **2007**, *68*, 1951–1964. [[CrossRef](#)]
87. Zahera, M.; Khan, S.A.; Khan, I.A.; Sharma, R.K.; Sinha, N.; Al-Shwaiman, H.A.; Al-Zahrani, R.R.; Elgorban, A.M.; Syed, A.; Khan, M.S. Cadmium oxide nanoparticles: An attractive candidate for novel therapeutic approaches. *Colloids Surf. A Physicochem. Eng. Asp.* **2020**, *585*, 124017. [[CrossRef](#)]
88. Wang, Z.; Zhang, H.; Zhang, L.; Yuan, J.; Yan, S.; Wang, C. Low-temperature synthesis of ZnO nanoparticles by solid-state pyrolytic reaction. *Nanotechnology* **2003**, *14*, 11–15. [[CrossRef](#)]
89. Nikam, A.V.; Prasad, B.L.V.; Kulkarni, A.A. Wet chemical synthesis of metal oxide nanoparticles: A review. *CrystEngComm* **2018**, *20*, 5091–5107. [[CrossRef](#)]
90. Mehra, S.; Bergerud, A.; Milliron, D.J.; Chan, E.M.; Salleo, A. Core/Shell Approach to Dopant Incorporation and Shape Control in Colloidal Zinc Oxide Nanorods. *Chem. Mater.* **2016**, *28*, 3454–3461. [[CrossRef](#)]
91. Park, J.; An, K.; Hwang, Y.; Park, J.-G.; Noh, H.-J.; Kim, J.-Y.; Park, J.-H.; Hwang, N.-M.; Hyeon, T. Ultra-large-scale syntheses of monodisperse nanocrystals. *Nat. Mater.* **2004**, *3*, 891–895. [[CrossRef](#)]
92. Song, H.-W.; Kim, N.-Y.; Park, J.-E.; Ko, J.-H.; Hickey, R.J.; Kim, Y.-H.; Park, S.-J. Shape-controlled syntheses of metal oxide nanoparticles by the introduction of rare-earth metals. *Nanoscale* **2017**, *9*, 2732–2738. [[CrossRef](#)]
93. Imagawa, H.; Suda, A.; Yamamura, K.; Sun, S. Monodisperse CeO<sub>2</sub> Nanoparticles and Their Oxygen Storage and Release Properties. *J. Phys. Chem. C* **2011**, *115*, 1740–1745. [[CrossRef](#)]
94. Deshmukh, S.M.; Tamboli, M.S.; Shaikh, H.; Babar, S.B.; Hiwarale, D.P.; Thate, A.G.; Shaikh, A.F.; Alam, M.A.; Khetre, S.M.; Bamane, S.R. A Facile Urea-Assisted Thermal Decomposition Process of TiO<sub>2</sub> Nanoparticles and Their Photocatalytic Activity. *Coatings* **2021**, *11*, 165. [[CrossRef](#)]
95. Mohandes, F.; Davar, F.; Salavati-Niasari, M. Magnesium oxide nanocrystals via thermal decomposition of magnesium oxalate. *J. Phys. Chem. Solids* **2010**, *71*, 1623–1628. [[CrossRef](#)]
96. Xiang, L.; Deng, X.Y.; Jin, Y. Experimental study on synthesis of NiO nano-particles. *Scr. Mater.* **2002**, *47*, 219–224. [[CrossRef](#)]
97. Qasem, M.A.A.; Aziz, M.A.; Qamaruddin, M.; Kim, J.-P.; Onaizi, S.A. Influence of Pamoic Acid as a Complexing Agent in the Thermal Preparation of NiO Nanoparticles: Application to Electrochemical Water Oxidation. *ChemistrySelect* **2018**, *3*, 573–580. [[CrossRef](#)]
98. Mohammadkish, M.; Hajisadeghi, H. Synthesis and growth mechanism of CdO nanoparticles prepared from thermal decomposition of CdSO<sub>3</sub> nanorods. *J. Mater. Sci. Mater. Electron.* **2016**, *27*, 6480–6487. [[CrossRef](#)]
99. Hu, X.; Gong, J.; Zhang, L.; Yu, J.C. Continuous Size Tuning of Monodisperse ZnO Colloidal Nanocrystal Clusters by a Microwave-Polyol Process and Their Application for Humidity Sensing. *Adv. Mater.* **2008**, *20*, 4845–4850. [[CrossRef](#)]
100. Soren, S.; Bessoi, M.; Parhi, P. A rapid microwave initiated polyol synthesis of cerium oxide nanoparticle using different cerium precursors. *Ceram. Int.* **2015**, *41*, 8114–8118. [[CrossRef](#)]
101. Wang, W.-W.; Zhu, Y.-J.; Ruan, M.-L. Microwave-assisted synthesis and magnetic property of magnetite and hematite nanoparticles. *J. Nanopart. Res.* **2007**, *9*, 419–426. [[CrossRef](#)]

102. Selvam, N.C.S.; Kumar, R.T.; Yogeenth, K.; Kennedy, L.J.; Sekaran, G.; Vijaya, J.J. Simple and rapid synthesis of Cadmium Oxide (CdO) nanospheres by a microwave-assisted combustion method. *Powder Technol.* **2011**, *211*, 250–255. [[CrossRef](#)]
103. Tohidian, Z.; Hashemi, S.; Boroujeni, K.P. Facile microwave-assisted synthesis of NiO nanoparticles and its effect on soybean (Glycine max). *IET Nanobiotechnol.* **2019**, *13*, 101–106. [[CrossRef](#)] [[PubMed](#)]
104. Dar, M.I.; Chandiran, A.K.; Grätzel, M.; Nazeeruddin, M.K.; Shivashankar, S.A. Controlled synthesis of TiO<sub>2</sub> nanoparticles and nanospheres using a microwave assisted approach for their application in dye-sensitized solar cells. *J. Mater. Chem. A* **2014**, *2*, 1662–1667. [[CrossRef](#)]
105. Wang, X.; Tian, J.; Fei, C.; Lv, L.; Wang, Y.; Cao, G. Rapid construction of TiO<sub>2</sub> aggregates using microwave assisted synthesis and its application for dye-sensitized solar cells. *RSC Adv.* **2015**, *5*, 8622–8629. [[CrossRef](#)]
106. Allahyar, S.; Taheri, M.; Abharya, A.; Mohammadi, K. Simple new synthesis of nickel oxide (NiO) in water using microwave irradiation. *J. Mater. Sci. Mater. Electron.* **2017**, *28*, 2846–2851. [[CrossRef](#)]
107. Hasanpoor, M.; Aliofkhaezrai, M.; Delavari, H. Microwave-assisted Synthesis of Zinc Oxide Nanoparticles. *Procedia Mater. Sci.* **2015**, *11*, 320–325. [[CrossRef](#)]
108. Cho, S.; Jung, S.-H.; Lee, K.-H. Morphology-Controlled Growth of ZnO Nanostructures Using Microwave Irradiation: From Basic to Complex Structures. *J. Phys. Chem. C* **2008**, *112*, 12769–12776. [[CrossRef](#)]
109. Sharma, D.; Sharma, S.; Kaith, B.S.; Rajput, J.; Kaur, M. Synthesis of ZnO nanoparticles using surfactant free in-air and microwave method. *Appl. Surf. Sci.* **2011**, *257*, 9661–9672. [[CrossRef](#)]
110. Seyedi, M.; Haratian, S.; Khaki, J.V. Mechanochemical Synthesis of Fe<sub>2</sub>O<sub>3</sub> Nanoparticles. *Procedia Mater. Sci.* **2015**, *11*, 309–313. [[CrossRef](#)]
111. Besenhard, M.O.; LaGrow, A.P.; Hodzic, A.; Kriechbaum, M.; Panariello, L.; Bais, G.; Loizou, K.; Damilos, S.; Cruz, M.M.; Thanh, N.T.K.; et al. Co-precipitation synthesis of stable iron oxide nanoparticles with NaOH: New insights and continuous production via flow chemistry. *Chem. Eng. J.* **2020**, *399*, 125740. [[CrossRef](#)]
112. Zhang, L.; Li, Y.; Zhang, Q.; Shi, G.; Wang, H. Fast Synthesis of Highly Dispersed Anatase TiO<sub>2</sub> Nanocrystals in a Microfluidic Reactor. *Chem. Lett.* **2011**, *40*, 1371–1373. [[CrossRef](#)]
113. Abou Hassan, A.; Sandre, O.; Cabuil, V.; Tabeling, P. Synthesis of iron oxide nanoparticles in a microfluidic device: Preliminary results in a coaxial flow millichannel. *Chem. Commun.* **2008**, *15*, 1783–1785. [[CrossRef](#)] [[PubMed](#)]
114. Gund, G.S.; Lokhande, C.D.; Park, H.S. Controlled synthesis of hierarchical nanoflake structure of NiO thin film for supercapacitor application. *J. Alloys Compd.* **2018**, *741*, 549–556. [[CrossRef](#)]
115. Cai, H.; Sun, B.; Chen, H.; Li, X.; Suo, H.; Zhao, C. Enhanced electrochemical glucose-sensing properties of NiO nanospheres modified with indium. *J. Mater. Sci.* **2017**, *52*, 11547–11553. [[CrossRef](#)]
116. Wei, Z.; Qiao, H.; Yang, H.; Zhang, C.; Yan, X. Characterization of NiO nanoparticles by anodic arc plasma method. *J. Alloys Compd.* **2009**, *479*, 855–858. [[CrossRef](#)]
117. Chouke, P.B.; Shrirame, T.; Potbhare, A.K.; Mondal, A.; Chaudhary, A.R.; Mondal, S.; Thakare, S.R.; Nepovimova, E.; Valis, M.; Kuca, K.; et al. Bioinspired metal/metal oxide nanoparticles: A road map to potential applications. *Mater. Today Adv.* **2022**, *16*, 100314. [[CrossRef](#)]
118. Cuong, H.N.; Pansambal, S.; Ghotekar, S.; Oza, R.; Hai, N.T.T.; Viet, N.M.; Nguyen, V.-H. New frontiers in the plant extract mediated biosynthesis of copper oxide (CuO) nanoparticles and their potential applications: A review. *Environ. Res.* **2022**, *203*, 111858. [[CrossRef](#)]
119. Pansambal, S.; Oza, R.; Borgave, S.; Chauhan, A.; Bardapurkar, P.; Vyas, S.; Ghotekar, S. Bioengineered cerium oxide (CeO<sub>2</sub>) nanoparticles and their diverse applications: A review. *Appl. Nanosci.* **2022**, 1–26. [[CrossRef](#)]
120. Jadoun, S.; Arif, R.; Jangid, N.K.; Meena, R.K. Green synthesis of nanoparticles using plant extracts: A review. *Environ. Chem. Lett.* **2021**, *19*, 355–374. [[CrossRef](#)]
121. Gade, A.K.; Bonde, P.; Ingle, A.P.; Marcato, P.D.; Durán, N.; Rai, M.K. Exploitation of *Aspergillus niger* for Synthesis of Silver Nanoparticles. *J. Biobased Mater. Bioenergy* **2008**, *2*, 243–247. [[CrossRef](#)]
122. Durán, N.; Marcato, P.D.; Alves, O.L.; de Souza, G.I.H.; Esposito, E. Mechanistic aspects of biosynthesis of silver nanoparticles by several *Fusarium oxysporum* strains. *J. Nanobiotechnol.* **2005**, *3*, 8. [[CrossRef](#)]
123. Mohammed, S.S.S.; Lawrance, A.V.; Sampath, S.; Sunderam, V.; Madhavan, Y. Facile green synthesis of silver nanoparticles from sprouted Zingiberaceae species: Spectral characterisation and its potential biological applications. *Mater. Technol.* **2022**, *37*, 533–546. [[CrossRef](#)]
124. Thakur, M.; Poojary, S.; Swain, N. Green Synthesis of Iron Oxide Nanoparticles and Its Biomedical Applications. In *Nanotechnology Applications in Health and Environmental Sciences*; Springer: Cham, Switzerland, 2021; pp. 83–109.
125. Lakshminarayanan, S.; Shereen, M.F.; Niraimathi, K.L.; Brindha, P.; Arumugam, A. One-pot green synthesis of iron oxide nanoparticles from *Bauhinia tomentosa*: Characterization and application towards synthesis of 1, 3 diolein. *Sci. Rep.* **2021**, *11*, 8643. [[CrossRef](#)] [[PubMed](#)]
126. Aravind, M.; Amalanathan, M.; Mary, M.S.M. Synthesis of TiO<sub>2</sub> nanoparticles by chemical and green synthesis methods and their multifaceted properties. *SN Appl. Sci.* **2021**, *3*, 409. [[CrossRef](#)]
127. Sun, Y.; Wang, S.; Zheng, J. Biosynthesis of TiO<sub>2</sub> nanoparticles and their application for treatment of brain injury—An in-vitro toxicity study towards central nervous system. *J. Photochem. Photobiol. B Biol.* **2019**, *194*, 1–5. [[CrossRef](#)] [[PubMed](#)]

128. Abinaya, S.; Kavitha, H.P.; Prakash, M.; Muthukrishnaraj, A. Green synthesis of magnesium oxide nanoparticles and its applications: A review. *Sustain. Chem. Pharm.* **2021**, *19*, 100368. [[CrossRef](#)]
129. Bouafia, A.; Laouini, S.E.; Ouahrani, M.R. A Review on Green Synthesis of CuO Nanoparticles using Plant Extract and Evaluation of Antimicrobial Activity. *Asian J. Res. Chem.* **2020**, *13*, 65. [[CrossRef](#)]
130. Lingaraju, K.; Naika, H.R.; Nagabhushana, H.; Jayanna, K.; Devaraja, S.; Nagaraju, G. Biosynthesis of Nickel oxide Nanoparticles from *Euphorbia heterophylla* (L.) and their biological application. *Arab. J. Chem.* **2020**, *13*, 4712–4719. [[CrossRef](#)]
131. Saraswathi, V.S.; Santhakumar, K. Photocatalytic activity against azo dye and cytotoxicity on MCF-7 cell lines of zirconium oxide nanoparticle mediated using leaves of *Lagerstroemia speciosa*. *J. Photochem. Photobiol. B Biol.* **2017**, *169*, 47–55. [[CrossRef](#)]
132. Vennila, R.; Kamaraj, P.; Arthanareeswari, M.; Sridharan, M.; Sudha, G.; Devikala, S.; Arockiaselvi, J.; Sivakumar, B.; Banu, A.H.; Rajeshwari, K. Biosynthesis of ZrO Nanoparticles And Its Natural Dye Sensitized Solar Cell Studies. *Mater. Today Proc.* **2018**, *5*, 8691–8698. [[CrossRef](#)]
133. van Tran, T.; Nguyen, D.T.C.; Kumar, P.S.; Din, A.T.M.; Jalil, A.A.; Vo, D.-V.N. Green synthesis of ZrO<sub>2</sub> nanoparticles and nanocomposites for biomedical and environmental applications: A review. *Environ. Chem. Lett.* **2022**, *20*, 1309–1331. [[CrossRef](#)]
134. Ghotekar, S. Green Synthesis of Fluorescent CdO Nanoparticles using *Leucaena leucocephala* L. Extract and their Biological Activities. *J. Bacteriol. Mycol. Open Access* **2017**, *5*, 00148. [[CrossRef](#)]
135. Lin, Y.-H.; Shen, L.-J.; Chou, T.-H.; Shih, Y.-H. Synthesis, Stability, and Cytotoxicity of Novel Cerium Oxide Nanoparticles for Biomedical Applications. *J. Clust. Sci.* **2021**, *32*, 405–413. [[CrossRef](#)]
136. Singh, K.R.; Nayak, V.; Sarkar, T.; Singh, R.P. Cerium oxide nanoparticles: Properties, biosynthesis and biomedical application. *RSC Adv.* **2020**, *10*, 27194–27214. [[CrossRef](#)]
137. Nelson, B.; Johnson, M.; Walker, M.; Riley, K.; Sims, C. Antioxidant Cerium Oxide Nanoparticles in Biology and Medicine. *Antioxidants* **2016**, *5*, 15. [[CrossRef](#)] [[PubMed](#)]
138. Ahmed, R.M.; Hasan, I. A review on properties and applications of TiO<sub>2</sub> and associated nanocomposite materials. *Mater. Today Proc.* **2021**. [[CrossRef](#)]
139. Chinthala, M.; Balakrishnan, A.; Venkataraman, P.; Gowtham, V.M.; Polagani, R.K. Synthesis and applications of nano-MgO and composites for medicine, energy, and environmental remediation: A review. *Environ. Chem. Lett.* **2021**, *19*, 4415–4454. [[CrossRef](#)]
140. Pilarska, A.A.; Klapiszewski, Ł.; Jesionowski, T. Recent development in the synthesis, modification and application of Mg(OH)<sub>2</sub> and MgO: A review. *Powder Technol.* **2017**, *319*, 373–407. [[CrossRef](#)]
141. Manyasree, D.; Peddi, K.M.; Ravikumar, R. CuO Nanoparticles: Synthesis, Characterization and Their Bactericidal Efficacy. *Int. J. Appl. Pharm.* **2017**, *9*, 71–74. [[CrossRef](#)]
142. Bonomo, M. Synthesis and characterization of NiO nanostructures: A review. *J. Nanopart. Res.* **2018**, *20*, 222. [[CrossRef](#)]
143. Mou, J.; Ren, Y.; Wang, J.; Wang, C.; Zou, Y.; Lou, K.; Zheng, Z.; Zhang, D. Nickel oxide nanoparticle synthesis and photocatalytic applications: Evolution from conventional methods to novel microfluidic approaches. *Microfluid. Nanofluid.* **2022**, *26*, 25. [[CrossRef](#)]
144. Ghotekar, S. A review on plant extract mediated biogenic synthesis of CdO nanoparticles and their recent applications. *Asian J. Green Chem.* **2019**, *3*, 187–200. [[CrossRef](#)]
145. Elsbahy, M.; Wooley, K.L. Design of polymeric nanoparticles for biomedical delivery applications. *Chem. Soc. Rev.* **2012**, *41*, 2545–2561. [[CrossRef](#)]
146. Ankamwar, B. Size and Shape Effect on Biomedical Applications of Nanomaterials. In *Biomedical Engineering—Technical Applications in Medicine*; InTech: London, UK, 2012.
147. Feng, Q.; Liu, Y.; Huang, J.; Chen, K.; Huang, J.; Xiao, K. Uptake, distribution, clearance, and toxicity of iron oxide nanoparticles with different sizes and coatings. *Sci. Rep.* **2018**, *8*, 2082. [[CrossRef](#)] [[PubMed](#)]
148. Andrade, R.G.D.; Veloso, S.R.S.; Castanheira, E.M.S. Shape Anisotropic Iron Oxide-Based Magnetic Nanoparticles: Synthesis and Biomedical Applications. *Int. J. Mol. Sci.* **2020**, *21*, 2455. [[CrossRef](#)] [[PubMed](#)]
149. Morones, J.R.; Elechiguerra, J.L.; Camacho, A.; Holt, K.; Kouri, J.B.; Ramírez, J.T.; Yacaman, M.J. The bactericidal effect of silver nanoparticles. *Nanotechnology* **2005**, *16*, 2346–2353. [[CrossRef](#)] [[PubMed](#)]
150. Utembe, W.; Potgieter, K.; Stefaniak, A.B.; Gulumian, M. Dissolution and biodurability: Important parameters needed for risk assessment of nanomaterials. *Part. Fibre Toxicol.* **2015**, *12*, 11. [[CrossRef](#)]
151. Michaelis, M.; Fischer, C.; Ciacchi, L.C.; Luttge, A. Variability of Zinc Oxide Dissolution Rates. *Environ. Sci. Technol.* **2017**, *51*, 4297–4305. [[CrossRef](#)]
152. He, H.; Cao, J.; Fei, X.; Duan, N. High-temperature annealing of ZnO nanoparticles increases the dissolution magnitude and rate in water by altering O vacancy distribution. *Environ. Int.* **2019**, *130*, 104930. [[CrossRef](#)]
153. He, Y.; Ingudam, S.; Reed, S.; Gehring, A.; Strobaugh, T.P.; Irwin, P. Study on the mechanism of antibacterial action of magnesium oxide nanoparticles against foodborne pathogens. *J. Nanobiotechnol.* **2016**, *14*, 54. [[CrossRef](#)]
154. Avramescu, M.-L.; Rasmussen, P.E.; Chénier, M.; Gardner, H.D. Influence of pH, particle size and crystal form on dissolution behaviour of engineered nanomaterials. *Environ. Sci. Pollut. Res.* **2017**, *24*, 1553–1564. [[CrossRef](#)]
155. Nikolova, M.P.; Chavali, M.S. Metal Oxide Nanoparticles as Biomedical Materials. *Biomimetics* **2020**, *5*, 27. [[CrossRef](#)] [[PubMed](#)]
156. Pham, B.T.T.; Colvin, E.K.; Pham, N.T.H.; Kim, B.J.; Fuller, E.S.; Moon, E.A.; Barbey, R.; Yuen, S.; Rickman, B.H.; Bryce, N.S.; et al. Biodistribution and Clearance of Stable Superparamagnetic Maghemite Iron Oxide Nanoparticles in Mice Following Intraperitoneal Administration. *Int. J. Mol. Sci.* **2018**, *19*, 205. [[CrossRef](#)]

157. Osaka, T.; Nakanishi, T.; Shanmugam, S.; Takahama, S.; Zhang, H. Effect of surface charge of magnetite nanoparticles on their internalization into breast cancer and umbilical vein endothelial cells. *Colloids Surf. B Biointerfaces* **2009**, *71*, 325–330. [[CrossRef](#)] [[PubMed](#)]
158. Augustine, R.; Mathew, A.P.; Sosnik, A. Metal Oxide Nanoparticles as Versatile Therapeutic Agents Modulating Cell Signaling Pathways: Linking Nanotechnology with Molecular Medicine. *Appl. Mater. Today* **2017**, *7*, 91–103. [[CrossRef](#)]
159. Schanen, B.C.; Das, S.; Reilly, C.M.; Warren, W.L.; Self, W.T.; Seal, S.; Drake, D.R. Immunomodulation and T Helper TH1/TH2 Response Polarization by CeO<sub>2</sub> and TiO<sub>2</sub> Nanoparticles. *PLoS ONE* **2013**, *8*, e62816. [[CrossRef](#)] [[PubMed](#)]
160. Lanone, S.; Rogerieux, F.; Geys, J.; Dupont, A.; Maillot-Marechal, E.; Boczkowski, J.; Lacroix, G.; Hoet, P. Comparative toxicity of 24 manufactured nanoparticles in human alveolar epithelial and macrophage cell lines. *Part. Fibre Toxicol.* **2009**, *6*, 14. [[CrossRef](#)] [[PubMed](#)]
161. Rambabu, D.; Mangili, V.; Kumbam, L.R.; Sagara, P.S.; Nakka, N.; Yogesh, M. Surface Coating and Functionalization of Metal and Metal Oxide Nanoparticles for Biomedical Applications. In *Metal Oxides for Biomedical and Biosensor Applications*; Elsevier: Amsterdam, The Netherlands, 2022; pp. 205–231.
162. Sun, S.-N.; Wei, C.; Zhu, Z.-Z.; Hou, Y.-L.; Venkatraman, S.S.; Xu, Z.-C. Magnetic iron oxide nanoparticles: Synthesis and surface coating techniques for biomedical applications. *Chin. Phys. B* **2014**, *23*, 037503. [[CrossRef](#)]
163. Arias, L.S.; Pessan, J.P.; Vieira, A.P.M.; de Lima, T.M.T.; Delbem, A.C.B.; Monteiro, D.R. Iron Oxide Nanoparticles for Biomedical Applications: A Perspective on Synthesis, Drugs, Antimicrobial Activity, and Toxicity. *Antibiotics* **2018**, *7*, 46. [[CrossRef](#)]
164. Raghu, S.N.V.; Onyenso, G.; Mohajernia, S.; Killian, M.S. Functionalization strategies to facilitate multi-depth, multi-molecule modifications of nanostructured oxides for triggered release applications. *Surf. Sci.* **2022**, *719*, 122024. [[CrossRef](#)]
165. Chaudhary, R.G.; Bhusari, G.S.; Tiple, A.D.; Rai, A.R.; Somkuvar, S.R.; Potbhare, A.K.; Lambat, T.L.; Ingle, P.P.; Abdala, A.A. Metal/Metal Oxide Nanoparticles: Toxicity, Applications, and Future Prospects. *Curr. Pharm. Des.* **2019**, *25*, 4013–4029. [[CrossRef](#)]
166. Soliman, M.G.; Pelaz, B.; Parak, W.J.; del Pino, P. Phase Transfer and Polymer Coating Methods toward Improving the Stability of Metallic Nanoparticles for Biological Applications. *Chem. Mater.* **2015**, *27*, 990–997. [[CrossRef](#)]
167. Aktan, M.K.; Coppola, G.A.; Van der Gucht, M.; Yoshioka, T.; Killian, M.S.; Lavigne, R.; Van der Eycken, E.; Steenackers, H.P.; Braem, A. Influence of polydopamine functionalization on the rapid protein immobilization by alternating current electrophoretic deposition. *Surf. Interfaces* **2022**, *34*, 102347. [[CrossRef](#)]
168. Sperling, R.A.; Parak, W.J. Surface modification, functionalization and bioconjugation of colloidal inorganic nanoparticles. *Philos. Trans. R. Soc. A Math. Phys. Eng. Sci.* **2010**, *368*, 1333–1383. [[CrossRef](#)]
169. Killian, M.S.; Schmuki, P. Influence of bioactive linker molecules on protein adsorption. *Surf. Interface Anal.* **2014**, *46*, 193–197. [[CrossRef](#)]
170. Farokhzad, O.C.; Karp, J.M.; Langer, R. Nanoparticle—Aptamer bioconjugates for cancer targeting. *Expert Opin. Drug Deliv.* **2006**, *3*, 311–324. [[CrossRef](#)] [[PubMed](#)]
171. Ahmad, F.; Salem-Bekhit, M.M.; Khan, F.; Alshehri, S.; Khan, A.; Ghoneim, M.M.; Wu, H.-F.; Taha, E.I.; Elbagory, I. Unique Properties of Surface-Functionalized Nanoparticles for Bio-Application: Functionalization Mechanisms and Importance in Application. *Nanomaterials* **2022**, *12*, 1333. [[CrossRef](#)]
172. Rajeshkumar, S.; Naik, P. Synthesis and biomedical applications of Cerium oxide nanoparticles—A Review. *Biotechnol. Rep.* **2018**, *17*, 1–5. [[CrossRef](#)]
173. Wu, S.; Weng, Z.; Liu, X.; Yeung, K.W.K.; Chu, P.K. Functionalized TiO<sub>2</sub> Based Nanomaterials for Biomedical Applications. *Adv. Funct. Mater.* **2014**, *24*, 5464–5481. [[CrossRef](#)]
174. Wintzheimer, S.; Genin, E.; Vellutini, L.; Le Bourdon, G.; Kessler, M.; Hackenberg, S.; Dembski, S.; Heuzé, K. Functionalisation of TiO<sub>2</sub> nanoparticles with a fluorescent organosilane: A synergy enabling their visualisation in biological cells and an enhanced photocatalytic activity. *Colloids Surf. B Biointerfaces* **2019**, *181*, 1019–1025. [[CrossRef](#)]
175. Fan, L.; Zhang, B.; Qiu, Z.; Dharanipragada, N.V.R.A.; Timmer, B.J.J.; Zhang, F.; Sheng, X.; Liu, T.; Meng, Q.; Inge, A.K.; et al. Molecular Functionalization of NiO Nanocatalyst for Enhanced Water Oxidation by Electronic Structure Engineering. *ChemSusChem* **2020**, *13*, 5901–5909. [[CrossRef](#)]
176. Ebnesajjad, S. Surface and Material Characterization Techniques. In *Surface Treatment of Materials for Adhesive Bonding*; William Andrew: Norwich, NY, USA, 2014; pp. 39–75. [[CrossRef](#)]
177. Chung, I.-M.; Rahuman, A.A.; Marimuthu, S.; Kirthi, A.V.; Anbarasan, K.; Rajakumar, G. An Investigation of the Cytotoxicity and Caspase-Mediated Apoptotic Effect of Green Synthesized Zinc Oxide Nanoparticles Using Eclipta prostrata on Human Liver Carcinoma Cells. *Nanomaterials* **2015**, *5*, 1317–1330. [[CrossRef](#)]
178. Wei, F.; Neal, C.J.; Sakthivel, T.S.; Kean, T.; Seal, S.; Coathup, M.J. Multi-functional cerium oxide nanoparticles regulate inflammation and enhance osteogenesis. *Mater. Sci. Eng. C* **2021**, *124*, 112041. [[CrossRef](#)]
179. Hirst, S.M.; Karakoti, A.S.; Tyler, R.D.; Sriranganathan, N.; Seal, S.; Reilly, C.M. Anti-inflammatory Properties of Cerium Oxide Nanoparticles. *Small* **2009**, *5*, 2848–2856. [[CrossRef](#)] [[PubMed](#)]
180. Balaji, S.; Mandal, B.K.; Vinod Kumar Reddy, L.; Sen, D. Biogenic Ceria Nanoparticles (CeO<sub>2</sub> NPs) for Effective Photocatalytic and Cytotoxic Activity. *Bioengineering* **2020**, *7*, 26. [[CrossRef](#)]
181. Rufus, A.; Sreeju, N.; Philip, D. Synthesis of biogenic hematite ( $\alpha$ -Fe<sub>2</sub>O<sub>3</sub>) nanoparticles for antibacterial and nanofluid applications. *RSC Adv.* **2016**, *6*, 94206–94217. [[CrossRef](#)]

182. Mallick, G.; Labh, J.; Giri, L.; Pandey, A.C.; Karna, S.P. Facile synthesis and electron transport properties of NiO nanostructures investigated by scanning tunneling microscopy. *AIP Adv.* **2017**, *7*, 085007. [[CrossRef](#)]
183. Al-Fakeh, M.S.; Alsaedi, R.O.; Amiri, N.; Allazzam, G.A. Synthesis, Characterization, and Antimicrobial of MnO and CdO Nanoparticles by Using a Calcination Method. *Coatings* **2022**, *12*, 215. [[CrossRef](#)]
184. El-Belely, E.F.; Farag, M.M.S.; Said, H.A.; Amin, A.S.; Azab, E.; Gobouri, A.A.; Fouda, A. Green Synthesis of Zinc Oxide Nanoparticles (ZnO-NPs) Using *Arthrospira platensis* (Class: Cyanophyceae) and Evaluation of their Biomedical Activities. *Nanomaterials* **2021**, *11*, 95. [[CrossRef](#)]
185. Miri, A.; Sarani, M. Biosynthesis, characterization and cytotoxic activity of CeO<sub>2</sub> nanoparticles. *Ceram. Int.* **2018**, *44*, 12642–12647. [[CrossRef](#)]
186. Singh, A.; Hussain, I.; Singh, N.B.; Singh, H. Uptake, translocation and impact of green synthesized nanoceria on growth and antioxidant enzymes activity of *Solanum lycopersicum* L. *Ecotoxicol. Environ. Saf.* **2019**, *182*, 109410. [[CrossRef](#)]
187. Zare, E.; Pourseyedi, S.; Khatami, M.; Darezereshki, E. Simple biosynthesis of zinc oxide nanoparticles using nature's source, and it's in vitro bio-activity. *J. Mol. Struct.* **2017**, *1146*, 96–103. [[CrossRef](#)]
188. Pugazhendhi, A.; Prabhu, R.; Muruganatham, K.; Shanmuganathan, R.; Natarajan, S. Anticancer, antimicrobial and photocatalytic activities of green synthesized magnesium oxide nanoparticles (MgONPs) using aqueous extract of *Sargassum wightii*. *J. Photochem. Photobiol. B Biol.* **2019**, *190*, 86–97. [[CrossRef](#)] [[PubMed](#)]
189. Younis, U.; Rahi, A.A.; Danish, S.; Ali, M.A.; Ahmed, N.; Datta, R.; Fahad, S.; Holatko, J.; Hammerschmidt, T.; Brtnicky, M.; et al. Fourier Transform Infrared Spectroscopy vibrational bands study of *Spinacia oleracea* and *Trigonella corniculata* under biochar amendment in naturally contaminated soil. *PLoS ONE* **2021**, *16*, e0253390. [[CrossRef](#)] [[PubMed](#)]
190. Fahelelbom, K.M.; Saleh, A.; Al-Tabakha, M.M.A.; Ashames, A.A. Recent applications of quantitative analytical FTIR spectroscopy in pharmaceutical, biomedical, and clinical fields: A brief review. *Rev. Anal. Chem.* **2022**, *41*, 21–33. [[CrossRef](#)]
191. Mahajan, R.; Suriyanarayanan, S.; Nicholls, I.A. Improved Solvothermal Synthesis of  $\gamma$ -Fe<sub>2</sub>O<sub>3</sub> Magnetic Nanoparticles for SiO<sub>2</sub> Coating. *Nanomaterials* **2021**, *11*, 1889. [[CrossRef](#)]
192. Sanchez Tobon, C.; Ljubas, D.; Mandić, V.; Panžić, I.; Matijašić, G.; Ćurković, L. Microwave-Assisted Synthesis of N/TiO<sub>2</sub> Nanoparticles for Photocatalysis under Different Irradiation Spectra. *Nanomaterials* **2022**, *12*, 1473. [[CrossRef](#)] [[PubMed](#)]
193. Fouda, A.; Awad, M.A.; Eid, A.M.; Saied, E.; Barghoth, M.G.; Hamza, M.F.; Awad, M.F.; Abdelbary, S.; Hassan, S.E.-D. An Eco-Friendly Approach to the Control of Pathogenic Microbes and *Anopheles stephensi* Malarial Vector Using Magnesium Oxide Nanoparticles (Mg-NPs) Fabricated by *Penicillium chrysogenum*. *Int. J. Mol. Sci.* **2021**, *22*, 5096. [[CrossRef](#)] [[PubMed](#)]
194. Greczynski, G.; Hultman, L. The same chemical state of carbon gives rise to two peaks in X-ray photoelectron spectroscopy. *Sci. Rep.* **2021**, *11*, 11195. [[CrossRef](#)] [[PubMed](#)]
195. Greczynski, G.; Hultman, L. Reliable determination of chemical state in x-ray photoelectron spectroscopy based on sample-work-function referencing to adventitious carbon: Resolving the myth of apparent constant binding energy of the C 1s peak. *Appl. Surf. Sci.* **2018**, *451*, 99–103. [[CrossRef](#)]
196. Biesinger, M.C. Accessing the robustness of adventitious carbon for charge referencing (correction) purposes in XPS analysis: Insights from a multi-user facility data review. *Appl. Surf. Sci.* **2022**, *597*, 153681. [[CrossRef](#)]
197. Greczynski, G.; Hultman, L. A step-by-step guide to perform X-ray photoelectron spectroscopy. *J. Appl. Phys.* **2022**, *132*, 011101. [[CrossRef](#)]
198. Alamdari, S.; Ghamsari, M.S.; Lee, C.; Han, W.; Park, H.-H.; Tafreshi, M.J.; Afarideh, H.; Ara, M.H.M. Preparation and Characterization of Zinc Oxide Nanoparticles Using Leaf Extract of *Sambucus ebulus*. *Appl. Sci.* **2020**, *10*, 3620. [[CrossRef](#)]
199. Bêche, E.; Charvin, P.; Perarnau, D.; Abanades, S.; Flamant, G. Ce 3d XPS investigation of cerium oxides and mixed cerium oxide (CexTiyOz). *Surf. Interface Anal.* **2008**, *40*, 264–267. [[CrossRef](#)]
200. Krill, G.; Kappler, J.-P.; Meyer, A.; Abadli, L.; Ravet, M.F. Surface and bulk properties of cerium atoms in several cerium intermetallic compounds: XPS and X-ray absorption measurements. *J. Phys. F Met. Phys.* **1981**, *11*, 1713–1725. [[CrossRef](#)]
201. Eslami, M.; Fedel, M.; Speranza, G.; Deflorian, F.; Zanella, C. Deposition and Characterization of Cerium-Based Conversion Coating on HPDC Low Si Content Aluminum Alloy. *J. Electrochem. Soc.* **2017**, *164*, C581–C590. [[CrossRef](#)]
202. Yamashita, T.; Hayes, P. Analysis of XPS spectra of Fe<sup>2+</sup> and Fe<sup>3+</sup> ions in oxide materials. *Appl. Surf. Sci.* **2008**, *254*, 2441–2449. [[CrossRef](#)]
203. Zhang, Y.; Li, L.; Ma, W.; Zhang, Y.; Yu, M.; Guo, J.; Lu, H.; Wang, C. Two-in-One Strategy for Effective Enrichment of Phosphopeptides Using Magnetic Mesoporous  $\gamma$ -Fe<sub>2</sub>O<sub>3</sub> Nanocrystal Clusters. *ACS Appl. Mater. Interfaces* **2013**, *5*, 614–621. [[CrossRef](#)] [[PubMed](#)]
204. Atuchin, V.V.; Kesler, V.G.; Pervukhina, N.V.; Zhang, Z. Ti 2p and O 1s core levels and chemical bonding in titanium-bearing oxides. *J. Electron. Spectrosc. Relat. Phenom.* **2006**, *152*, 18–24. [[CrossRef](#)]
205. Wanger, C.D.; Riggs, W.M.; Davis, L.E.; Moulder, J.F.; Muilenberg, G.E. *Handbook of X-ray Photoelectron Spectroscopy*; Perkin-Elmer Corp.: Eden Prairie, MN, USA, 1992; ISBN 9780964812413.
206. Le Febvrier, A.; Jensen, J.; Eklund, P. Wet-cleaning of MgO(001): Modification of surface chemistry and effects on thin film growth investigated by x-ray photoelectron spectroscopy and time-of-flight secondary ion mass spectroscopy. *J. Vac. Sci. Technol. A Vac. Surf. Films* **2017**, *35*, 021407. [[CrossRef](#)]
207. Biju, V. Ni 2p X-ray photoelectron spectroscopy study of nanostructured nickel oxide. *Mater. Res. Bull.* **2007**, *42*, 791–796. [[CrossRef](#)]

208. Jeejamol, D.J.; Raj, A.M.E.; Jayakumari, K.; Ravidhas, C. Optimization of CdO nanoparticles by Zr<sup>4+</sup> doping for better photocatalytic activity. *J. Mater. Sci. Mater. Electron.* **2018**, *29*, 97–116. [[CrossRef](#)]
209. Killian, M.S.; Seiler, S.; Wagener, V.; Hahn, R.; Ebensperger, C.; Meyer, B.; Schmuki, P. Interface Chemistry and Molecular Bonding of Functional Ethoxysilane-Based Self-Assembled Monolayers on Magnesium Surfaces. *ACS Appl. Mater. Interfaces* **2015**, *7*, 9006–9014. [[CrossRef](#)] [[PubMed](#)]
210. Tang, Y.; Rajendran, P.; Veeraraghavan, V.P.; Hussain, S.; Balakrishna, J.P.; Chinnathambi, A.; Alharbi, S.A.; Alahmadi, T.A.; Rengarajan, T.; Mohan, S.K. Osteogenic differentiation and mineralization potential of zinc oxide nanoparticles from *Scutellaria baicalensis* on human osteoblast-like MG-63 cells. *Mater. Sci. Eng. C* **2021**, *119*, 111656. [[CrossRef](#)] [[PubMed](#)]
211. Augustine, R. Skin bioprinting: A novel approach for creating artificial skin from synthetic and natural building blocks. *Prog. Biomater.* **2018**, *7*, 77–92. [[CrossRef](#)] [[PubMed](#)]
212. Augustine, R.; Dan, P.; Schlachet, I.; Rouxel, D.; Menu, P.; Sosnik, A. Chitosan ascorbate hydrogel improves water uptake capacity and cell adhesion of electrospun poly(epsilon-caprolactone) membranes. *Int. J. Pharm.* **2019**, *559*, 420–426. [[CrossRef](#)]
213. Lansdown, A.B.G.; Mirastschijski, U.; Stubbs, N.; Scanlon, E.; Ågren, M.S. Zinc in wound healing: Theoretical, experimental, and clinical aspects. *Wound Repair Regen.* **2007**, *15*, 2–16. [[CrossRef](#)]
214. Raguvaran, R.; Manuja, B.K.; Chopra, M.; Thakur, R.; Anand, T.; Kalia, A.; Manuja, A. Sodium alginate and gum acacia hydrogels of ZnO nanoparticles show wound healing effect on fibroblast cells. *Int. J. Biol. Macromol.* **2017**, *96*, 185–191. [[CrossRef](#)]
215. Chen, J.; Patil, S.; Seal, S.; McGinnis, J.F. Rare earth nanoparticles prevent retinal degeneration induced by intracellular peroxides. *Nat. Nanotechnol.* **2006**, *1*, 142–150. [[CrossRef](#)]
216. Davan, R.; Prasad, R.G.S.V.; Jakka, V.S.; Aparna, R.S.L.; Phani, A.R.; Jacob, B.; Salins, P.C.; Raju, D.B. Cerium Oxide Nanoparticles Promotes Wound Healing Activity in In-Vivo Animal Model. *J. Bionanosci.* **2012**, *6*, 78–83. [[CrossRef](#)]
217. Naseri-Nosar, M.; Farzamfar, S.; Sahrpeyma, H.; Ghorbani, S.; Bastami, F.; Vaez, A.; Salehi, M. Cerium oxide nanoparticle-containing poly(epsilon-caprolactone)/gelatin electrospun film as a potential wound dressing material: In vitro and in vivo evaluation. *Mater. Sci. Eng. C* **2017**, *81*, 366–372. [[CrossRef](#)]
218. Wu, H.; Li, F.; Wang, S.; Lu, J.; Li, J.; Du, Y.; Sun, X.; Chen, X.; Gao, J.; Ling, D. Ceria nanocrystals decorated mesoporous silica nanoparticle based ROS-scavenging tissue adhesive for highly efficient regenerative wound healing. *Biomaterials* **2018**, *151*, 66–77. [[CrossRef](#)] [[PubMed](#)]
219. Pai, B.G.; Kulkarni, A.V.; Jain, S. Study of smart antibacterial PCL-xFe<sub>3</sub>O<sub>4</sub> thin films using mouse NIH-3T3 fibroblast cells in vitro. *J. Biomed. Mater. Res. Part B Appl. Biomater.* **2019**, *105*, 795–804. [[CrossRef](#)] [[PubMed](#)]
220. Grumezescu, A.M.; Holban, A.M.; Andronescu, E.; Mogoşanu, G.D.; Vasile, B.S.; Chifiriuc, M.C.; Lazar, V.; Andrei, E.; Constantinescu, A.; Maniu, H. Anionic polymers and 10nm Fe<sub>3</sub>O<sub>4</sub>@UA wound dressings support human foetal stem cells normal development and exhibit great antimicrobial properties. *Int. J. Pharm.* **2014**, *463*, 146–154. [[CrossRef](#)]
221. Bunea, M.C.; Vasile, E.; Galateanu, B.; Hudita, A.; Serban, M.; Zaharia, C. Silk Fibroin Films Decorated with Magnetic Nanoparticles for Wound Healing Applications. *Mater. Plast.* **2017**, *54*, 83–87. [[CrossRef](#)]
222. Anghel, I.; Holban, A.M.; Grumezescu, A.M.; Andronescu, E.; Ficai, A.; Anghel, A.G.; Maganu, M.; Lazăr, V.; Chifiriuc, M.C. Modified wound dressing with phyto-nanostructured coating to prevent staphylococcal and pseudomonal biofilm development. *Nanoscale Res. Lett.* **2012**, *7*, 690. [[CrossRef](#)] [[PubMed](#)]
223. Wu, J.; Zhu, J.; Wu, Q.; An, Y.; Wang, K.; Xuan, T.; Zhang, J.; Song, W.; He, H.; Song, L.; et al. Mussel-Inspired Surface Immobilization of Heparin on Magnetic Nanoparticles for Enhanced Wound Repair via Sustained Release of a Growth Factor and M2 Macrophage Polarization. *ACS Appl. Mater. Interfaces* **2021**, *13*, 2230–2244. [[CrossRef](#)]
224. Li, X.; Wei, Z.; Zhang, W.; Lv, H.; Li, J.; Wu, L.; Zhang, H.; Yang, B.; Zhu, M.; Jiang, J. Anti-Inflammatory Effects of Magnetically Targeted Mesenchymal Stem Cells on Laser-Induced Skin Injuries in Rats. *Int. J. Nanomed.* **2020**, *15*, 5645–5659. [[CrossRef](#)]
225. Khader, A.; Arinzeh, T.L. Biodegradable zinc oxide composite scaffolds promote osteochondral differentiation of mesenchymal stem cells. *Biotechnol. Bioeng.* **2020**, *117*, 194–209. [[CrossRef](#)]
226. Garino, N.; Sanvitale, P.; Dumontel, B.; Laurenti, M.; Colilla, M.; Izquierdo-Barba, I.; Cauda, V.; Vallet-Regí, M. Zinc oxide nanocrystals as a nanoantibiotic and osteoinductive agent. *RSC Adv.* **2019**, *9*, 11312–11321. [[CrossRef](#)]
227. Zhou, G.; Gu, G.; Li, Y.; Zhang, Q.; Wang, W.; Wang, S.; Zhang, J. Effects of Cerium Oxide Nanoparticles on the Proliferation, Differentiation, and Mineralization Function of Primary Osteoblasts In Vitro. *Biol. Trace Elem. Res.* **2013**, *153*, 411–418. [[CrossRef](#)]
228. Yuan, K.; Mei, J.; Shao, D.; Zhou, F.; Qiao, H.; Liang, Y.; Li, K.; Tang, T. Cerium Oxide Nanoparticles Regulate Osteoclast Differentiation Bidirectionally by Modulating the Cellular Production of Reactive Oxygen Species. *Int. J. Nanomed.* **2020**, *15*, 6355–6372. [[CrossRef](#)] [[PubMed](#)]
229. Li, J.; Wen, J.; Li, B.; Li, W.; Qiao, W.; Shen, J.; Jin, W.; Jiang, X.; Yeung, K.W.K.; Chu, P.K. Valence State Manipulation of Cerium Oxide Nanoparticles on a Titanium Surface for Modulating Cell Fate and Bone Formation. *Adv. Sci.* **2018**, *5*, 1700678. [[CrossRef](#)] [[PubMed](#)]
230. Singh, R.K.; Patel, K.D.; Lee, J.H.; Lee, E.-J.; Kim, J.-H.; Kim, T.-H.; Kim, H.-W. Potential of Magnetic Nanofiber Scaffolds with Mechanical and Biological Properties Applicable for Bone Regeneration. *PLoS ONE* **2014**, *9*, e91584. [[CrossRef](#)] [[PubMed](#)]
231. Cojocar, F.D.; Balan, V.; Popa, M.I.; Lobiuc, A.; Antoniac, A.; Antoniac, I.V.; Verestiuc, L. Biopolymers—Calcium phosphates composites with inclusions of magnetic nanoparticles for bone tissue engineering. *Int. J. Biol. Macromol.* **2019**, *125*, 612–620. [[CrossRef](#)] [[PubMed](#)]

232. Lee, Y.-J.; Lee, S.-C.; Jee, S.C.; Sung, J.-S.; Kadam, A.A. Surface functionalization of halloysite nanotubes with supermagnetic iron oxide, chitosan and 2-D calcium-phosphate nanoflakes for synergistic osteoconduction enhancement of human adipose tissue-derived mesenchymal stem cells. *Colloids Surf. B Biointerfaces* **2019**, *173*, 18–26. [[CrossRef](#)]
233. Zeng, X.B.; Hu, H.; Xie, L.Q.; Lan, F.; Jiang, W.; Wu, Y.; Gu, Z.W. Magnetic responsive hydroxyapatite composite scaffolds construction for bone defect repair. *Int. J. Nanomed.* **2012**, *7*, 3365. [[CrossRef](#)]
234. Tanasa, E.; Zaharia, C.; Hudita, A.; Radu, I.-C.; Costache, M.; Galateanu, B. Impact of the magnetic field on 3T3-E1 preosteoblasts inside SMART silk fibroin-based scaffolds decorated with magnetic nanoparticles. *Mater. Sci. Eng. C* **2020**, *110*, 110714. [[CrossRef](#)]
235. Sung, H.; Ferlay, J.; Siegel, R.L.; Laversanne, M.; Soerjomataram, I.; Jemal, A.; Bray, F. Global Cancer Statistics 2020: GLOBOCAN Estimates of Incidence and Mortality Worldwide for 36 Cancers in 185 Countries. *CA Cancer J. Clin.* **2021**, *71*, 209–249. [[CrossRef](#)]
236. Arruebo, M.; Vilaboa, N.; Sáez-Gutierrez, B.; Lambea, J.; Tres, A.; Valladares, M.; González-Fernández, Á. Assessment of the Evolution of Cancer Treatment Therapies. *Cancers* **2011**, *3*, 3279–3330. [[CrossRef](#)]
237. Danhier, F.; Feron, O.; Pr at, V. To exploit the tumor microenvironment: Passive and active tumor targeting of nanocarriers for anti-cancer drug delivery. *J. Control. Release* **2010**, *148*, 135–146. [[CrossRef](#)]
238. Chandrasekaran, M.; Pandurangan, M. In Vitro Selective Anti-Proliferative Effect of Zinc Oxide Nanoparticles Against Co-Cultured C<sub>2</sub>C<sub>12</sub> Myoblastoma Cancer and 3T<sub>3</sub>-L1 Normal Cells. *Biol. Trace Elem. Res.* **2016**, *172*, 148–154. [[CrossRef](#)] [[PubMed](#)]
239. Wahab, R.; Kaushik, N.K.; Kaushik, N.; Choi, E.H.; Umar, A.; Dwivedi, S.; Musarrat, J.; Al-Khedhairi, A.A. ZnO Nanoparticles Induces Cell Death in Malignant Human T98G Gliomas, KB and Non-Malignant HEK Cells. *J. Biomed. Nanotechnol.* **2013**, *9*, 1181–1189. [[CrossRef](#)] [[PubMed](#)]
240. Premanathan, M.; Karthikeyan, K.; Jeyasubramanian, K.; Manivannan, G. Selective toxicity of ZnO nanoparticles toward Gram-positive bacteria and cancer cells by apoptosis through lipid peroxidation. *Nanomed. Nanotechnol. Biol. Med.* **2011**, *7*, 184–192. [[CrossRef](#)]
241. Pandurangan, M.; Enkhtaivan, G.; Kim, D.H. Anticancer studies of synthesized ZnO nanoparticles against human cervical carcinoma cells. *J. Photochem. Photobiol. B Biol.* **2016**, *158*, 206–211. [[CrossRef](#)] [[PubMed](#)]
242. Padmanabhan, A.; Kaushik, M.; Niranjana, R.; Richards, J.S.; Ebright, B.; Venkatasubbu, G.D. Zinc oxide nanoparticles induce oxidative and proteotoxic stress in ovarian cancer cells and trigger apoptosis independent of p53-mutation status. *Appl. Surf. Sci.* **2019**, *487*, 807–818. [[CrossRef](#)] [[PubMed](#)]
243. Majeed, S.; Danish, M.; Ismail, M.H.B.; Ansari, M.T.; Ibrahim, M.N.M. Anticancer and apoptotic activity of biologically synthesized zinc oxide nanoparticles against human colon cancer HCT-116 cell line- in vitro study. *Sustain. Chem. Pharm.* **2019**, *14*, 100179. [[CrossRef](#)]
244. Chakraborti, S.; Chakraborty, S.; Saha, S.; Manna, A.; Banerjee, S.; Adhikary, A.; Sarwar, S.; Hazra, T.K.; Das, T.; Chakrabarti, P. PEG-functionalized zinc oxide nanoparticles induce apoptosis in breast cancer cells through reactive oxygen species-dependent impairment of DNA damage repair enzyme NEIL2. *Free Radic. Biol. Med.* **2017**, *103*, 35–47. [[CrossRef](#)]
245. Rahman, H.S.; Azizi, S.; Namvar, F.; Mohamad, R.; Rasedee, A.; Soltani, M.; Rahim, R.A. Green synthesis, characterization, and anticancer activity of hyaluronan/zinc oxide nanocomposites. *OncoTargets Ther.* **2016**, *9*, 4549–4559. [[CrossRef](#)]
246. KC, B.; Paudel, S.N.; Rayamajhi, S.; Karna, D.; Adhikari, S.; Shrestha, B.G.; Bisht, G. Enhanced preferential cytotoxicity through surface modification: Synthesis, characterization and comparative in vitro evaluation of TritonX-100 modified and unmodified zinc oxide nanoparticles in human breast cancer cell (MDA-MB-231). *Chem. Cent. J.* **2016**, *10*, 16. [[CrossRef](#)]
247. Wu, H.; Zhang, J. Chitosan-based zinc oxide nanoparticle for enhanced anticancer effect in cervical cancer: A physicochemical and biological perspective. *Saudi Pharm. J.* **2018**, *26*, 205–210. [[CrossRef](#)]
248. Singh, T.A.; Das, J.; Sil, P.C. Zinc oxide nanoparticles: A comprehensive review on its synthesis, anticancer and drug delivery applications as well as health risks. *Adv. Colloid Interface Sci.* **2020**, *286*, 102317. [[CrossRef](#)]
249. Zhang, J.; Wu, D.; Li, M.-F.; Feng, J. Multifunctional Mesoporous Silica Nanoparticles Based on Charge-Reversal Plug-Gate Nanovalves and Acid-Decomposable ZnO Quantum Dots for Intracellular Drug Delivery. *ACS Appl. Mater. Interfaces* **2015**, *7*, 26666–26673. [[CrossRef](#)] [[PubMed](#)]
250. Cai, X.; Luo, Y.; Zhang, W.; Du, D.; Lin, Y. pH-Sensitive ZnO Quantum Dots–Doxorubicin Nanoparticles for Lung Cancer Targeted Drug Delivery. *ACS Appl. Mater. Interfaces* **2016**, *8*, 22442–22450. [[CrossRef](#)]
251. Wang, X.; Li, X.; Ito, A.; Sogo, Y.; Watanabe, Y.; Tsuji, N.M. Hollow ZnO Nanospheres Enhance Anticancer Immunity by Promoting CD4 + and CD8 + T Cell Populations In Vivo. *Small* **2017**, *13*, 1701816. [[CrossRef](#)] [[PubMed](#)]
252. Akbarian, M.; Mahjoub, S.; Elahi, S.M.; Zabihi, E.; Tashakkorian, H. Green synthesis, formulation and biological evaluation of a novel ZnO nanocarrier loaded with paclitaxel as drug delivery system on MCF-7 cell line. *Colloids Surf. B Biointerfaces* **2020**, *186*, 110686. [[CrossRef](#)] [[PubMed](#)]
253. Dhivya, R.; Ranjani, J.; Rajendhran, J.; Mayandi, J.; Annaraj, J. Enhancing the anti-gastric cancer activity of curcumin with biocompatible and pH sensitive PMMA-AA/ZnO nanoparticles. *Mater. Sci. Eng. C* **2018**, *82*, 182–189. [[CrossRef](#)]
254. Ezhuthupurakkal, P.B.; Ariraman, S.; Arumugam, S.; Subramanian, N.; Muthuvel, S.K.; Kumpati, P.; Rajamani, B.; Chinnasamy, T. Anticancer potential of ZnO nanoparticle-ferulic acid conjugate on Huh-7 and HepG2 cells and diethyl nitrosamine induced hepatocellular cancer on Wistar albino rat. *Nanomed. Nanotechnol. Biol. Med.* **2018**, *14*, 415–428. [[CrossRef](#)]
255. Abbasian, M.; Hasanzadeh, P.; Mahmoodzadeh, F.; Salehi, R. Novel cationic cellulose-based nanocomposites for targeted delivery of methotrexate to breast cancer cells. *J. Macromol. Sci. Part A* **2020**, *57*, 99–115. [[CrossRef](#)]

256. Hassan, H.F.H.; Mansour, A.M.; Abo-Youssef, A.M.H.; Elsadek, B.E.M.; Messiha, B.A.S. Zinc oxide nanoparticles as a novel anticancer approach; in vitro and in vivo evidence. *Clin. Exp. Pharmacol. Physiol.* **2017**, *44*, 235–243. [[CrossRef](#)]
257. DeLong, R.; Mitchell, J.; Morris, R.T.; Comer, J.; Hurst, M.; Ghosh, K.; Wanekaya, A.; Mudge, M.; Schaeffer, A.; Washington, L.; et al. Enzyme and Cancer Cell Selectivity of Nanoparticles: Inhibition of 3-D Metastatic Phenotype and Experimental Melanoma by Zinc Oxide. *J. Biomed. Nanotechnol.* **2017**, *13*, 221–231. [[CrossRef](#)]
258. Condello, M.; De Berardis, B.; Ammendolia, M.G.; Barone, F.; Condello, G.; Degan, P.; Meschini, S. ZnO nanoparticle tracking from uptake to genotoxic damage in human colon carcinoma cells. *Toxicol. Vitro.* **2016**, *35*, 169–179. [[CrossRef](#)]
259. Zijno, A.; De Angelis, I.; De Berardis, B.; Andreoli, C.; Russo, M.T.; Pietraforte, D.; Scorza, G.; Degan, P.; Ponti, J.; Rossi, F.; et al. Different mechanisms are involved in oxidative DNA damage and genotoxicity induction by ZnO and TiO<sub>2</sub> nanoparticles in human colon carcinoma cells. *Toxicol. Vitro.* **2015**, *29*, 1503–1512. [[CrossRef](#)] [[PubMed](#)]
260. Asik, M.R.; Gowdhami, B.; Jaabir, M.S.; Archunan, G.; Suganthi, N. Anticancer potential of zinc oxide nanoparticles against cervical carcinoma cells synthesized via biogenic route using aqueous extract of *Gracilaria edulis*. *Mater. Sci. Eng. C* **2019**, *103*, 109840. [[CrossRef](#)]
261. Baskar, G.; Chandhuru, J.; Sheraz Fahad, K.; Praveen, A.S.; Chamundeeswari, M.; Muthukumar, T. Anticancer activity of fungal l-asparaginase conjugated with zinc oxide nanoparticles. *J. Mater. Sci. Mater. Med.* **2015**, *26*, 43. [[CrossRef](#)]
262. Alarifi, S.; Ali, D.; Alkahtani, S.; Verma, A.; Ahamed, M.; Ahmed, M.; Alhadlaq, H.A. Induction of oxidative stress, DNA damage, and apoptosis in a malignant human skin melanoma cell line after exposure to zinc oxide nanoparticles. *Int. J. Nanomed.* **2013**, *8*, 983. [[CrossRef](#)]
263. Wu, B.; Wu, J.; Liu, S.; Shen, Z.; Chen, L.; Zhang, X.-X.; Ren, H.-Q. Combined effects of graphene oxide and zinc oxide nanoparticle on human A549 cells: Bioavailability, toxicity and mechanisms. *Environ. Sci. Nano* **2019**, *6*, 635–645. [[CrossRef](#)]
264. Bai, K.-J.; Chuang, K.-J.; Ma, C.-M.; Chang, T.-Y.; Chuang, H.-C. Human lung adenocarcinoma cells with an EGFR mutation are sensitive to non-autophagic cell death induced by zinc oxide and aluminium-doped zinc oxide nanoparticles. *J. Toxicol. Sci.* **2017**, *42*, 437–444. [[CrossRef](#)]
265. Generalov, R.; Kuan, W.B.; Chen, W.; Kristensen, S.; Juzenas, P. Radiosensitizing effect of zinc oxide and silica nanocomposites on cancer cells. *Colloids Surf. B Biointerfaces* **2015**, *129*, 79–86. [[CrossRef](#)]
266. Tripathy, N.; Ahmad, R.; Ko, H.A.; Khang, G.; Hahn, Y.-B. Enhanced anticancer potency using an acid-responsive ZnO-incorporated liposomal drug-delivery system. *Nanoscale* **2015**, *7*, 4088–4096. [[CrossRef](#)]
267. Guo, D.; Wu, C.; Jiang, H.; Li, Q.; Wang, X.; Chen, B. Synergistic cytotoxic effect of different sized ZnO nanoparticles and daunorubicin against leukemia cancer cells under UV irradiation. *J. Photochem. Photobiol. B Biol.* **2008**, *93*, 119–126. [[CrossRef](#)]
268. Yuan, L.; Wang, Y.; Wang, J.; Xiao, H.; Liu, X. Additive effect of zinc oxide nanoparticles and isoorientin on apoptosis in human hepatoma cell line. *Toxicol. Lett.* **2014**, *225*, 294–304. [[CrossRef](#)] [[PubMed](#)]
269. Fakhar-e-Alam, M.; Ali, S.M.U.; Ibupoto, Z.H.; Kimleang, K.; Atif, M.; Kashif, M.; Loong, F.K.; Hashim, U.; Willander, M. Sensitivity of A-549 human lung cancer cells to nanoporous zinc oxide conjugated with Photofrin. *Lasers Med. Sci.* **2012**, *27*, 607–614. [[CrossRef](#)] [[PubMed](#)]
270. Puvvada, N.; Rajput, S.; Kumar, B.N.P.; Sarkar, S.; Konar, S.; Brunt, K.R.; Rao, R.R.; Mazumdar, A.; Das, S.K.; Basu, R.; et al. Novel ZnO hollow-nanocarriers containing paclitaxel targeting folate-receptors in a malignant pH-microenvironment for effective monitoring and promoting breast tumor regression. *Sci. Rep.* **2015**, *5*, 11760. [[CrossRef](#)] [[PubMed](#)]
271. Hariharan, R.; Senthilkumar, S.; Suganthi, A.; Rajarajan, M. Synthesis and characterization of doxorubicin modified ZnO/PEG nanomaterials and its photodynamic action. *J. Photochem. Photobiol. B Biol.* **2012**, *116*, 56–65. [[CrossRef](#)]
272. Colon, J.; Hsieh, N.; Ferguson, A.; Kupelian, P.; Seal, S.; Jenkins, D.W.; Baker, C.H. Cerium oxide nanoparticles protect gastrointestinal epithelium from radiation-induced damage by reduction of reactive oxygen species and upregulation of superoxide dismutase 2. *Nanomed. Nanotechnol. Biol. Med.* **2010**, *6*, 698–705. [[CrossRef](#)]
273. Madero-Visbal, R.A.; Alvarado, B.E.; Colon, J.F.; Baker, C.H.; Wason, M.S.; Isley, B.; Seal, S.; Lee, C.M.; Das, S.; Mañón, R. Harnessing nanoparticles to improve toxicity after head and neck radiation. *Nanomed. Nanotechnol. Biol. Med.* **2012**, *8*, 1223–1231. [[CrossRef](#)]
274. Tarnuzzer, R.W.; Colon, J.; Patil, S.; Seal, S. Vacancy Engineered Ceria Nanostructures for Protection from Radiation-Induced Cellular Damage. *Nano Lett.* **2005**, *5*, 2573–2577. [[CrossRef](#)]
275. Colon, J.; Herrera, L.; Smith, J.; Patil, S.; Komanski, C.; Kupelian, P.; Seal, S.; Jenkins, D.W.; Baker, C.H. Protection from radiation-induced pneumonitis using cerium oxide nanoparticles. *Nanomed. Nanotechnol. Biol. Med.* **2009**, *5*, 225–231. [[CrossRef](#)]
276. Wason, M.S.; Colon, J.; Das, S.; Seal, S.; Turkson, J.; Zhao, J.; Baker, C.H. Sensitization of pancreatic cancer cells to radiation by cerium oxide nanoparticle-induced ROS production. *Nanomed. Nanotechnol. Biol. Med.* **2013**, *9*, 558–569. [[CrossRef](#)]
277. Cheng, G.; Guo, W.; Han, L.; Chen, E.; Kong, L.; Wang, L.; Ai, W.; Song, N.; Li, H.; Chen, H. Cerium oxide nanoparticles induce cytotoxicity in human hepatoma SMMC-7721 cells via oxidative stress and the activation of MAPK signaling pathways. *Toxicol. Vitro.* **2013**, *27*, 1082–1088. [[CrossRef](#)]
278. Singh, S.; Kumar, A.; Karakoti, A.; Seal, S.; Self, W.T. Unveiling the mechanism of uptake and sub-cellular distribution of cerium oxide nanoparticles. *Mol. Biosyst.* **2010**, *6*, 1813–1820. [[CrossRef](#)] [[PubMed](#)]
279. Alili, L.; Sack, M.; von Montfort, C.; Giri, S.; Das, S.; Carroll, K.S.; Zanger, K.; Seal, S.; Brenneisen, P. Downregulation of Tumor Growth and Invasion by Redox-Active Nanoparticles. *Antioxid. Redox Signal* **2013**, *19*, 765–778. [[CrossRef](#)] [[PubMed](#)]

280. Giri, S.; Karakoti, A.; Graham, R.P.; Maguire, J.L.; Reilly, C.M.; Seal, S.; Rattan, R.; Shridhar, V. Nanoceria: A Rare-Earth Nanoparticle as a Novel Anti-Angiogenic Therapeutic Agent in Ovarian Cancer. *PLoS ONE* **2013**, *8*, e54578. [[CrossRef](#)] [[PubMed](#)]
281. Wason, M.S.; Zhao, J. Cerium oxide nanoparticles: Potential applications for cancer and other diseases. *Am. J. Transl. Res.* **2013**, *5*, 126–131. [[PubMed](#)]
282. Lin, W.; Huang, Y.; Zhou, X.-D.; Ma, Y. Toxicity of Cerium Oxide Nanoparticles in Human Lung Cancer Cells. *Int. J. Toxicol.* **2006**, *25*, 451–457. [[CrossRef](#)]
283. Jana, S.K.; Banerjee, P.; Das, S.; Seal, S.; Chaudhury, K. Redox-active nanoceria depolarize mitochondrial membrane of human colon cancer cells. *J. Nanopart. Res.* **2014**, *16*, 2441. [[CrossRef](#)]
284. Renu, G.; Rani, V.V.D.; Nair, S.V.; Subramanian, K.R.V.; Lakshmanan, V.-K. Development of Cerium Oxide Nanoparticles and Its Cytotoxicity in Prostate Cancer Cells. *Adv. Sci. Lett.* **2012**, *6*, 17–25. [[CrossRef](#)]
285. Kumari, M.; Singh, S.P.; Chinde, S.; Rahman, M.F.; Mahboob, M.; Grover, P. Toxicity Study of Cerium Oxide Nanoparticles in Human Neuroblastoma Cells. *Int. J. Toxicol.* **2014**, *33*, 86–97. [[CrossRef](#)]
286. Nourmohammadi, E.; Khoshdel-Sarkarizi, H.; Nedaeinia, R.; Sadeghnia, H.R.; Hasanzadeh, L.; Darroudi, M.; Oskuee, R.K. Evaluation of anticancer effects of cerium oxide nanoparticles on mouse fibrosarcoma cell line. *J. Cell. Physiol.* **2019**, *234*, 4987–4996. [[CrossRef](#)]
287. Muhammad, F.; Wang, A.; Qi, W.; Zhang, S.; Zhu, G. Intracellular Antioxidants Dissolve Man-Made Antioxidant Nanoparticles: Using Redox Vulnerability of Nanoceria to Develop a Responsive Drug Delivery System. *ACS Appl. Mater. Interfaces* **2014**, *6*, 19424–19433. [[CrossRef](#)]
288. Das, J.; Choi, Y.-J.; Han, J.W.; Reza, A.M.M.T.; Kim, J.-H. Nanoceria-mediated delivery of doxorubicin enhances the anti-tumour efficiency in ovarian cancer cells via apoptosis. *Sci. Rep.* **2017**, *7*, 9513. [[CrossRef](#)] [[PubMed](#)]
289. Sulthana, S.; Banerjee, T.; Kallu, J.; Vuppala, S.R.; Heckert, B.; Naz, S.; Shelby, T.; Yambem, O.; Santra, S. Combination Therapy of NSCLC Using Hsp90 Inhibitor and Doxorubicin Carrying Functional Nanoceria. *Mol. Pharm.* **2017**, *14*, 875–884. [[CrossRef](#)] [[PubMed](#)]
290. Zhang, Y.; Wu, X.; Hou, C.; Shang, K.; Yang, K.; Tian, Z.; Pei, Z.; Qu, Y.; Pei, Y. Dual-responsive dithio-polydopamine coated porous CeO<sub>2</sub> nanorods for targeted and synergistic drug delivery. *Int. J. Nanomed.* **2018**, *13*, 2161–2173. [[CrossRef](#)] [[PubMed](#)]
291. Kalashnikova, I.; Mazar, J.; Neal, C.J.; Rosado, A.L.; Das, S.; Westmoreland, T.J.; Seal, S. Nanoparticle delivery of curcumin induces cellular hypoxia and ROS-mediated apoptosis via modulation of Bcl-2/Bax in human neuroblastoma. *Nanoscale* **2017**, *9*, 10375–10387. [[CrossRef](#)]
292. Xie, J.; Huang, J.; Li, X.; Sun, S.; Chen, X. Iron Oxide Nanoparticle Platform for Biomedical Applications. *Curr. Med. Chem.* **2009**, *16*, 1278–1294. [[CrossRef](#)] [[PubMed](#)]
293. Corot, C.; Robert, P.; Idée, J.-M.; Port, M. Recent advances in iron oxide nanocrystal technology for medical imaging. *Adv. Drug Deliv. Rev.* **2006**, *58*, 1471–1504. [[CrossRef](#)]
294. Indira, T.K.; Lakshmi, P.K. Magnetic Nanoparticles—A Review. *Int. J. Pharm. Sci. Nanotechnol.* **2010**, *3*, 1035–1042. [[CrossRef](#)]
295. Giustini, A.J.; Petryk, A.A.; Cassim, S.M.; Tate, J.A.; Baker, I.; Hoopes, P.J. Magnetic Nanoparticle Hyperthermia in Cancer Treatment. *Nano Life* **2010**, *1*, 17–32. [[CrossRef](#)]
296. Hilger, I.; Hiergeist, R.; Hergt, R.; Winnefeld, K.; Schubert, H.; Kaiser, W.A. Thermal Ablation of Tumors Using Magnetic Nanoparticles. *Investig. Radiol.* **2002**, *37*, 580–586. [[CrossRef](#)]
297. Xie, J.; Lee, S.; Chen, X. Nanoparticle-based theranostic agents. *Adv. Drug Deliv. Rev.* **2010**, *62*, 1064–1079. [[CrossRef](#)]
298. Zhu, L.; Zhou, Z.; Mao, H.; Yang, L. Magnetic nanoparticles for precision oncology: Theranostic magnetic iron oxide nanoparticles for image-guided and targeted cancer therapy. *Nanomedicine* **2017**, *12*, 73–87. [[CrossRef](#)] [[PubMed](#)]
299. Plichta, Z.; Horák, D.; Mareková, D.; Turnovcová, K.; Kaiser, R.; Jendelová, P. Poly [N-(2-hydroxypropyl)methacrylamide]-Modified Magnetic  $\gamma$ -Fe<sub>2</sub>O<sub>3</sub> Nanoparticles Conjugated with Doxorubicin for Glioblastoma Treatment. *ChemMedChem* **2020**, *15*, 96–104. [[CrossRef](#)] [[PubMed](#)]
300. Li, S.; Zhang, R.; Wang, D.; Feng, L.; Cui, K. Synthesis of hollow maghemite ( $\gamma$ -Fe<sub>2</sub>O<sub>3</sub>) particles for magnetic field and pH-responsive drug delivery and lung cancer treatment. *Ceram. Int.* **2021**, *47*, 7457–7464. [[CrossRef](#)]
301. Lungu, I.I.; Nistorescu, S.; Badea, M.A.; Petre, A.-M.; Udrea, A.-M.; Banici, A.-M.; Fleacă, C.; Andronesco, E.; Dinischiotu, A.; Dumitrache, F.; et al. Doxorubicin-Conjugated Iron Oxide Nanoparticles Synthesized by Laser Pyrolysis: In Vitro Study on Human Breast Cancer Cells. *Polymers* **2020**, *12*, 2799. [[CrossRef](#)]
302. Plichta, Z.; Kozak, Y.; Panchuk, R.; Sokolova, V.; Epple, M.; Kobylinska, L.; Jendelová, P.; Horák, D. Cytotoxicity of doxorubicin-conjugated poly[N-(2-hydroxypropyl)methacrylamide]-modified  $\gamma$ -Fe<sub>2</sub>O<sub>3</sub> nanoparticles towards human tumor cells. *Beilstein J. Nanotechnol.* **2018**, *9*, 2533–2545. [[CrossRef](#)] [[PubMed](#)]
303. Quan, Q.; Xie, J.; Gao, H.; Yang, M.; Zhang, F.; Liu, G.; Lin, X.; Wang, A.; Eden, H.S.; Lee, S.; et al. HSA Coated Iron Oxide Nanoparticles as Drug Delivery Vehicles for Cancer Therapy. *Mol. Pharm.* **2011**, *8*, 1669–1676. [[CrossRef](#)]
304. MubarakAli, D.; Manzoor, M.A.; Sabarinathan, A.; Devi, C.A.; Rekha, P.; Thajuddin, N.; Lee, S.-Y. An investigation of antibiofilm and cytotoxic property of MgO nanoparticles. *Biocatal. Agric. Biotechnol.* **2019**, *18*, 101069. [[CrossRef](#)]
305. Karthik, K.; Dhanuskodi, S.; Gobinath, C.; Prabukumar, S.; Sivaramakrishnan, S. Fabrication of MgO nanostructures and its efficient photocatalytic, antibacterial and anticancer performance. *J. Photochem. Photobiol. B Biol.* **2019**, *190*, 8–20. [[CrossRef](#)]
306. Mangalampalli, B.; Dumala, N.; Grover, P. Acute oral toxicity study of magnesium oxide nanoparticles and microparticles in female albino Wistar rats. *Regul. Toxicol. Pharmacol.* **2017**, *90*, 170–184. [[CrossRef](#)]

307. Blanco, E.; Shen, H.; Ferrari, M. Principles of nanoparticle design for overcoming biological barriers to drug delivery. *Nat. Biotechnol.* **2015**, *33*, 941–951. [[CrossRef](#)]
308. Yuan, W.; Li, Z.; Xie, X.; Zhang, Z.-Y.; Bian, L. Bisphosphonate-based nanocomposite hydrogels for biomedical applications. *Bioact. Mater.* **2020**, *5*, 819–831. [[CrossRef](#)] [[PubMed](#)]
309. Khalid, A.; Norello, R.; Abraham, A.N.; Tetienne, J.-P.; Karle, T.J.; Lui, E.W.C.; Xia, K.; Tran, P.A.; O'Connor, A.J.; Mann, B.G.; et al. Biocompatible and Biodegradable Magnesium Oxide Nanoparticles with In Vitro Photostable Near-Infrared Emission: Short-Term Fluorescent Markers. *Nanomaterials* **2019**, *9*, 1360. [[CrossRef](#)] [[PubMed](#)]
310. Busi, S.; Rajkumari, J. Microbially synthesized nanoparticles as next generation antimicrobials: Scope and applications. In *Nanoparticles in Pharmacotherapy*; William Andrew Publishing: Norwich, NY, USA, 2019; pp. 485–524.
311. Fahmy, H.; El-Hakin, M.; Nady, D.; Mostafa, Y.; Mohamed, F.; Yasien, A.; Moustafa, M.; Elmsery, B.; Yousef, H. Review on MgO nanoparticles multifunctional role in the biomedical field: Properties and applications. *Nanomed. J.* **2022**, *9*, 1–14. [[CrossRef](#)]
312. Letchumanan, D.; Sok, S.P.M.; Ibrahim, S.; Nagoor, N.H.; Arshad, N.M. Plant-Based Biosynthesis of Copper/Copper Oxide Nanoparticles: An Update on Their Applications in Biomedicine, Mechanisms, and Toxicity. *Biomolecules* **2021**, *11*, 564. [[CrossRef](#)]
313. Hu, Y.-P.; Wang, Y.; Zi, X.-Y.; Su, J.; Zhang, H.-X.; Zhang, X.-R.; Zhu, H.-Y.; Li, J.-X.; Yin, M.; Yang, F. Cuprous oxide nanoparticles selectively induce apoptosis of tumor cells. *Int. J. Nanomed.* **2012**, *7*, 2641. [[CrossRef](#)]
314. Siddiqui, M.A.; Alhadlaq, H.A.; Ahmad, J.; Al-Khedhairi, A.A.; Musarrat, J.; Ahamed, M. Copper Oxide Nanoparticles Induced Mitochondria Mediated Apoptosis in Human Hepatocarcinoma Cells. *PLoS ONE* **2013**, *8*, e69534. [[CrossRef](#)]
315. Wang, C.; Cao, S.; Tie, X.; Qiu, B.; Wu, A.; Zheng, Z. Induction of cytotoxicity by photoexcitation of TiO<sub>2</sub> can prolong survival in glioma-bearing mice. *Mol. Biol. Rep.* **2011**, *38*, 523–530. [[CrossRef](#)]
316. Zeni, P.F.; Dos Santos, D.P.; Canevarolo, R.R.; Yunes, J.A.; Padilha, F.F.; Júnior, R.L.C.D.A.; Egues, S.M.; Hernández-Macedo, M.L. Photocatalytic and Cytotoxic Effects of Nitrogen-Doped TiO<sub>2</sub> Nanoparticles on Melanoma Cells. *J. Nanosci. Nanotechnol.* **2018**, *18*, 3722–3728. [[CrossRef](#)]
317. Nešić, M.; Žakula, J.; Korićanac, L.; Stepić, M.; Radoičić, M.; Popović, I.; Šaponjić, Z.; Petković, M. Light controlled metallo-drug delivery system based on the TiO<sub>2</sub>-nanoparticles and Ru-complex. *J. Photochem. Photobiol. A Chem.* **2017**, *347*, 55–66. [[CrossRef](#)]
318. Hou, Z.; Zhang, Y.; Deng, K.; Chen, Y.; Li, X.; Deng, X.; Cheng, Z.; Lian, H.; Li, C.; Lin, J. UV-Emitting Upconversion-Based TiO<sub>2</sub> Photosensitizing Nanoplatform: Near-Infrared Light Mediated in Vivo Photodynamic Therapy via Mitochondria-Involved Apoptosis Pathway. *ACS Nano* **2015**, *9*, 2584–2599. [[CrossRef](#)]
319. Lucky, S.S.; Idris, N.M.; Li, Z.; Huang, K.; Soo, K.C.; Zhang, Y. Titania Coated Upconversion Nanoparticles for Near-Infrared Light Triggered Photodynamic Therapy. *ACS Nano* **2015**, *9*, 191–205. [[CrossRef](#)]
320. Venkatasubbu, G.D.; Ramasamy, S.; Reddy, G.P.; Kumar, J. In vitro and In vivo anticancer activity of surface modified paclitaxel attached hydroxyapatite and titanium dioxide nanoparticles. *Biomed. Microdevices* **2013**, *15*, 711–726. [[CrossRef](#)] [[PubMed](#)]
321. Liu, E.; Zhou, Y.; Liu, Z.; Li, J.; Zhang, D.; Chen, J.; Cai, Z. Cisplatin Loaded Hyaluronic Acid Modified TiO<sub>2</sub> Nanoparticles for Neoadjuvant Chemotherapy of Ovarian Cancer. *J. Nanomater.* **2015**, *2015*, 390358. [[CrossRef](#)]
322. Parodi, A.; Quattrocchi, N.; van de Ven, A.L.; Chiappini, C.; Evangelopoulos, M.; Martinez, J.O.; Brown, B.S.; Khaled, S.Z.; Yazdi, I.K.; Enzo, M.V.; et al. Synthetic nanoparticles functionalized with biomimetic leukocyte membranes possess cell-like functions. *Nat. Nanotechnol.* **2013**, *8*, 61–68. [[CrossRef](#)] [[PubMed](#)]
323. Delalat, B.; Sheppard, V.C.; Ghaemi, S.R.; Rao, S.; Prestidge, C.A.; McPhee, G.; Rogers, M.-L.; Donoghue, J.F.; Pillay, V.; Johns, T.G.; et al. Targeted drug delivery using genetically engineered diatom biosilica. *Nat. Commun.* **2015**, *6*, 8791. [[CrossRef](#)]
324. Decuzzi, P.; Godin, B.; Tanaka, T.; Lee, S.-Y.; Chiappini, C.; Liu, X.; Ferrari, M. Size and shape effects in the biodistribution of intravascularly injected particles. *J. Control. Release* **2010**, *141*, 320–327. [[CrossRef](#)]
325. Kafshgari, M.H.; Mazare, A.; Distaso, M.; Goldmann, W.H.; Peukert, W.; Fabry, B.; Schmuki, P. Intracellular Drug Delivery with Anodic Titanium Dioxide Nanotubes and Nanocylinders. *ACS Appl. Mater. Interfaces* **2019**, *11*, 14980–14985. [[CrossRef](#)]
326. Kafshgari, M.H.; Kah, D.; Mazare, A.; Nguyen, N.T.; Distaso, M.; Peukert, W.; Goldmann, W.H.; Schmuki, P.; Fabry, B. Anodic Titanium Dioxide Nanotubes for Magnetically Guided Therapeutic Delivery. *Sci. Rep.* **2019**, *9*, 14336. [[CrossRef](#)]
327. Abbasi, B.A.; Iqbal, J.; Mahmood, T.; Ahmad, R.; Kanwal, S.; Afridi, S. Plant-mediated synthesis of nickel oxide nanoparticles (NiO) via Geranium wallichianum: Characterization and different biological applications. *Mater. Res. Express* **2019**, *6*, 0850a7. [[CrossRef](#)]
328. Zhang, Y.; Mahdavi, B.; Mohammadhosseini, M.; Rezaei-Seresht, E.; Paydarfard, S.; Qorbani, M.; Karimian, M.; Abbasi, N.; Ghaneialvar, H.; Karimi, E. Green synthesis of NiO nanoparticles using Calendula officinalis extract: Chemical characterization, antioxidant, cytotoxicity, and anti-esophageal carcinoma properties. *Arab. J. Chem.* **2021**, *14*, 103105. [[CrossRef](#)]
329. Tabassum, N.; Kumar, D.; Verma, D.; Bohara, R.A.; Singh, M.P. Zirconium oxide (ZrO<sub>2</sub>) nanoparticles from antibacterial activity to cytotoxicity: A next-generation of multifunctional nanoparticles. *Mater. Today Commun.* **2021**, *26*, 102156. [[CrossRef](#)]
330. El Zowalaty, M.; Al-Fahdawi, M.Q.; Al-Qubaisi, M.S.; Alhassan, F.; Rosli, R.; Webster, T.J.; Naadja, S.-E.; Taufiq-Yap, Y.H.; Abdullah, R. Cytotoxicity and physicochemical characterization of iron-manganese-doped sulfated zirconia nanoparticles. *Int. J. Nanomed.* **2015**, *10*, 5739–5750. [[CrossRef](#)] [[PubMed](#)]
331. Balaji, S.; Mandal, B.K.; Ranjan, S.; Dasgupta, N.; Chidambaram, R. Nano-zirconia—Evaluation of its antioxidant and anticancer activity. *J. Photochem. Photobiol. B Biol.* **2017**, *170*, 125–133. [[CrossRef](#)] [[PubMed](#)]
332. Dizaj, S.M.; Lotfipour, F.; Barzegar-Jalali, M.; Zarrintan, M.H.; Adibkia, K. Antimicrobial activity of the metals and metal oxide nanoparticles. *Mater. Sci. Eng. C* **2014**, *44*, 278–284. [[CrossRef](#)]

333. Besinis, A.; De Peralta, T.; Handy, R.D. The antibacterial effects of silver, titanium dioxide and silica dioxide nanoparticles compared to the dental disinfectant chlorhexidine on *Streptococcus mutans* using a suite of bioassays. *Nanotoxicology* **2014**, *8*, 1–16. [[CrossRef](#)]
334. Webster, T.J.; Seil, J.T. Antimicrobial applications of nanotechnology: Methods and literature. *Int. J. Nanomed.* **2012**, *7*, 2767–2781. [[CrossRef](#)]
335. Khosro, A.; Mahmood, A.B.; Mohammad, B.J.; Gobad, M.; Mehdi, S.A. Evaluation and optimization of factors affecting novel diclofenac sodium-eudragit RS100 nanoparticles. *Afr. J. Pharm. Pharmacol.* **2012**, *6*, 941–947. [[CrossRef](#)]
336. Buzea, C.; Pacheco, I.I.; Robbie, K. Nanomaterials and nanoparticles: Sources and toxicity. *Biointerphases* **2007**, *2*, MR17–MR71. [[CrossRef](#)]
337. Pal, S.; Tak, Y.K.; Song, J.M. Does the Antibacterial Activity of Silver Nanoparticles Depend on the Shape of the Nanoparticle? A Study of the Gram-Negative Bacterium *Escherichia coli*. *Appl. Environ. Microbiol.* **2007**, *73*, 1712–1720. [[CrossRef](#)]
338. Egger, S.; Lehmann, R.P.; Height, M.J.; Loessner, M.J.; Schuppler, M. Antimicrobial Properties of a Novel Silver-Silica Nanocomposite Material. *Appl. Environ. Microbiol.* **2009**, *75*, 2973–2976. [[CrossRef](#)]
339. Yun, H.; Kim, J.D.; Choi, H.C.; Lee, C.W. Antibacterial Activity of CNT-Ag and GO-Ag Nanocomposites Against Gram-negative and Gram-positive Bacteria. *Bull. Korean Chem. Soc.* **2013**, *34*, 3261–3264. [[CrossRef](#)]
340. Iavicoli, I.; Fontana, L.; Leso, V.; Bergamaschi, A. The Effects of Nanomaterials as Endocrine Disruptors. *Int. J. Mol. Sci.* **2013**, *14*, 16732–16801. [[CrossRef](#)] [[PubMed](#)]
341. Pelletier, D.A.; Suresh, A.K.; Holton, G.A.; McKeown, C.K.; Wang, W.; Gu, B.; Mortensen, N.P.; Allison, D.P.; Joy, D.C.; Allison, M.R.; et al. Effects of Engineered Cerium Oxide Nanoparticles on Bacterial Growth and Viability. *Appl. Environ. Microbiol.* **2010**, *76*, 7981–7989. [[CrossRef](#)] [[PubMed](#)]
342. Ravishankar, T.N.; Ramakrishnappa, T.; Nagaraju, G.; Rajanaika, H. Synthesis and Characterization of CeO<sub>2</sub> Nanoparticles via Solution Combustion Method for Photocatalytic and Antibacterial Activity Studies. *ChemistryOpen* **2015**, *4*, 146–154. [[CrossRef](#)] [[PubMed](#)]
343. Azam, A.; Ahmed, A.S.; Oves, M.; Khan, M.; Memic, A. Size-dependent antimicrobial properties of CuO nanoparticles against Gram-positive and -negative bacterial strains. *Int. J. Nanomed.* **2012**, *7*, 3527–3535. [[CrossRef](#)]
344. Mahapatra, O.; Bhagat, M.; Gopalakrishnan, C.; Arunachalam, K.D. Ultrafine dispersed CuO nanoparticles and their antibacterial activity. *J. Exp. Nanosci.* **2008**, *3*, 185–193. [[CrossRef](#)]
345. Ahamed, M.; Alhadlaq, H.A.; Khan, M.A.M.; Karuppiyah, P.; Al-Dhabi, N.A. Synthesis, Characterization, and Antimicrobial Activity of Copper Oxide Nanoparticles. *J. Nanomater.* **2014**, *2014*, 637858. [[CrossRef](#)]
346. Jin, T.; He, Y. Antibacterial activities of magnesium oxide (MgO) nanoparticles against foodborne pathogens. *J. Nanopart. Res.* **2011**, *13*, 6877–6885. [[CrossRef](#)]
347. Vidic, J.; Stankic, S.; Haque, F.; Ciric, D.; Le Goffic, R.; Vidy, A.; Jupille, J.; Delmas, B. Selective antibacterial effects of mixed ZnMgO nanoparticles. *J. Nanopart. Res.* **2013**, *15*, 1595. [[CrossRef](#)]
348. Yamamoto, O.; Ohira, T.; Alvarez, K.; Fukuda, M. Antibacterial characteristics of CaCO<sub>3</sub>-MgO composites. *Mater. Sci. Eng. B* **2010**, *173*, 208–212. [[CrossRef](#)]
349. Allahverdiyev, A.M.; Abamor, E.S.; Bagirova, M.; Rafailovich, M. Antimicrobial effects of TiO<sub>2</sub> and Ag<sub>2</sub>O nanoparticles against drug-resistant bacteria and leishmania parasites. *Future Microbiol.* **2011**, *6*, 933–940. [[CrossRef](#)] [[PubMed](#)]
350. Haghighi, F.; Roudbar Mohammadi, S.; Mohammadi, P.; Hosseinkhani, S.; Shipour, R. Antifungal activity of TiO<sub>2</sub> nanoparticles and EDTA on *Candida albicans* biofilms. *Infect. Epidemiol. Microbiol.* **2013**, *1*, 33–38.
351. Roy, A.S.; Parveen, A.; Koppalkar, A.R.; Prasad, M.V.N.A. Effect of Nano-Titanium Dioxide with Different Antibiotics against Methicillin-Resistant *Staphylococcus Aureus*. *J. Biomater. Nanobiotechnol.* **2010**, *1*, 37–41. [[CrossRef](#)]
352. Carré, G.; Hamon, E.; Ennahar, S.; Estner, M.; Lett, M.-C.; Horvatovich, P.; Gies, J.-P.; Keller, V.; Keller, N.; Andre, P. TiO<sub>2</sub> Photocatalysis Damages Lipids and Proteins in *Escherichia coli*. *Appl. Environ. Microbiol.* **2014**, *80*, 2573–2581. [[CrossRef](#)]
353. Saraf, R. Cost effective and Monodispersed Zinc Oxide Nanoparticles Synthesis and their Characterization. *Int. J. Adv. Appl. Sci.* **2013**, *2*, 85–88. [[CrossRef](#)]
354. Azam, A.; Ahmed, A.S.; Oves, M.; Khan, M.S.; Habib, S.S.; Memic, A. Antimicrobial activity of metal oxide nanoparticles against Gram-positive and Gram-negative bacteria: A comparative study. *Int. J. Nanomed.* **2012**, *7*, 6003–6009. [[CrossRef](#)]
355. Ravishankar Rai, V.; Jamuna Bai, A. Nanoparticles and Their Potential Application as Antimicrobials. In *Science against Microbial Pathogens: Communicating Current Research and Technological Advances*; Formatex Research Center: Badajoz, Spain, 2011; pp. 197–209.
356. Fellahi, O.; Sarma, R.K.; Das, M.R.; Saikia, R.; Marcon, L.; Coffinier, Y.; Hadjersi, T.; Maamache, M.; Boukherroub, R. The antimicrobial effect of silicon nanowires decorated with silver and copper nanoparticles. *Nanotechnology* **2013**, *24*, 495101. [[CrossRef](#)]
357. Mohammadi, G.; Nokhodchi, A.; Barzegar-Jalali, M.; Lotfipour, F.; Adibkia, K.; Ehyaei, N.; Valizadeh, H. Physicochemical and anti-bacterial performance characterization of clarithromycin nanoparticles as colloidal drug delivery system. *Colloids Surf. B Biointerfaces* **2011**, *88*, 39–44. [[CrossRef](#)]
358. Dwivedi, S.; Siddiqui, M.A.; Farshori, N.N.; Ahamed, M.; Musarrat, J.; Al-Khedhairi, A.A. Synthesis, characterization and toxicological evaluation of iron oxide nanoparticles in human lung alveolar epithelial cells. *Colloids Surf. B Biointerfaces* **2014**, *122*, 209–215. [[CrossRef](#)]

359. Padmavathy, N.; Vijayaraghavan, R. Enhanced bioactivity of ZnO nanoparticles—An antimicrobial study. *Sci. Technol. Adv. Mater.* **2008**, *9*, 035004. [[CrossRef](#)]
360. Hosseinkhani, P.; Zand, A.M.; Imani, S.; Rezayi, M.; Rezaei, Z.S. Determining the antibacterial effect of ZnO nanoparticle against the pathogenic bacterium, *Shigella dysenteriae* (type 1). *Int. J. Nano Dimens.* **2011**, *1*, 279–285.
361. Zarrindokht, E.K.; Pegah, C. Antibacterial activity of ZnO nanoparticle on Gram-positive and Gram-negative bacteria. *Afr. J. Microbiol. Res.* **2012**, *5*, 1368–1373. [[CrossRef](#)]
362. Ghasemi, F.; Jalal, R. Antimicrobial action of zinc oxide nanoparticles in combination with ciprofloxacin and ceftazidime against multidrug-resistant *Acinetobacter baumannii*. *J. Glob. Antimicrob. Resist.* **2016**, *6*, 118–122. [[CrossRef](#)] [[PubMed](#)]
363. Sarwar, S.; Chakraborti, S.; Bera, S.; Sheikh, I.A.; Hoque, K.M.; Chakrabarti, P. The antimicrobial activity of ZnO nanoparticles against *Vibrio cholerae*: Variation in response depends on biotype. *Nanomed. Nanotechnol. Biol. Med.* **2016**, *12*, 1499–1509. [[CrossRef](#)]
364. Manzoor, U.; Siddique, S.; Ahmed, R.; Noreen, Z.; Bokhari, H.; Ahmad, I. Antibacterial, Structural and Optical Characterization of Mechano-Chemically Prepared ZnO Nanoparticles. *PLoS ONE* **2016**, *11*, e0154704. [[CrossRef](#)]
365. Jafari, A.R.; Mosavi, T.; Mosavari, N.; Majid, A.; Movahedzadeh, F.; Tebyaniyan, M.; Kamalzadeh, M.; Dehgan, M.; Jafari, S.; Arastoo, S. Mixed metal oxide nanoparticles inhibit growth of *Mycobacterium tuberculosis* into THP-1 cells. *Int. J. Mycobacteriol.* **2016**, *5*, S181–S183. [[CrossRef](#)]
366. Cioffi, N.; Rai, M. (Eds.) Nano-Antimicrobials. In *Synthesis and Characterization of Novel Nano Antimicrobials*; Springer: Berlin/Heidelberg, Germany, 2012.
367. Sawai, J.; Kojima, H.; Igarashi, H.; Hashimoto, A.; Shoji, S.; Sawaki, T.; Hakoda, A.; Kawada, E.; Kokugan, T.; Shimizu, M. Antibacterial characteristics of magnesium oxide powder. *World J. Microbiol. Biotechnol.* **2000**, *16*, 187–194. [[CrossRef](#)]
368. Sondi, I.; Salopek-Sondi, B. Silver nanoparticles as antimicrobial agent: A case study on *E. coli* as a model for Gram-negative bacteria. *J. Colloid Interface Sci.* **2004**, *275*, 177–182. [[CrossRef](#)]
369. Heckert, E.G.; Karakoti, A.S.; Seal, S.; Self, W.T. The role of cerium redox state in the SOD mimetic activity of nanoceria. *Biomaterials* **2008**, *29*, 2705–2709. [[CrossRef](#)]
370. Sener, G.; Hilton, S.A.; Osmond, M.J.; Zgheib, C.; Newsom, J.P.; Dewberry, L.; Singh, S.; Sakthivel, T.S.; Seal, S.; Liechty, K.W.; et al. Injectable, self-healable zwitterionic cryogels with sustained microRNA-cerium oxide nanoparticle release promote accelerated wound healing. *Acta Biomater.* **2020**, *101*, 262–272. [[CrossRef](#)]
371. Dewberry, L.K.; Zgheib, C.; Hilton, S.A.; Seal, S.; Newsom, J.; Krebs, M.D.; Hu, J.; Xu, J.; Liechty, K.W. Cerium Oxide Nanoparticle-miR146a Decreases Inflammation in a Murine Dextran Sodium Sulfate Colitis Model. *J. Am. Coll. Surg.* **2019**, *229*, S91. [[CrossRef](#)]
372. Gowri, S.; Gandhi, R.R.; Sundrarajan, M. Structural, Optical, Antibacterial and Antifungal Properties of Zirconia Nanoparticles by Biobased Protocol. *J. Mater. Sci. Technol.* **2014**, *30*, 782–790. [[CrossRef](#)]
373. Kumaresan, M.; Anand, K.V.; Govindaraju, K.; Tamilselvan, S.; Kumar, V.G. Seaweed *Sargassum wightii* mediated preparation of zirconia (ZrO<sub>2</sub>) nanoparticles and their antibacterial activity against gram positive and gram negative bacteria. *Microb. Pathog.* **2018**, *124*, 311–315. [[CrossRef](#)] [[PubMed](#)]
374. Ghomi, A.R.G.; Mohammadi-Khanaposhti, M.; Vahidi, H.; Kobarfard, F.; Reza, M.A.S.; Barabadi, H. Fungus-mediated extracellular biosynthesis and characterization of zirconium nanoparticles using standard penicillium species and their preliminary bactericidal potential: A novel biological approach to nanoparticle synthesis. *Iran. J. Pharm. Res. IJPR* **2019**, *18*, 2101–2110. [[CrossRef](#)]
375. Skheel, A.Z.; Jaduaa, M.H.; Abd, A.N. Biosynthesis of Cadmium Oxide Nanoparticles (CdO NPS) Using Aqueous Rhizome Extract of Curcuma for Biological Applications. In *AIP Conference Proceedings*; AIP Publishing LLC.: Melville, NY, USA, 2022; p. 020030.
376. Xu, C.; Qu, X. Cerium oxide nanoparticle: A remarkably versatile rare earth nanomaterial for biological applications. *NPG Asia Mater.* **2014**, *6*, e90. [[CrossRef](#)]
377. Applerot, G.; Lellouche, J.; Lipovsky, A.; Nitzan, Y.; Lubart, R.; Gedanken, A.; Banin, E. Understanding the Antibacterial Mechanism of CuO Nanoparticles: Revealing the Route of Induced Oxidative Stress. *Small* **2012**, *8*, 3326–3337. [[CrossRef](#)]
378. Gunawan, C.; Teoh, W.Y.; Marquis, C.P.; Amal, R. Cytotoxic Origin of Copper(II) Oxide Nanoparticles: Comparative Studies with Micron-Sized Particles, Leachate, and Metal Salts. *ACS Nano* **2011**, *5*, 7214–7225. [[CrossRef](#)]
379. Misra, S.K.; Nuseibeh, S.; Dybowska, A.; Berhanu, D.; Tetley, T.D.; Valsami-Jones, E. Comparative study using spheres, rods and spindle-shaped nanoplatelets on dispersion stability, dissolution and toxicity of CuO nanomaterials. *Nanotoxicology* **2014**, *8*, 422–432. [[CrossRef](#)] [[PubMed](#)]
380. Heinlaan, M.; Ivask, A.; Blinova, I.; Dubourguier, H.-C.; Kahru, A. Toxicity of nanosized and bulk ZnO, CuO and TiO<sub>2</sub> to bacteria *Vibrio fischeri* and crustaceans *Daphnia magna* and *Thamnocephalus platyurus*. *Chemosphere* **2008**, *71*, 1308–1316. [[CrossRef](#)]
381. Horie, M.; Fujita, K.; Kato, H.; Endoh, S.; Nishio, K.; Komaba, L.K.; Nakamura, A.; Miyauchi, A.; Kinugasa, S.; Hagihara, Y.; et al. Association of the physical and chemical properties and the cytotoxicity of metal oxide nanoparticles: Metal ion release, adsorption ability and specific surface area. *Metallomics* **2012**, *4*, 350–360. [[CrossRef](#)]
382. Leung, Y.H.; Chan, C.M.N.; Ng, A.M.C.; Chan, H.T.; Chiang, M.W.L.; Djurišić, A.B.; Ng, Y.H.; Jim, W.Y.; Guo, M.Y.; Leung, F.C.C.; et al. Antibacterial activity of ZnO nanoparticles with a modified surface under ambient illumination. *Nanotechnology* **2012**, *23*, 475703. [[CrossRef](#)] [[PubMed](#)]

383. Liu, Y.; He, L.; Mustapha, A.; Li, H.; Hu, Z.Q.; Lin, M. Antibacterial activities of zinc oxide nanoparticles against *Escherichia coli* O157:H7. *J. Appl. Microbiol.* **2009**, *107*, 1193–1201. [[CrossRef](#)] [[PubMed](#)]
384. Gogniat, G.; Thyssen, M.; Denis, M.; Pulgarin, C.; Dukan, S. The bactericidal effect of TiO<sub>2</sub> photocatalysis involves adsorption onto catalyst and the loss of membrane integrity. *FEMS Microbiol. Lett.* **2006**, *258*, 18–24. [[CrossRef](#)] [[PubMed](#)]
385. Karlsson, H.L.; Toprak, M.S.; Fadeel, B. Toxicity of Metal and Metal Oxide Nanoparticles. In *Handbook on the Toxicology of Metals*; Academic Press: Cambridge, MA, USA, 2022; pp. 87–126.
386. Wang, J.J.; Sanderson, B.J.S.; Wang, H. Cyto- and genotoxicity of ultrafine TiO<sub>2</sub> particles in cultured human lymphoblastoid cells. *Mutat. Res. Toxicol. Environ. Mutagen.* **2007**, *628*, 99–106. [[CrossRef](#)]
387. Kang, S.J.; Kim, B.M.; Lee, Y.J.; Chung, H.W. Titanium dioxide nanoparticles trigger p53-mediated damage response in peripheral blood lymphocytes. *Environ. Mol. Mutagen.* **2008**, *49*, 399–405. [[CrossRef](#)]
388. Falck, G.C.M.; Lindberg, H.K.; Suhonen, S.; Vippola, M.; Vanhala, E.; Catalán, J.; Savolainen, K.; Norppa, H. Genotoxic effects of nanosized and fine TiO<sub>2</sub>. *Hum. Exp. Toxicol.* **2009**, *28*, 339–352. [[CrossRef](#)]
389. Magdolenova, Z.; Bilaničová, D.; Pojana, G.; Fjellsbø, L.M.; Hudecova, A.; Hasplova, K.; Marcomini, A.; Dusinska, M. Impact of agglomeration and different dispersions of titanium dioxide nanoparticles on the human related in vitro cytotoxicity and genotoxicity. *J. Environ. Monit.* **2012**, *14*, 455–464. [[CrossRef](#)]
390. Akhal'tseva, L.V.; Moshkov, N.E.; Ingel', F.I.; Iurtseva, N.A.; Iurchenko, V.V. Effect of titanium dioxide nano- and microparticles on the values of the micronucleus test using human blood lymphocytes in culture. *Gig. Sanit.* **2011**, *5*, 61–63.
391. Dobrzyńska, M.M.; Gajowik, A.; Radzikowska, J.; Lankoff, A.; Dušínská, M.; Kruszewski, M. Genotoxicity of silver and titanium dioxide nanoparticles in bone marrow cells of rats in vivo. *Toxicology* **2014**, *315*, 86–91. [[CrossRef](#)]
392. Kao, Y.-Y.; Chen, Y.-C.; Cheng, T.-J.; Chiung, Y.-M.; Liu, P.-S. Zinc Oxide Nanoparticles Interfere With Zinc Ion Homeostasis to Cause Cytotoxicity. *Toxicol. Sci.* **2012**, *125*, 462–472. [[CrossRef](#)]
393. Sahu, D.; Kannan, G.M.; Vijayaraghavan, R.; Anand, T.; Khanum, F. Nanosized Zinc Oxide Induces Toxicity in Human Lung Cells. *ISRN Toxicol.* **2013**, *2013*, 316075. [[CrossRef](#)] [[PubMed](#)]
394. Huang, C.-C.; Aronstam, R.S.; Chen, D.-R.; Huang, Y.-W. Oxidative stress, calcium homeostasis, and altered gene expression in human lung epithelial cells exposed to ZnO nanoparticles. *Toxicol. Vitr.* **2010**, *24*, 45–55. [[CrossRef](#)] [[PubMed](#)]
395. Wu, W.; Samet, J.M.; Peden, D.B.; Bromberg, P.A. Phosphorylation of p65 Is Required for Zinc Oxide Nanoparticle-Induced Interleukin 8 Expression in Human Bronchial Epithelial Cells. *Environ. Health Perspect.* **2010**, *118*, 982–987. [[CrossRef](#)] [[PubMed](#)]
396. Ng, K.W.; Khoo, S.P.K.; Heng, B.C.; Setyawati, M.I.; Tan, E.C.; Zhao, X.; Xiong, S.; Fang, W.; Leong, D.T.; Loo, J.S.C. The role of the tumor suppressor p53 pathway in the cellular DNA damage response to zinc oxide nanoparticles. *Biomaterials* **2011**, *32*, 8218–8225. [[CrossRef](#)] [[PubMed](#)]
397. George, S.; Pokhrel, S.; Xia, T.; Gilbert, B.; Ji, Z.; Schowalter, M.; Rosenauer, A.; Damoiseaux, R.; Bradley, K.A.; Mädler, L.; et al. Use of a Rapid Cytotoxicity Screening Approach To Engineer a Safer Zinc Oxide Nanoparticle through Iron Doping. *ACS Nano* **2010**, *4*, 15–29. [[CrossRef](#)]
398. Hanley, C.; Thurber, A.; Hanna, C.; Punnoose, A.; Zhang, J.; Wingett, D.G. The Influences of Cell Type and ZnO Nanoparticle Size on Immune Cell Cytotoxicity and Cytokine Induction. *Nanoscale Res. Lett.* **2009**, *4*, 1409–1420. [[CrossRef](#)]
399. Park, E.-J.; Choi, J.; Park, Y.-K.; Park, K. Oxidative stress induced by cerium oxide nanoparticles in cultured BEAS-2B cells. *Toxicology* **2008**, *245*, 90–100. [[CrossRef](#)]
400. Hussain, S.; Al-Nsour, F.; Rice, A.B.; Marshburn, J.; Yingling, B.; Ji, Z.; Zink, J.I.; Walker, N.J.; Garantziotis, S. Cerium Dioxide Nanoparticles Induce Apoptosis and Autophagy in Human Peripheral Blood Monocytes. *ACS Nano* **2012**, *6*, 5820–5829. [[CrossRef](#)]
401. Mahmoudi, M.; Sant, S.; Wang, B.; Laurent, S.; Sen, T. Superparamagnetic iron oxide nanoparticles (SPIONs): Development, surface modification and applications in chemotherapy. *Adv. Drug Deliv. Rev.* **2011**, *63*, 24–46. [[CrossRef](#)]
402. Yang, W.J.; Lee, J.H.; Hong, S.C.; Lee, J.; Lee, J.; Han, D.-W. Difference between Toxicities of Iron Oxide Magnetic Nanoparticles with Various Surface-Functional Groups against Human Normal Fibroblasts and Fibrosarcoma Cells. *Materials* **2013**, *6*, 4689–4706. [[CrossRef](#)]
403. Sarkar, A.; Sil, P.C. Iron oxide nanoparticles mediated cytotoxicity via PI3K/AKT pathway: Role of quercetin. *Food Chem. Toxicol.* **2014**, *71*, 106–115. [[CrossRef](#)] [[PubMed](#)]
404. Naqvi, S.; Samim, M.; Abdin, M.Z.; Ahmed, F.J.; Maitra, A.N.; Prashant, C.K.; Dinda, A.K. Concentration-dependent toxicity of iron oxide nanoparticles mediated by increased oxidative stress. *Int. J. Nanomed.* **2010**, *5*, 983. [[CrossRef](#)]
405. Ma, J.Y.; Zhao, H.; Mercer, R.R.; Barger, M.; Rao, M.; Meighan, T.; Schwegler-Berry, D.; Castranova, V.; Ma, J.K. Cerium oxide nanoparticle-induced pulmonary inflammation and alveolar macrophage functional change in rats. *Nanotoxicology* **2011**, *5*, 312–325. [[CrossRef](#)]
406. Ma, J.Y.; Mercer, R.R.; Barger, M.; Schwegler-Berry, D.; Scabilloni, J.; Ma, J.K.; Castranova, V. Induction of pulmonary fibrosis by cerium oxide nanoparticles. *Toxicol. Appl. Pharmacol.* **2012**, *262*, 255–264. [[CrossRef](#)]
407. Donaldson, K.; Brown, D.M.; Clouter, A.; Duffin, R.; MacNee, W.; Renwick, L.; Tran, L.; Stone, V. The Pulmonary Toxicology of Ultrafine Particles. *J. Aerosol Med.* **2002**, *15*, 213–220. [[CrossRef](#)]
408. Renwick, L.C.; Brown, D.; Clouter, A.; Donaldson, K. Increased inflammation and altered macrophage chemotactic responses caused by two ultrafine particle types. *Occup. Environ. Med.* **2004**, *61*, 442–447. [[CrossRef](#)]
409. Trouiller, B.; Reliene, R.; Westbrook, A.; Solaimani, P.; Schiestl, R.H. Titanium Dioxide Nanoparticles Induce DNA Damage and Genetic Instability In vivo in Mice. *Cancer Res.* **2009**, *69*, 8784–8789. [[CrossRef](#)]

410. Sycheva, L.P.; Zhurkov, V.S.; Iurchenko, V.V.; Daugel-Dauge, N.O.; Kovalenko, M.A.; Krivtsova, E.K.; Durnev, A.D. Investigation of genotoxic and cytotoxic effects of micro- and nanosized titanium dioxide in six organs of mice in vivo. *Mutat. Res. Toxicol. Environ. Mutagen.* **2011**, *726*, 8–14. [[CrossRef](#)]
411. Lindberg, H.K.; Falck, G.C.-M.; Catalán, J.; Koivisto, A.J.; Suhonen, S.; Järventausta, H.; Rossi, E.M.; Nykäsenoja, H.; Peltonen, Y.; Moreno, C.; et al. Genotoxicity of inhaled nanosized TiO<sub>2</sub> in mice. *Mutat. Res. Toxicol. Environ. Mutagen.* **2012**, *745*, 58–64. [[CrossRef](#)]
412. Cho, W.-S.; Duffin, R.; Howie, S.E.; Scotton, C.J.; Wallace, W.A.; MacNee, W.; Bradley, M.; Megson, I.L.; Donaldson, K. Progressive severe lung injury by zinc oxide nanoparticles; the role of Zn<sup>2+</sup> dissolution inside lysosomes. *Part. Fibre Toxicol.* **2011**, *8*, 27. [[CrossRef](#)]
413. Yang, Z.; Han, D.; Tian, Y.; Zhang, T.; Ren, G. Nano-zinc oxide damages spatial cognition capability via over-enhanced long-term potentiation in hippocampus of Wistar rats. *Int. J. Nanomed.* **2011**, *6*, 1453–1461. [[CrossRef](#)]
414. Elshama, S.S.; El-Kenawy, A.E.M.; Osman, H.E.H. Histopathological study of zinc oxide nanoparticle-induced neurotoxicity in rats. *Curr. Top. Toxicol.* **2017**, *13*, 95–103.
415. Li, C.-H.; Shen, C.-C.; Cheng, Y.-W.; Huang, S.-H.; Wu, C.-C.; Kao, C.-C.; Liao, J.-W.; Kang, J.-J. Organ biodistribution, clearance, and genotoxicity of orally administered zinc oxide nanoparticles in mice. *Nanotoxicology* **2012**, *6*, 746–756. [[CrossRef](#)]
416. Saman, S.; Moradhaseli, S.; Shokouhian, A.; Ghorbani, M. Histopathological Effects of ZnO Nanoparticles on Liver and Heart Tissues in Wistar Rats. *Adv. Biores.* **2013**, *4*, 83–88.
417. Esmaeillou, M.; Moharamnejad, M.; Hsankhani, R.; Tehrani, A.A.; Maadi, H. Toxicity of ZnO nanoparticles in healthy adult mice. *Environ. Toxicol. Pharmacol.* **2013**, *35*, 67–71. [[CrossRef](#)]
418. An, S.S.A.; Kim, Y.-R.; Park, J.-I.; Lee, E.J.; Park, S.H.; Seong, N.-W.; Kim, J.-H.; Kim, G.-Y.; Meang, E.-H.; Hong, J.-S.; et al. Toxicity of 100 nm zinc oxide nanoparticles: A report of 90-day repeated oral administration in Sprague Dawley rats. *Int. J. Nanomed.* **2014**, *9*, 109–126. [[CrossRef](#)]
419. Hong, J.-S.; Park, M.-K.; Kim, M.-S.; Lim, J.-H.; Park, G.-J.; Maeng, E.-H.; Shin, J.-H.; Kim, M.-K.; Jeong, J.; Park, J.-A.; et al. Prenatal development toxicity study of zinc oxide nanoparticles in rats. *Int. J. Nanomed.* **2014**, *9*, 159–171. [[CrossRef](#)]
420. Jan, T.-R.; Shen, C.-C.; Wang, C.-C.; Liao, M.-H. A single exposure to iron oxide nanoparticles attenuates antigen-specific antibody production and T-cell reactivity in ovalbumin-sensitized BALB/c mice. *Int. J. Nanomed.* **2011**, *6*, 1229–1235. [[CrossRef](#)]
421. Reinert, M.; Schlachter, E.K.; Bregy, A.; Lönnfors-Weitzel, T.; Vajtai, I.; Bernau, V.J.; Weitzel, T.; Mordasini, P.; Slotboom, J.; Herrmann, G.; et al. Metabolic pathway and distribution of superparamagnetic iron oxide nanoparticles: In vivo study. *Int. J. Nanomed.* **2011**, *6*, 1793–1800. [[CrossRef](#)]
422. Malindretos, P.; Sarafidis, P.A.; Rudenco, I.; Raptis, V.; Makedou, K.; Makedou, A.; Grekas, D.M. Slow Intravenous Iron Administration Does Not Aggravate Oxidative Stress and Inflammatory Biomarkers during Hemodialysis: A Comparative Study between Iron Sucrose and Iron Dextran. *Am. J. Nephrol.* **2007**, *27*, 572–579. [[CrossRef](#)]
423. Anzai, Y.; Piccoli, C.W.; Outwater, E.K.; Stanford, W.; Bluemke, D.A.; Nurenberg, P.; Saini, S.; Maravilla, K.R.; Feldman, D.E.; Schmiedl, U.P.; et al. Evaluation of Neck and Body Metastases to Nodes with Ferumoxtran 10-enhanced MR Imaging: Phase III Safety and Efficacy Study. *Radiology* **2003**, *228*, 777–788. [[CrossRef](#)]
424. Gu, L.; Fang, R.H.; Sailor, M.J.; Park, J.-H. In Vivo Clearance and Toxicity of Monodisperse Iron Oxide Nanocrystals. *ACS Nano* **2012**, *6*, 4947–4954. [[CrossRef](#)]
425. Pacchierotti, F.; Bellusci, M.; La Barbera, A.; Padella, F.; Mancuso, M.; Pasquo, A.; Grollino, M.G.; Leter, G.; Nardi, E.; Cremisini, C.; et al. Biodistribution and acute toxicity of a nanofluid containing manganese iron oxide nanoparticles produced by a mechanochemical process. *Int. J. Nanomed.* **2014**, *9*, 1919–1929. [[CrossRef](#)]
426. Patil, U.S.; Adireddy, S.; Jaiswal, A.; Mandava, S.H.; Lee, B.R.; Chrisey, D.B. In Vitro/In Vivo Toxicity Evaluation and Quantification of Iron Oxide Nanoparticles. *Int. J. Mol. Sci.* **2015**, *16*, 24417–24450. [[CrossRef](#)]